

THE CHEMICAL BIOLOGY AND BIOINORGANIC CHEMISTRY OF YEAST
PHOSPHATIDYLINOSITOL TRANSFER PROTEIN

A Dissertation

by

DANISH KHAN

Submitted to the Office of Graduate and Professional Studies of
Texas A&M University
in partial fulfillment of the requirements for the degree of

DOCTOR OF PHILOSOPHY

| | |
|---------------------|------------------|
| Chair of Committee, | Vytas Bankaitis |
| Committee Members, | Dorothy Shippen |
| | Frank Raushel |
| | Tadhg Begley |
| Head of Department, | Gregory Reinhart |

August 2018

Major Subject: Biochemistry

Copyright 2018 Danish Khan

ABSTRACT

Phosphatidylinositol Transfer Proteins are an enigmatic family of proteins present across the plant and animal kingdoms. They act as diversifiers of phosphoinositide signaling and regulate diverse cellular processes such as membrane trafficking in yeast, polarized root hair growth in plants and neural stem cell development in mouse. Model organism *Saccharomyces cerevisiae* has provided opportunities to study Sec14, a prototype PITP, in detail. Sec14 orchestrates a kinase dependent phosphoinositide signaling pathway in cells that co-ordinates phosphatidylcholine metabolism with *trans*Golgi network/endosomal dynamics. It is essential to the infectivity of many fungal pathogens and is thus an attractive drug target. Small molecule inhibitors belonging to nitrophenyl piperazin methanone (NPPM) scaffold have been developed but their mode of action is not clear.

Using genetic screens and *in vitro* reconstitutions of phosphatidylinositol transfer activity, I studied the mechanism by which NPPMs inhibit Sec14. I identified a motif associated with Sec14 that allows pan-fungal predictions of sensitivity to NPPMs. My work showed that Sec14 from fungal pathogen *Candida glabrata* is sensitive to NPPMs. Two new classes of Sec14 inhibitors belonging to picolinamide and benzamide scaffolds, were identified and rigorously validated. These small molecules are potential lead compounds for novel anti-fungal drug development.

I also studied Sfh5, a Sec14 homolog from yeast. I discovered that Sfh5 is a heme binding protein. Using Electron Paramagnetic Resonance and Mössbauer spectroscopy, I determined the biophysical properties of the heme iron center. This is the first known instance of a PITP that binds heme. The structure of Sfh5 was solved at 2.7Å resolution through X-Ray crystallography, revealing a novel mode of heme binding. We also identified specific mutations in Sfh5 that weakened or abrogated heme binding. My studies reveal an allosteric relationship between

phosphatidylinositol and heme binding sites of the protein. Finally, I show that when Sfh5 is unable to bind heme, it acquires robust phosphatidylinositol transfer and signaling abilities.

These studies open avenues for development of a new class of anti-fungal drugs and offer new insights into the structure and functions of PITPs.

ACKNOWLEDGEMENTS

I would like to thank my committee chair, Prof. Vytas Bankaitis, and my committee members, Prof. Dorothy Shippen, Prof. Frank Raushel and Prof. Tadhg Begley, for their guidance and support throughout the course of this research.

Thanks also go to my friends and colleagues in the laboratory for making my time at Texas A&M University a great experience.

Finally, thanks to my dearest family for their love and encouragement.

CONTRIBUTORS AND FUNDING SOURCES

This work was supported by a dissertation committee consisting of Professor Vytas Bankaitis [advisor], Professor Dorothy Shippen, Professor Frank Raushel of Department of Biochemistry and Biophysics, and Professor Tadhg Begley of Department of Chemistry.

Ashutosh Tripathi of Bankaitis Lab helped with all the bioinformatic analyses presented in this work. The study presented in Chapter III was done in collaboration with the Dr. Dominic Hoepfner's group at Novartis, Switzerland, with contributions from group members led by: Gabriel Schaaf at Institute of Crop Science, Bonn, Germany; Fulvia Bono at Max Planck Institute for Developmental Biology, Tübingen, Germany and Herbert Waldmann at Max Planck Institute for Molecular Physiology, Dortmund, Germany.

The work presented in Chapter IV was done in collaboration with Professor James Sacchettini and Professor Paul Lindahl's groups at Department of Biochemistry and Biophysics. Chapter IV has not been published yet. Gulcin Gulten and Anup Agarwal of Sacchettini Lab processed the X-Ray crystallization data. Joshua Wofford of Lindahl Lab has collected and analyzed the data from Mössbauer experiments presented in the study. I have performed all the rest of the experiments presented here.

My work in the Bankaitis lab was funded by the National Institutes of Health [GM44530 to V.B.] and Robert A. Welch Foundation [BE-0017 to V.B.]. The Deutsche Forschungsgemeinschaft and Max Plank Gesellschaft funded work from the labs of Gabriel Schaaf and Fulvia Bono, respectively. The Robert A. Welch foundation grants to the laboratories of Professor Paul Lindahl [A-1170 to P.L.] and Professor James Sacchettini [A-0015 to J.S.] are also acknowledged.

NOMENCLATURE

| | |
|-------------------|--|
| [³ H] | Tritium |
| Au | <i>Candida auris</i> |
| Ca | <i>Candida albicans</i> |
| Cg | <i>Candida glabrata</i> |
| Cn | <i>Cryptococcus neoformans</i> |
| CRISPR | Clustered Regularly Interspaced Short Palindromic Repeats |
| DAG | Diacylglycerol |
| EPR | Electron Paramagnetic Resonance |
| HIP | Haploinsufficiency Profiling |
| HOP | Homozygous Profiling |
| ICP-MS | Inductively Coupled Plasma Mass Spectrometry |
| IFI | Invasive Fungal Infections |
| LBD | Lipid Binding Domain |
| M | Molar |
| m | 10 ⁻³ |
| MDS | Molecular Dynamics Simulation |
| NHE | Normal Hydrogen Electrode |
| nM | Nanomolar |
| NPPM | Nitrophenyl(4-(2-methoxyphenyl) piperazin-1-yl) methanones |
| PDB | Protein Databank File |
| PH | Pleckstrin Homology |
| Pik1 | Phosphatidylinositol-4-phosphate kinase 1 |

| | |
|------------|---|
| PIP | Phosphoinositide Phosphate |
| PITP | Phosphatidylinositol Transfer Protein |
| Plb1 | Phospholipase B 1 |
| PTB | Phospho-Tyrosine Binding |
| PtdCho | Phosphatidylcholine |
| PtdIns | Phosphatidylinositol |
| PtdSer | Phosphatidylserine |
| PtdEtn | Phosphatidylethanolamine |
| PX | Phox Homology |
| SAR | Structure Activity Relationship |
| SDS-PAGE | Sodium Dodecyl Sulfate Polyacrylamide Gel Electrophoresis |
| <i>SFH</i> | Sec14 Fourteen Homolog |
| Sfh1 | Sec14 Homolog 1 |
| Sfh2 | Sec14 Homolog 2 |
| Sfh3 | Sec14 Homolog 3 |
| Sfh4 | Sec14 Homolog 4 |
| Sfh5 | Sec14 Homolog 5 |
| SMI | Small Molecular Inhibitor |
| Stt4 | Staurosporine and Temperature sensitive |
| TGN | <i>Trans</i> -Golgi Network |
| UV-vis | Ultraviolet-visible |
| WT | Wild Type |
| YPD | Yeast Peptone Dextrose |

TABLE OF CONTENTS

| | Page |
|---|------|
| ABSTRACT..... | ii |
| ACKNOWLEDGEMENTS..... | iv |
| CONTRIBUTORS AND FUNDING SOURCES | v |
| NOMENCLATURE | vi |
| TABLE OF CONTENTS..... | viii |
| LIST OF FIGURES | xii |
| LIST OF TABLES..... | xiii |
| CHAPTER I INTRODUCTION AND LITERATURE REVIEW | 1 |
| PITP Structure and Function: Unity in Diversity | 3 |
| Sec14 Homologs in <i>S. cerevisiae</i> | 7 |
| Structural Features of Sec14..... | 8 |
| Sec14 in fungal pathogens | 10 |
| Fungal Resistance: An Emerging Problem..... | 11 |
| Scope and Nature of the <i>Candida</i> Threat..... | 13 |
| Therapeutic Approaches for Treating Candidiasis | 14 |
| The Resistance Rises..... | 15 |
| Opportunities For New Anti-Microbial Strategies | 17 |
| Specificity of NPPMs towards Sec14..... | 18 |
| Non-NPPM drugs and their inhibition of Sec14..... | 22 |
| Pharmacophore and Future SMI Design Considerations..... | 24 |
| References..... | 27 |
| CHAPTER II STRUCTURAL ELEMENTS THAT GOVERN SEC14-LIKE PHOSPHATIDYLINOSITOL TRANSFER PROTEIN SENSITIVITIES TO POTENT SMALL MOLECULE INHIBITORS | 32 |
| Disclaimer for Chapter II..... | 32 |
| Summary..... | 33 |
| Introduction..... | 34 |

| | |
|---|-----|
| Results..... | 36 |
| Discussion..... | 59 |
| Materials and Methods..... | 65 |
| References..... | 77 |
| | |
| CHAPTER III TARGET IDENTIFICATION AND MECHANISM OF ACTION OF PICOLINAMIDE AND BENZAMIDE BASED CHEMOTYPES WITH ANTIFUNGAL PROPERTIES | 81 |
| Disclaimer for Chapter III..... | 81 |
| Summary..... | 82 |
| Introduction..... | 83 |
| Results..... | 84 |
| Discussion..... | 107 |
| Materials and Methods..... | 110 |
| References..... | 116 |
| | |
| CHAPTER IV SFH5, A SEC14 HOMOLOG, IS A HEME BINDING PROTEIN | 122 |
| Summary..... | 122 |
| Introduction..... | 123 |
| Results..... | 126 |
| Discussion..... | 144 |
| Materials and Methods..... | 148 |
| References..... | 153 |
| | |
| CHAPTER V CONCLUSIONS AND FUTURE DIRECTIONS..... | 156 |
| Conclusions..... | 157 |
| Future Directions | 158 |
| References..... | 165 |
| | |
| APPENDIX A PLASMID INVENTORY..... | 166 |
| | |
| APPENDIX B PROTOCOLS OF NOVEL TECHNIQUES | 168 |

LIST OF FIGURES

| | Page |
|---|------|
| Figure 1-1 Diversification of PtdIns-4-P signaling by PITP molecules | 4 |
| Figure 1-2 Crystal structures of Sec14 and Sec14 Homolog 1 | 12 |
| Figure 1-3 Chemical structures of NPPMs 4130-1278, 6748-481 and 5564-701 | 20 |
| Figure 1-4 Ergoline scaffold compound that shows anti-Sec14 activity | 23 |
| Figure 2-1 Comparisons of NPPM 6748-481 docking poses in the hydrophobic pockets of Sec14 and Sfh1 | 39 |
| Figure 2-2 A rational approach for engineering Sfh1 sensitivity to NPPM 6748-481 | 40 |
| Figure 2-3 Functional characterization of NPPM-resistant Sec14 proteins..... | 46 |
| Figure 2-4 The Sec14 VV motif is not conserved among closely related Sec14 PtdIns/PtdCho-transfer proteins | 49 |
| Figure 2-5 The VV motif is a signature of NPPM-sensitive yeast Sec14-like PtdIns/PtdCho-transfer proteins | 55 |
| Figure 2-6 Functional analysis of the VV motif in Sec14 | 58 |
| Figure 2-7 The Ser173 coordination envelope..... | 64 |
| Figure 3-1 Chemogenomic profiling and hypersensitivity validation | 88 |
| Figure 3-2 Synthesis of a collection of benz- and picolinamides for structure-activity relationship study | 92 |
| Figure 3-3 Analysis of lipid-transfer inhibition with recombinant Sec14p | 93 |
| Figure 3-4 Structural and functional analysis of Sec14p-compound interactions. | 98 |
| Figure 4-1 Visual properties of <i>E. coli</i> cells when expressing Sfh5 and picture of the purified protein. | 127 |
| Figure 4-2 Recombinant Sfh5 protein binds heme | 128 |

| | | |
|-------------|--|-----|
| Figure 4-3 | Structural features of Sfh5 protein | 132 |
| Figure 4-4 | Surface electrostatic potentials of “closed” and “open” forms of Sfh5 | 134 |
| Figure 4-5 | The iron co-ordination architecture of Sfh5 protein | 135 |
| Figure 4-6 | Determination of Reduction Potential of Sfh5 protein | 138 |
| Figure 4-7 | Mutations in proximal residues renders Sfh5 defective to heme binding..... | 139 |
| Figure 4-8 | Electron Paramagnetic Resonance spectra for Sfh5 protein and mutants..... | 141 |
| Figure 4-9 | Mössbauer spectra of Sfh5p and mutants..... | 142 |
| Figure 4-10 | PtdIns transfer assay with purified, recombinant Sfh5 protein | 143 |
| Figure 4-11 | <i>In vivo</i> complementation assay with Sfh5 mutants | 145 |
| Figure 5-1 | Crystallization efforts directed towards Sec14 from <i>C. albicans</i> and promising new chemical scaffolds..... | 160 |
| Figure 5-2 | Analysis of new Sec14 mutants that do not reside in the binding pocket..... | 164 |

LIST OF TABLES

| | Page |
|---|------|
| Table 2-1 Intrinsic PtdIns-transfer activities for NPPM ^R Sec14 | 48 |
| Table 2-2 Intrinsic PtdIns-transfer activities for Sec14-like PITPs and VV-motif variants.. | 54 |
| Table 2-3 Gene replacement cassette plasmids | 67 |
| Table 2-4 Primer sequences | 68 |
| Table 2-5 Protein expression plasmids | 72 |
| Table 3-1 Structures and IC ₅₀ values for active compounds..... | 85 |
| Table 3-2 Crystal structure model refinement parameters for Sec14-compound 2 complex | 100 |
| Table 3-3 Growth inhibitory concentrations against pathogenic fungi | 106 |
| Table 4-1 Crystal structure model refinement parameters for Sfh5 | 131 |

CHAPTER I

INTRODUCTION AND LITERATURE REVIEW

Phosphatidylinositol (PtdIns) is a major cellular phospholipid that serves as a metabolic precursor for diverse polyanionic lipids. A six-carbon polyol, the inositol headgroup on PtdIns hosts five hydroxyl moieties that can be phosphorylated in a combinatorial fashion to generate an ensemble of chemically distinct phosphoinositides (PIPs). Although low in abundance, PIPs affect nearly all aspects of cellular functioning. These include cell signaling, modulation of membrane proteins and ion channels, regulation of membrane trafficking to and from plasma membrane, to name a few (Balla et al., 2013; Di Paolo et al., 2006; Cong et al., 2017). It is likely that the structural and functional diversity of PIPs has played a major role in the evolution of complex eukaryotic lifeforms (Michell et al., 2008).

In *Saccharomyces cerevisiae*, a phosphatidylinositol (PtdIns) molecule can be phosphorylated to yield five phosphoinositide species. These include phosphatidylinositol-3-phosphate (PtdIns-3-P), phosphatidylinositol-4-phosphate (PtdIns-4-P), phosphatidylinositol-3,5-*bis*phosphate (PtdIns-3,5-P) and phosphatidylinositol-4,5-*bis*phosphate (PtdIns-4,5-P) (Liu et al., 2010). By binding to or recruiting effectors at membrane-cytosol interface, individual PIP molecules can orchestrate signal transduction events that are resolved spatially and temporally. Multiple ‘PIP detecting domains’ have been discovered that interpret the chemical diversity of phosphoinositides. Proteins containing the pleckstrin homology (PH), phox-homology (PX) or phosphotyrosine binding (PTB) domains show headgroup specific recognition for multiple PIP species (Di Paolo et al., 2006; Kutateladze 2010).

In proteins with FERM (for **F**our-point-one, **E**zrin, **R**adixin, **M**oesin) or MARCKS (for **M**yrystoylated **A**lanine-**R**ich **C** **K**inase **S**ubstrate) domains, basic patches allow electrostatic interactions with PIPs (Gambhir et al., 2004; Narayan et al., 2006; Bankaitis et al., 2010). Proteins containing these modules are often helped by ancillary proteins that sharpen their PIP-specificity. These detection events are then followed by downstream signaling pathways that lead to discrete biological outcomes. An added layer of control is imposed by phosphoinositide phosphatases that hydrolyze the phosphoryl groups from PIPs as well as kinases that populate PIPs in the first place. These checks and balances on the population of PIPs are integral to maintenance of cellular homeostasis (Balla et al., 2013; Di Paolo et al., 2006; Liu et. al, 2010).

Although the model of ‘PIP detection’ followed by downstream signaling events is rational, it is predicated excessively on PIP identities. The metabolic linkage between PIP mediated lipid signaling, and generation and maintenance of bulk lipid pools remain understudied. Analyzing this issue in the context of PtdIns-4-P signaling is particularly insightful (Bankaitis et al., 2010).

There are two known PtdIns-4-P kinases in yeast, Stt4 and Pik1. Stt4 mediated PtdIns-4-P generation plays major roles in the overall maintenance of key cellular structures viz. lipid droplets, cytoskeleton, cell wall and vacuoles (Audhya et. al. 2002; Baird et. al. 2008; Ren et al., 2014). The polymorphic nature of PtdIns-4-P signaling cannot be explained by models that only account for post-production events in the life cycle of a PtdIns-4-P molecule. Moreover, kinases are biologically insufficient enzymes that do not produce enough PtdIns-4-P molecules to trigger a signaling cascade. Work from our lab and others have shown that an enigmatic class of proteins, called the Phosphatidylinositol Transfer Proteins (PITPs) regulate PtdIns-4-P production in response to specific metabolic cues (Figure 1-1).

PITPs prime PtdIns-4-P signaling by boosting the activity of kinases. This mechanism does not involve PITP mediated transport of lipids from one membrane to another. Our work has demonstrated that PITPs execute an energy-independent exchange reaction between membrane PtdIns and a second counter-lipid ligand that acts as a metabolic cue for signaling. This localized extraction of PtdIns provides the kinase with an otherwise inaccessible substrate that triggers PtdIns-4-P production. This represents an additional layer of regulation over phosphoinositide signaling that is distinct from the action of a kinase or the identity of PIP generated (Schaaf et al., 2008; Bankaitis et al., 2010; Schaaf et al., 2011).

PITP Structure and Function: Unity in Diversity

PITPs constitute an ancient family of proteins that are present throughout the plant and animal kingdoms (Huang et al., 2017). They owe their nomenclature to a narrow description of their *in vitro* abilities, namely, their mediation of energy-independent transfer of PtdIns between membranes. The term PITP by itself does not exclude any other phospholipid (PL) transfer ability that may additionally reside in the protein.

PITPs fall into two evolutionarily distinct groups based on their primary sequence similarity and secondary structure features, namely, Sec14-like proteins and the START (steroidogenic acute response related transfer domain)-like proteins. Fungal and plant PITPs are Sec14-like, while metazoan PITPs are classified as START-like. Despite their structural heterogeneity, all PITPs can transfer PtdIns. As non-enzymatic proteins, PITPs do not chemically modify a phospholipid. Instead, they execute a lipid exchange cycle involving complex structural dynamics, that allow them channel PtdIns molecules to PtdIns-4-kinases (Grabon et al., 2015; Bankaitis et al., 2010).

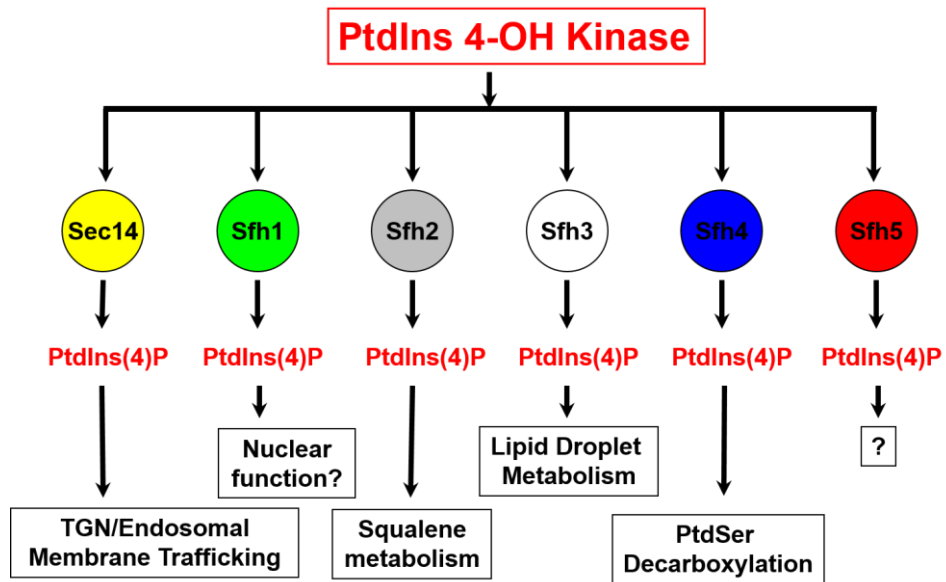


Figure 1-1. Diversification of PtdIns-4-P signaling by PTP molecules

The activity of Stt4, a PtdIns-4-OH kinase in yeast, is regulated by individual PTP proteins (shown in circles). These result in diverse metabolic outcomes in cells. The PTPs whose cellular roles are not clear, are indicated with ‘?’.

The discovery of single nucleotide polymorphisms in PITP domains have been linked to multiple metabolic disorders and diseases, highlight the importance of this family of proteins. Inherited conditions such as cerebellar ataxia of Cayman type, Bothnia retinal disorder and cone-rod dystrophy have been associated with mutations in the PITP domains of relevant proteins (Nile et al., 2010). Derangements in development of mice neocortex and stunted root hair growth in *Arabidopsis* have been observed in mutant PITPs (Xie et al., 2017; Huang et al., 2018).

With the help of well-established techniques of genetic manipulation, valuable insights have been gained as to how PITPs executes their biological functions in yeasts. Sec14 is the prototype member of the yeast PITPs. It is an essential protein that co-ordinates the *trans*-Golgi Network endosomal system mediated membrane trafficking, with lipid metabolic pathways. *In vitro* transfer assays have shown that Sec14 can transfer both PtdIns and phosphatidylcholine (PtdCho) and that both these activities must reside on the same protein molecule for stimulation of PtdIns-4-OH kinase activity (Schaaf et al., 2008).

Kinases are considered to be biologically insufficient enzymes. Although PtdIns, the kinase substrate, is present in membranes, they are not accessible to them for catalysis. In response to metabolic cues emanating from PtdCho production, Sec14 is proposed to extract PtdIns from membrane and ‘present’ it to the kinase for phosphorylation, overcoming a critical kinase handicap. It does so by executing a series of abortive exchanges where it attempts to extract and bind PtdIns, even as the protein is already occupied by PtdCho. The slow egress of PtdCho provide ample opportunities for the extracted PtdIns to be made available to the kinases. The relative kinetics of PtdIns/PtdCho binding and transfer has been studied using small angle neutron scattering. It has been shown that the time taken by PtdIns molecule to complete a phospholipid exchange reaction is ~15 times faster than the same for PtdCho (Sugiura, et al., 2016; Nakano et

al., 2007). This supports the notion that PtdCho occupancy in Sec14 frustrates attempts by PtdIns to access the lipid pocket. In view of these properties. Sec14-like PITPs have been envisioned as ‘nanoreactors’, a sort of one-stop-shop scaffold for metabolic signaling and organization, that integrates PtdCho metabolism with PtdIns-4-P signaling (Ile et al., 2006; Grabon et al., 2015).

Identification of multiple ‘bypass Sec14’ mutants, support this conclusion. These mutants have been identified in seven distinct alleles of enzymes belonging to two metabolically distinct categories. The first category includes enzymes from the CDP-Choline/Kennedy pathway. This biosynthetic pathway metabolizes diacylglycerol (DAG) to produce PtdCho. The second category of mutations were mapped to *SAC1*, a PtdIns-4-P phosphatase, and *KESI*, an oxysterol binding protein that sequesters PtdIns-4-P molecules. These mutations allow cellular viability even in the absence of Sec14, i.e. they allow cells to ‘bypass’ the normal Sec14 requirement (Cleves et al., 1989; Cleves et al., 1991; Bankaitis et al., 2010).

The bypass mutants strongly argue in favor of a model where Sec14 regulates lipid metabolism, instead of merely effecting vectoral lipid transport between undefined cellular membranes. Such bulk models would predict that the essential requirement of Sec14 would be obviated in cells that have been engineered to overproduce PtdIns. In practice, Sec14 remains essential despite enhanced PtdIns levels. Alternatively, a 90% reduction in expression levels of *SEC14* fails to impose metabolic penalties on cells, arguing strongly in favor of a lipid signaling role for Sec14. By tuning PtdIns-4-P production to PtdCho synthesis and DAG consumption, Sec14 integrates multiple metabolic pathways (Cleves et al., 1991; Kearns et al., 1997; Bankaitis et al., 1990).

Sec14 Homologs in *S. cerevisiae*

There are five proteins encoded by the yeast genome who share similarity with Sec14. These numbers vary between 42% to 76% and the proteins are named as Sec Fourteen Homolog 1 through 5 (i.e. Sfh1, Sfh2, Sfh3, Sfh4 and Sfh5). The SFH proteins are biochemically distinct from Sec14p and are considered non-classical members of the PITP family of proteins. While all five SFH proteins can bind and transfer PtdIns to some extent *in vitro*, they are unable to transfer PtdCho. Their role in phosphoinositide signaling and lipid metabolism in yeast is an area of active study (Li et al., 2000; Schaaf et al., 2011; Ren et al., 2014).

None of the SFH proteins are essential for cell viability, either individually or collectively. In a temperature sensitive yeast strain (*sec14ts-1*) where Sec14 can be inactivated by growing the yeast at 37°C instead of 25°C, only SFH2, SFH4 or SFH5 were each able to rescue the growth defect upon overexpression. These observations notwithstanding, SFH proteins are understood to have Sec14-independent roles in cell. (Li et. al, 2000)

Out of all the SFH proteins, SFH3 has been studied in extensive detail and found to be linked with lipid droplet metabolism (Ren et al., 2014). Lipid droplets have recently gained prominence as dynamic organelles that play an important role in cells. Unlike conventional organelles that are bound by membrane bilayers, lipid droplets have a phospholipid monolayer surrounding a core of neutral lipids such as triacylglycerol and proteins. They are regarded as ‘depots’ for fat in cells that are under tight metabolic control. Defects in lipid droplet metabolism have been linked to disorders associated with excess fat storage such as obesity, non-alcoholic fatty liver disease and diabetes.

Sfh3 has been found to associate with bulk lipid droplets in vegetative cells where it functions to inhibit neutral lipid distribution. The Sfh3 mediated production of PtdIns-4-P was

implicated in the inhibition of lipid droplet utilization, thereby establishing a formal link between phosphoinositide signaling and lipid droplet homeostasis. Under conditions of nutrient stress, however, diploid yeast cells prefer to sporulate and enter a meiotic stage. The nucleus divides into four haploids that are enveloped by a membrane termed ‘pro-spore membrane’. Sfh3 was found to associate with a subset of lipid droplet pools that were rich in lipid hydrolases and closely associated with the pro-spore membranes. It inhibited the process of pro-spore membrane biogenesis in a manner dependent upon its ability to bind PtdIns. Thus, Sfh3 was found to execute two distinct functions in metabolically distinct lipid droplet pools (Ren et al., 2014).

Another SFH protein - Sfh4p has been implicated in decarboxylation of phosphatidylserine (PtdSer) to produce phosphatidylethanolamine (PtdEth). Our lab has previously shown that Sfh4 is not only capable of potentiating Ptd-4-kinase activity, but that it has a non-canonical role in the ‘phosphatidylserine decarboxylation 2’ pathway. Sfh4p has also been suggested to be involved in intermembrane contact sites between endoplasmic reticulum (ER) and mitochondria, where PtdSer can be transferred (Wu et al., 2000).

Sfh1 has been exploited as a structural proxy for Sec14 due to its high similarity with Sec14. It has been co-crystallized with PtdIns, PtdCho and PtdEth and has served to massively enhance our understanding of Sec14 protein dynamics. There is little information available about the other SFH proteins and what roles, if any, they play in cells. The rudimentary nature of our knowledge of these proteins offers real avenues for their studies in future.

Structural features of Sec14

Multiple crystal structures of Sec14 and Sec14-like proteins have been solved. These include Sec14, Sfh1, Sfh3 as well as the structurally related α -tocopherol transfer protein (α TTP) and

mammalian Sec14L2 protein, to name a few (Sha et al., 1998; Stocker et al., 2003; Min et al., 2003; Schaaf et al., 2008; Ren et al., 2014). These structures outline certain basic features of Sec14-like proteins that are summarized below.

Sec14 domains adopt a classical fold termed ‘CRAL TRIO’. The N-terminal lobe is populated by 3-4 α helices that organize to form tripod like structure. The central feature of these proteins is a lipid binding pocket or chamber. Parallel β pleated sheets constitute the hydrophobic floor of the pocket, that are lent structural support by multiple 3_{10} helices on one side. A series of α helices delineates the pocket on the other end. An α helical chain gates the pocket that is conformationally very flexible. Studies with Sec14 have shown that the gate swings into an “open” confirmation in non-phospholipid bound structures of Sec14. The gate is “closed” in lipid bound structures of Sec14, moving by $\sim 20\text{\AA}$ during every structural transition. The importance of opening and closing of the helical gate to lipid exchange was demonstrated by cross-linking experiments (Figure 1-2) (Schaaf et al., 2008; Ryan et al., 2008; Sha et al., 1997). These massive conformational changes are regulated by substructures situated behind the lipid binding pocket. A “gating module” held together by a series of hydrogen bonded helices and loops, that themselves are conformationally rigid but can transmit ‘open’ and ‘close’ instructions to the gating helix. Mutations in the gating module that impair its ability to form a series of hydrogen bonds makes the protein conformationally immobile and has been associated with many diseases. The crystal structures also identified unique binding sites for the phospholipids. PtdCho head group settled at a site deep within the protein, while PtdIns headgroup assumed a position just beneath the protein surface. The acyl chains of both phospholipids occupied a common space. Residues coordinating the PtdIns, PtdCho as well as the glycerol backbone are conserved throughout Sec14 homologs. These unique residues constitute ‘barcodes’ that predict the PtdIns/PtdCho binding abilities of

Sec14 and Sec14-like proteins (Ryan et al., 2007; Schaaf et al. 2008, Grabon et al. 2015; Grabon et al., 2017).

An Electron Paramagnetic Resonance (EPR) study of Sec14 found suggested that a polarity gradient within the Sec14 cavity could explain the energy independent nature of lipid exchange reaction of Sec14 (Smirnova et al., 2007; Schaaf et al., 2011). The crystal structures support the notion of a hydrophobic gradient operating within the pocket. During an exchange cycle, a phospholipid has an option to partition from membrane bilayer to the pocket. It is plausible that the membrane pocket provides a more favorable energetic environment thereby making it energetically more favorable for the phospholipid to partition into it. When releasing the bound phospholipid, it is possible that the protein reorients the chamber polarity by realigning the molecules present inside. Mapping out the energetics of a phospholipid exchange reaction remains an outstanding conundrum.

Sec14 in Fungal Pathogens

Sec14-like proteins have been reported to play major roles in fungal pathogens. Many fungi are dimorphic in nature, that is, they show a morphogenic transition between yeast and hyphal forms that is critical to their pathogenicity. Such transitions are complex in nature, marked by massive changes in the fungi metabolome (Klein et al., 2007). Sec14 has been implicated in regulation of dimorphic transition in multiple organisms including *Kluveromyces lactis* and *Candida albicans* (Lopez et al., 1994; Riggle et al., 1997). It has been observed that Under conditions of Sec14 depletion, *C. albicans* is unable to form filaments and its pathogenicity is remarkably compromised (Monteoliva et al., 1996). A critical role of Sec14 has also been seen in *Cryptococcus neoformans*. The virulence of *C. neoformans* is critically dependent upon its ability to secrete pro-

pathogenic factors into its host (Oliviera et al., 2010; Chayakulkeeree et al., 2011). One such factor – *Cryptococcal* Phospholipase B1 or CnPlb1 is a major determinant of *C. neoformans* infection in host phagocytes and was found to be secreted in a Sec14 dependent manner. CnPlb1 contains multiple enzymatic activities, all of which serve to mobilize fatty acids from host cell membranes and diminish host immune responses. The role of Sec14 as a pro-membrane trafficking protein makes it an attractive drug target in *C. neoformans* and similar fungal pathogens. Given the shrinking arsenal of antifungal drugs and global emergence of fungal resistance, it is important to develop new antifungals (Schmiedel et al., 2016).

Fungal Resistance: An Emerging Problem

Growing resistance to anti-fungal agents has led to fears of an impending global health emergency. While superficial fungal infections in humans are commonplace, invasive fungal infections (IFIs) are life-threatening. They account for a mortality rate of upto 42%, surpassing fatalities associated viral and bacterial infections that are otherwise more communicable. More than 90% of reported deaths due to fungal infections are attributed to pathogens from *Aspergillus*, *Candida*, *Cryptococcus* and *Pneumocystis* genera (Monk et al., 2008; Brown et al., 2012; Fisher et al., 2018).

Invasive candidiasis manifests itself as a nosocomial infection that puts hospitalized neonates, immunocompromised patients, organ transplant and chemotherapy recipients at major risk (Kullberg et al., 2015). Difficulty in diagnosis of IFIs and lack of reliable epidemiological data has complicated efforts to appreciate the true extent of this nuisance. Furthermore, the number of tools needed to combat fungal infections are limited in number and potency. Emergence of ever more virulent fungi that defy conventional treatment paradigms has led to a prioritization of searches for new *drugs* and *drug-targets* (Fisher et al., 2012).

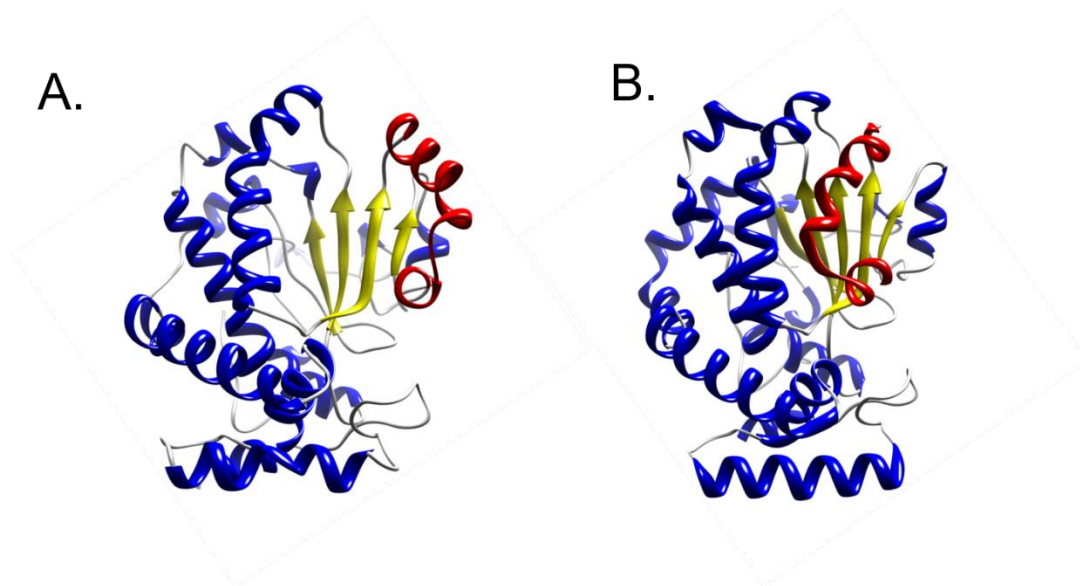


Figure 1-2. Crystal structures of Sec14 and Sec14 Homolog 1

(A) Sec14 (PDB ID 1AUA) crystallizes in an “open” confirmation. The hydrophobic floor of the lipid binding pocket is made by β pleated sheets (in yellow). In red, is the α helical gate that lines the pocket door. The helix is repositioned $\sim 20\text{\AA}$ away from the pocket in Sec14.

(B) Sfh1 (PDB ID 3BLQ) crystallizes in a “closed” conformation. The bound lipid has been removed from the pocket for purposes of clarity. The α helix colored in red is present in a conformation that closes the hydrophobic pocket.

Scope and Nature of the *Candida* Threat

While members of *Candida* spp. populate the gastrointestinal tract in all humans, they generally do not give rise to invasive infections. The tract acts as a natural barrier and prevents fungal proliferation. The switch from such commensal to opportunistic behavior may be induced when host immunity is weakened or a surgery causes disruption in the mucosal barrier. The primary source of invasive candidiasis in hospital patients though are intravascular catheter tubes contaminated with fungal biofilm. Patients undergoing chemotherapy, hemodialysis or surgical procedures are particularly vulnerable, as are the elderly and newborn babies. The incubation period between exposure of *Candida* and onset of fulminant sepsis symptoms is ~7-10 days. Invasive candidiasis includes bloodstream infections (candidemia) as well as the harder-to-detect organ candidiasis which is manifested by pathophysiologies in kidney, liver, spleen, eyes or lungs (Antinori et al., 2016; DuPont et al., 2009).

Although there are ~20 pathogenic species of *Candida*, 92% of all isolates from candidemia patients belong to 5 species: *C. albicans*, *C. glabrata*, *C. krusei*, *C. parapsilosis* and *C. tropicalis* (Guinea et al., 2014). Their strategies to circumvent the host immune system vary as do their virulent traits. For example, most *Candida* spp. are dimorphic and show a morphogenic transition between yeast and hyphal forms that is critical to their pathogenicity. In contrast, *C. glabrata* does not form filamentous hyphae and is more closely related to non-pathogenic *Saccharomyces cerevisiae*, than to *C. albicans* (Kurtzman et al., 1998). Differences in carbohydrate composition of cell walls also impact fungal sensing by human hosts. *C. parapsilosis* was found to elicit higher cytokine proliferation upon recognition by human peripheral blood mononuclear cells, than *C. albicans* while perturbations in carbohydrate content of *C. albicans* affected the rate at which they were phagocytosed (Lewis et al., 2012; Estrada et al., 2012).

The distribution of *Candida* species varies with geography. In the US, *C. albicans* infections account for about half of all infections, while the proportion of *C. glabrata* infection has increased to ~33% over the past decade. Globally, the distribution of *C. parapsilosis* and *C. tropicalis* are rising while that of *C. albicans* is falling, although it still dominates the etiological landscape of IFIs (Pfaller et al., 2014; Lamoth et al., 2018).

Therapeutic Approaches for Treating Candidiasis

In the absence of any anti-fungal vaccine, the medicinal strategies for combating invasive candidiasis revolve around FDA-approved compounds from three classes of molecules: polyenes, azoles and echinocandins. The panoply of mechanisms through which these drugs act is narrow, as are their targets. Despite their smaller genomes, members of *Candida* species have close phylogenetic relationship with humans. Depending upon the stringency with which they are compared, *Candida* has homologs for about 30-50% of human genes (Zeng et al., 2001). This mandates careful selection of fungal drug targets as the starting point for any drug discovery approach.

Polyenes such as Amphotericin B are some of the oldest antifungals that have remained mostly refractory to fungal resistance. They exert their toxic effects by binding ergosterol in fungal plasma membranes with sub-micromolar dissociation constants, followed by membrane perforation. Their inability to bind cholesterol - ergosterol's mammalian analog - make them particularly selective towards fungi (Gray et al., 2012). Due to their poor bioavailability, new generation polyenes have been complexed with lipids to further improve their potency (Ostrosky-Zeichner et al., 2010).

Azoles (such as fluconazole) target ergosterol biosynthesis by inhibiting the lanosterol 14- α -demethylase enzyme (also known as ERG11) at endoplasmic reticulum, inhibiting growth of most of *Candida* spp. Echinocandins class of drugs are non-competitive inhibitors of the β -1,3-D glucan synthase complex encoded by FKS genes. They are lipo-peptidic in nature and inhibit cell wall synthesis. In contrast to the superior pharmacokinetic properties of azoles, echinocandins suffer from poor bioavailability. The last anti-fungal drug from the echinocandin class, anidulafungin, was approved by the FDA more than a decade ago (Fisher et al., 2012, Filipuzzi et al 2016). The chitinous cell wall of fungus is also come into focus as an attractive drug target. Chitin synthase inhibitors like Nikkomycin Z are currently in the drug development pipeline (Shubitz et al., 2014).

The Resistance Rises

Not surprisingly, many *Candida* isolates have emerged that are resistant to multiple classes of drugs. These include both naturally resistant species and those that have acquire resistance over time. Development of new drugs is a time-taking and costly enterprise. In this incessant cat-and-mouse game of beating resistance pathogens with new drug formulations, all 'wins' need to be considered as essentially temporary.

While some *Candida* spp. are innately resistant to azoles, like *C. kruzei*, excessive prophylactic use of fluconazole has induced resistance in others. In both *C. albicans* and *C. glabrata* resistance to voriconazole, a new generation azole, has also been observed (Castanheira et al., 2014, Denning et al., 2015). Aneuploidies in sections of chromosomes coding for ERG11 (the target of fluconazole), drug efflux pumps and PAC1 - a transcriptional activator of ATP binding cassette (ABC)-transporter genes, have been found in azole resistant *C. albicans* isolates.

Remarkably, in the absence of selection pressure of drugs, this aneuploidy is lost. A clinical therapy that supplements azoles with drugs capable of perturbing chromosomal aneuploidy may help overcome azole resistance in *C. albicans*. (Selmecki et al., 2006). A similar polytherapeutic approach has been tested against fluconazole resistant *C. glabrata*. Multiple mutations in transcription factor CgPdr1 makes it constitutionally active, thereby upregulating multiple ATP transporter genes. Discovery of small molecules that block CgPdr1 mediated transcriptional activation have been shown to confer sensitivity to azoles in otherwise resistant *C. glabrata* isolates (Nishikawa et al., 2016; Monk et al., 2008).

In 2001, caspofungin was the first echinocandin based drug to be approved by the FDA and quickly became the first-line agents for treating invasive candidiasis. Echinocandin based drugs have remained mostly impervious to resistance by *C. albicans*, the notable exception being *C. glabrata* (Park et al., 2005). Clusters of mutations in the FKS (glucan synthase) genes have been associated with loss of sensitivity to multiple echinocandins, more so in patients with previous exposures (Pfaller et al., 2014; Farmakiotis et al. 2014; Arendrup et al., 2014). Although resistance to amphotericin B is rare, isolates of *C. albicans*, *C. glabrata* and *C. tropicalis* have been identified that are insensitive to it (Sterling et al., 1996; Krogh-Madsen et al., 2006; Mesa-Arango et al., 2016).

One multi-drug resistant pathogen that has garnered significant attention recently is *Candida auris* (Satoh et al., 2009; Lamoth et al., 2018; Fisher et al., 2018; Chaudhary et al., 2017). Spread primarily through nosocomial infections, *C. auris* was identified in Japan in 2009. As of 18th May 2018, 279 confirmed cases of *C. auris* have been reported within US. Traditional methods of identification that rely on fungal phenotypes routinely misidentify *C. auris* as *C. haemulonii* or *C. famata*, making its diagnosis very cumbersome. Sequencing the D1/D2 region of

28S rDNA and the internal transcribed spacer region of rDNA can identify it with confidence as can some mass spectrometry techniques. Most U.S. isolates show complete resistance to azoles while ~30% have Amphotericin B resistance. This leaves treatment with echinocandins as the only viable option. A new echinocandin-class drug called rezafungin has shown promise in treatment of *C. auris* based candidiasis in mouse model and is slated to enter phase 3 clinical trial later this year (Hager et al., 2018). However, around 2% of all isolates in US have also shown echinocandin resistance making them essentially impervious to all three classes of antifungals. *C. auris* has rapidly spread to >50 countries and this trend is likely to continue, prompting the US Center for Drug Control (CDC) to characterized *C. auris* as a ‘serious global health threat’.

Opportunities For New Anti-Microbial Strategies

Given these dire predictions, the importance of developing new drugs cannot possibly be overstated. that act via unconventional mechanisms Small molecules that hijack cellular immune machinery as a way to selectively degrade fungi have been proposed. These bifunctional molecules consist of a ‘targeting ligand’ that is specific to fungal chitin and a ‘recruitment ligand’ that can bind to pre-existing antibodies. This leads to enhanced neutrophil surveillance around the fungus leading to their phagocytosis. Through simultaneous targeting of unique components of fungal cell wall and host immune system, there is scope for diversification of these molecules to yield potent antifungals (Chirkin et al., 2017).

A similar strategy to selectively degrade protein molecules within cells has shown great potential. Proteolysis-targeting chimeras or PROTACs are bifunctional molecules that recruit cellular proteasomal machinery to target proteins for ubiquitin mediated degradation. They have been successfully used to target hyperactive receptor tyrosine kinases and androgen receptors in

cancerous cells (Raina et al., 2016; Burslem et al., 2018). Whether this technology can be adapted to target fungal pathogens, remains untested. The fungal cell imposes a considerable barrier for any drug seeking to exploit internal cellular machinery of fungi. Potential uses may involve selective degradation of pro-dimorphic transition proteins thereby arresting the progress of pathogen at a less virulent stage. While it is impossible to predict the success of any novel pharmacological modality, emergence of ever more resistant pathogens, require that all options be considered, including targeting Sec14 proteins.

Specificity of NPPMs towards Sec14

Of the small molecules that target Sec14 activity, the nitrophenyl(4-(2-methoxyphenyl) piperazin-1-yl) methanones (NPPMs) are the best understood (Nile et al., 2016). These molecules have been shown to be robust inhibitors of Sec14p in vivo and in vitro. Identified in a genome-wide screen with synthetic chemical compounds that impacted affecting yeast growth, NPPM 4130-1278 (Figure 1-3) showed specificity against Sec14. A search for compounds with better clogP values was undertaken and additional derivatives were identified that were ~10x more potent than the original compound.

Based on these findings, our lab generated a focused compound library and the ‘hit’ candidate was optimized. Dose-response experiments showed that NPPM sensitivity was related to cellular Sec14 levels. An optimized compound NPPM 6748-481, was identified as the most water-soluble bioactive compound and the most potent growth inhibitor of all. The half- maximum inhibitory concentration (IC₅₀) for 6748-481 was ~2.9µM for wild-type cells. To measure the impact of drug intoxication on the functional abilities of Sec14, we adapted an in vitro lipid transfer assay to accurately measure profile Sec14’s sensitivity to the candidate small molecule inhibitors.

The representative NPPMs 6748-481 and 4130-1276 displayed potent and dose-dependent inhibitions of Sec14-catalyzed [³H]PtdIns transfer in a purified system and the IC₅₀ values ranged from 175nM to 283 nM (Nile et al., 2014).

These SMIs were projected to inhibit Sec14 by loading into the phospholipid binding pocket and blocking any subsequent rounds of phospholipid exchange. Available data projects that NPPM invades the hydrophobic lipid-binding pocket of Sec14 during a lipid-exchange cycle where the inhibitor engages both residues within PtdIns -and PtdCho-acyl chain space and residues essential for coordination of the PtdCho headgroup. Computational docking simulations further indicated distinct Sec14 residues that were crucial for its inhibition.

The modeling studies projected that the activated aryl halide moiety of 6748-481 oriented itself towards the polar sub-region of the PtdCho binding pocket where it engages barcode residues via a network of hydrogen bonds, halogen bonds and polar interaction. It engaged with one residue, Ser173, via a halogen bond. Ser173 is a key component of the PtdCho headgroup-coordinating substructure of Sec14 and is highly conserved. The rest of the ring system comprising of piperazine and phenyl rings fit snugly into the amphipathic pocket of the PtdCho binding site. Rational mutagenesis experiments based on computational modeling further validated the binding of NPPMs to the PtdCho binding site and surrounding residues that engaged in NPPM binding (Nile et al., 2014).

In addition to the computational modeling that proffered multiple binding modes, rational mutagenesis experiments further validated the binding specificities of NPPMs. An extensive library of compounds around the NPPM scaffold was then generated to study structure-activity relationship (SAR) of NPPMs in the context of Sec14 inhibition. SAR further elaborated on the

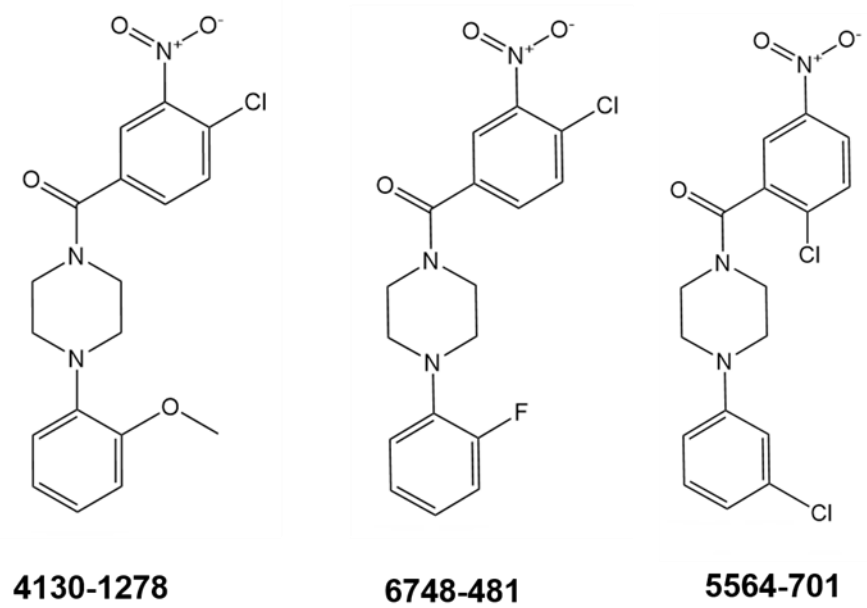


Figure 1-3. Chemical structures of NPPMs 4130-1278, 6748-481 and 5564-701

contributions of each functional group on NPPMs and explained the structural determinants critical for binding and potency.

An obligatory requirement for ortho-Cl in the Cl nitrophenyl (i.e., activated aryl halide) NPPM moiety was reported. Either halogen removal or halogen shift to the para position resulted in decreased drug potency. The critical ortho-Cl on the nitrophenyl ring was replaced with other halogens that suggested a halogen bonding mechanism for NPPM binding. The linker ketone that connected the Cl nitrophenyl and piperazinyl groups was also found to be critical for the activity of the molecule. Its modification reduced NPPM potency in vitro by ~30-fold. The NO₂ was also important to NPPM potency as it oriented the nitrophenyl moiety to the polar sub-region of the binding pocket. Its removal resulted in an approximately 10-fold increase in IC₅₀ value in phospholipid transfer assays (Nile et al., 2014).

Addition of hydrophobic functional groups to the NPPM fluorobenzene tail further enhanced the potency approximately 4-fold. However, extending the linker group that connected the piperazinyl and fluorobenzene groups by a single carbon reduced NPPM potency, highlighting the steric restrictions for binding. Both in vivo and in vitro assays validated the SAR and highlighted the critical functional groups for potency and specificity of NPPMs and future SMI design (Nile et al., 2014).

NPPMs were also found to be exquisitely selective for Sec14 as a target. Even though yeast expresses five other Sec14-like PITP, i.e. the SFH proteins, none of these proteins were found to be sensitive to inhibition by NPPMs. This selectivity is, in most cases, accounted for by the mechanism by which NPPMs are bound by Sec14.

Because four of the other five yeast Sec14-like PITPs (Sfh2–Sfh5) do not conserve the PtdCho-coordinating residues, the NPPM resistance of those proteins is readily explained by their

lack of a structural barcode essential for NPPM binding. The discovery of PITP-directed inhibitors offers exciting tools for clinical dissection of distinct phosphoinositide pools within cells. Moreover, with the identification of multiple anti-Sec14 inhibitors with potent anti-fungal properties, these first generation of Sec14 specific SMIs offer proof-of-concept/ template to design potent inhibitors for pathogenic *Candida* species.

Non-NPPM drugs and their inhibition of Sec14

In another chemogenomic screen, Dr. Dominic Hoepfner's group at Novartis, found that chemicals belonging to the ergoline compound scaffold showed anti-fungal activity with selectivity over mammalian cells. Terming the compound as NGx04, they investigated the protein-ligand interactions and found the inhibited protein to be Sec14. Identification of compound specific mutations supported their conclusions. The research study demonstrated that NGx04 inhibits the growth of *C. neoformans* isolated from clinic and that NGx04 analogues have comparable and even higher potency against *C. neoformans*. Besides, showing inhibitory activity against wild type *C. neoformans* strain, NGx04 analogues showed fungicidal activity against a fluconazole resistant *C. neoformans* strain (Figure 1-4) (Filipuzzi et al., 2016). Computational docking of NGx04 to Sec14 suggested its putative binding site to be the PtdCho binding pocket. Rational mutagenesis based on computational modeling further highlighted residues critical for ligand binding. Furthermore, the residues discovered to be engaging NPPMs were also found to be conserved in engaging NGx04 in *C. neoformans* Sec14. NGx04 also showed selectivity for fungal species over mammalian cells. Structural overlay of the *S. cerevisiae* Sec14p and human orthologue Sec14L2 crystal structure showed that although having a similar overall structure fold, the SMI binding pockets of the two proteins differed considerably. Human Sec14L2 formed a smaller and more

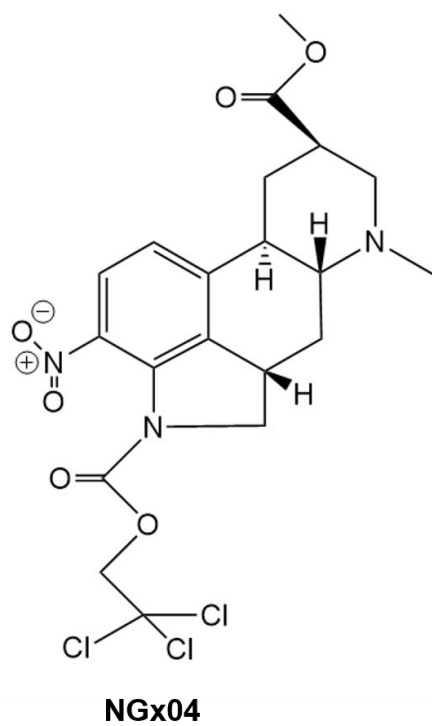


Figure 1-4. Ergoline scaffold compound that shows anti-Sec14 activity.

hydrophobic pocket compared to yeast Sec14, with only one-fourth of all residues conserved among the two binding pockets, thereby explaining the selectivity of ergoline drug.

The *S. cerevisiae* and *C. neoformans* Sec14s show 53% sequence similarity of the residues in the lipid-binding pocket, which is distinct from their overall similarity. Ergoline and its analogues were then tested on two clinical isolates and shown to inhibit *C. neoformans* growth in the tested dose ranges. Ergoline and its analogues also showed fungicidal effect on fluconazole-sensitive as well as fluconazole-resistant *C. neoformans* strains. Given the rising instances of azole resistance, as discussed earlier, ergolines indicate potential as potent fungicidal agents against fluconazole-resistant strains of *C. neoformans*.

Pharmacophore and Future SMI Design Considerations.

The advent of SMIs for Sec14-like P1TP offers new prospects for targeting pathogenic *Candida* species. The NPPM along with new anti-Sec14 inhibitors from the benzamide/picolinamide scaffolds being reported in Chapter III, provide a proof-of-concept for designing potent anti-fungal compounds. Structural superimposition of binding models of NPPM and ergoline on the crystal structure of Sec14::picolinamide complex firmly establish the pharmacophoric points for optimizing the potency of SMIs. In addition to structural models, extensive SAR from number of analogues has provided a wealth of information on microenvironment of SMI binding pocket. Saturation mutagenesis, and functional variomics has further deepen our understanding of sensitivity/resistance mechanism and highlighted critical residues for binding.

Based on structural overlay and SAR, pharmacophore model indicates an obligatory requirement of halogen at para position on H1 phenyl ring. For example, Cl- group in NPPM, and Br- in picolinamide are optimally placed at the para position and interact via halogen bond to back

bone of Tyr151. The hydrophobic planar ring system (H1) is also essential for inhibitor activity as it:

(i) acts as a scaffold to properly position halide functional group, and interacts with Val154 and Val155 via van der Waals interaction, and

(ii) provides a planar ring system which stacks within a hydrophobic sub-pocket composed of residues Tyr151, Val154, Val155 and Arg208. These stacking interactions lend significant stability to scaffold binding. These residues will be further discussed in chapter II.

However, in case of *C. albicans*, *C. auris* and some other pathogenic species where the Val154 and Val155 residues are substituted by larger residues and present steric hindrance; a smaller 5-member ring system may interact optimally. Based on docking solutions, polar substitutions at meta-position of H1 ring that engaged Ser173 seemed to be tolerated and may increase inhibitor potency. The carboxyl oxygen of the carboxamide or the keto group in NPPM was required for the activity of the compounds as it is a hydrogen bond acceptor and engages residue Ser201 in hydrogen bonding interactions. A vicinal nitrogen or polar functionality also favorably contributes to the binding at this position as it engages Ser175 or Glu124.

The methylene group linker that connects the carboxamide/piperazine group and planar ring H1 with the proximal hydrophobic planar ring system (H2) also contributed to the activity of the SMIs. SAR reported that the methylene group is well tolerated and likely orients the planar ring H2 in a conformation favorable for docking to the amphipathic region of the binding cavity. However, extending the linker region, or substitution of methyl or phenyl group on the linker, is incompatible with inhibition of Sec14 activity. Several modifications of the hydrophobic planar ring system H2 were investigated that affected the potencies of active NPPMs. A hydrophobic ring system was optimal in this region; however, part of the binding pocket is lined by G124 and any

substitution or modification of ring system that access the G124 may increase the potency of SMIs. Such functional 'hot spots' are critical for binding activity and re-structuring the scaffold to engage these residues can increase SMIs potency and selectivity.

In sum, discovery of small molecule inhibitors of Sec14 have opened new doors for anti-fungal drug development. The PITPs represent a druggable target in many fungal pathogens. The wealth of structural and functional information about PITPs generated over the last three decades should greatly help exploitation of PITPs as potent pharmacological targets.

References

Baird D, Stefan C, Audhya A, Weys S, Emr SD. Assembly of the PtdIns 4-kinase Stt4 complex at the plasma membrane requires Ypp1 and Efr3. *The Journal of Cell Biology*. 2008;183(6):1061-74.

Balla T. Phosphoinositides: tiny lipids with giant impact on cell regulation. *Physiological Reviews*. 2013;93(3):1019-137.

Bankaitis VA, Mousley CJ, Schaaf G. The Sec14 superfamily and mechanisms for crosstalk between lipid metabolism and lipid signaling. *Trends in Biochemical Sciences*. 2010;35(3):150-60.

Bromley D, Anderson PC, Daggett V. Structural consequences of mutations to the alpha-tocopherol transfer protein associated with the neurodegenerative disease ataxia with vitamin E deficiency. *Biochemistry*. 2013;52(24):4264-73.

Brown GD, Denning DW, Gow NA, Levitz SM, Netea MG, White TC. Hidden killers: human fungal infections. *Sci Transl Med*. 2012;4(165):165rv13.

Chang-Ileto B, Frere SG, Di Paolo G. Acute manipulation of phosphoinositide levels in cells. *Methods Cell Biol*. 2012;108:187-207.

Chayakulkeeree M, Johnston SA, Oei JB, Lev S, Williamson PR, Wilson CF, et al. SEC14 is a specific requirement for secretion of phospholipase B1 and pathogenicity of *Cryptococcus neoformans*. *Mol Microbiol*. 2011;80(4):1088-101.

D'Angelo G, Vicinanza M, Di Campli A, De Matteis MA. The multiple roles of PtdIns(4)P -- not just the precursor of PtdIns(4,5)P₂. *J Cell Sci*. 2008;121(Pt 12):1955-63.

Di Paolo G, De Camilli P. Phosphoinositides in cell regulation and membrane dynamics. *Nature*. 2006;443(7112):651-7.

Estrada-Mata E, Navarro-Arias MJ, Perez-Garcia LA, Mellado-Mojica E, Lopez MG, Csonka K, et al. Members of the *Candida parapsilosis* Complex and *Candida albicans* are Differentially Recognized by Human Peripheral Blood Mononuclear Cells. *Front Microbiol*. 2015;6:1527.

Filipuzzi I, Cotesta S, Perruccio F, Knapp B, Fu Y, Studer C, et al. High-Resolution Genetics Identifies the Lipid Transfer Protein Sec14p as Target for Antifungal Ergolines. *PLoS Genet*. 2016;12(11):e1006374.

Fisher MC, Hawkins NJ, Sanglard D, Gurr SJ. Worldwide emergence of resistance to antifungal drugs challenges human health and food security. *Science*. 2018;360(6390):739-42.

Gambhir A, Hangyas-Mihalyne G, Zaitseva I, Cafiso DS, Wang J, Murray D, et al. Electrostatic sequestration of PIP2 on phospholipid membranes by basic/aromatic regions of proteins. *Biophysical Journal*. 2004;86(4):2188-207.

Grabon A, Khan D, Bankaitis VA. Phosphatidylinositol transfer proteins and instructive regulation of lipid kinase biology. *Biochimica et Biophysica Acta*. 2015;1851(6):724-35.

Grabon A, Orlowski A, Tripathi A, Vuorio J, Javanainen M, Rog T, et al. Dynamics and energetics of the mammalian phosphatidylinositol transfer protein phospholipid exchange cycle. *The Journal of Biological Chemistry*. 2017;292(35):14438-55.

Gray KC, Palacios DS, Dailey I, Endo MM, Uno BE, Wilcock BC, et al. Amphotericin primarily kills yeast by simply binding ergosterol. *Proceedings of the National Academy of Sciences of the United States of America*. 2012;109(7):2234-9.

Hager CL, Larkin EL, Long L, Zohra Abidi F, Shaw KJ, Ghannoum MA. *In vitro* and *In vivo* Evaluation of the Antifungal Activity of APX001A/APX001 against *Candida auris*. *Antimicrob Agents Chemother*. 2018;62(3).

Hager CL, Larkin EL, Long LA, Ghannoum MA, Evaluation of the efficacy of rezafungin, a novel echinocandin, in the treatment of disseminated *Candida auris* infection using an immunocompromised mouse model. *Antimicrob Agents Chemother*. 2018(33-45)

Huang J, Ghosh R, Tripathi A, Lonnfors M, Somerharju P, Bankaitis VA. Two-ligand priming mechanism for potentiated phosphoinositide synthesis is an evolutionarily conserved feature of Sec14-like phosphatidylinositol and phosphatidylcholine exchange proteins. *Molecular Biology of the Cell*. 2016;27(14):2317-30.

Huang J, Mousley CJ, Dacquay L, Maitra N, Drin G, He C, et al. A Lipid Transfer Protein Signaling Axis Exerts Dual Control of Cell-Cycle and Membrane Trafficking Systems. *Developmental Cell*. 2018;44(3):378-91 e5.

Ile KE, Schaaf G, Bankaitis VA. Phosphatidylinositol transfer proteins and cellular nanoreactors for lipid signaling. *Nature Chemical Biology*. 2006;2(11):576-83.

Kearns BG, McGee TP, Mayinger P, Gedvilaite A, Phillips SE, Kagiwada S, et al. Essential role for diacylglycerol in protein transport from the yeast Golgi complex. *Nature*. 1997;387(6628):101-5.

Kim YJ, Hernandez ML, Balla T. Inositol lipid regulation of lipid transfer in specialized membrane domains. *Trends in Cell Biology*. 2013;23(6):270-8.

Klein BS, Tebbets B. Dimorphism and virulence in fungi. *Curr Opin Microbiol*. 2007;10(4):314-9.

Kullberg BJ, Arendrup MC. Invasive Candidiasis. *N Engl J Med*. 2015;373(15):1445-56.

Kurtzman CP, Robnett CJ. Identification and phylogeny of ascomycetous yeasts from analysis of nuclear large subunit (26S) ribosomal DNA partial sequences. *Antonie Van Leeuwenhoek*. 1998;73(4):331-71.

Lamoth F, Lockhart SR, Berkow EL, Calandra T. Changes in the epidemiological landscape of invasive candidiasis. *J Antimicrob Chemother*. 2018;73:i4-i13.

Lewis LE, Bain JM, Lowes C, Gillespie C, Rudkin FM, Gow NA, et al. Stage specific assessment of *Candida albicans* phagocytosis by macrophages identifies cell wall composition and morphogenesis as key determinants. *PLoS Pathog*. 2012;8(3):e1002578.

Li X, Xie Z, Bankaitis VA. Phosphatidylinositol/phosphatidylcholine transfer proteins in yeast. *Biochimica et Biophysica Acta*. 2000;1486(1):55-71.

Liu Y, Bankaitis VA. Phosphoinositide phosphatases in cell biology and disease. *Progress in Lipid Research*. 2010;49(3):201-17.

Lopez MC, Nicaud JM, Skinner HB, Vergnolle C, Kader JC, Bankaitis VA, et al. A phosphatidylinositol/phosphatidylcholine transfer protein is required for differentiation of the dimorphic yeast *Yarrowia lipolytica* from the yeast to the mycelial form. *The Journal of Cell Biology*. 1994;125(1):113-27.

McLaughlin S, Murray D. Plasma membrane phosphoinositide organization by protein electrostatics. *Nature*. 2005;438(7068):605-11.

Min KC, Kovall RA, Hendrickson WA. Crystal structure of human alpha-tocopherol transfer protein bound to its ligand: implications for ataxia with vitamin E deficiency. *Proceedings of the National Academy of Sciences of the United States of America*. 2003;100(25):14713-8.

Monk BC, Goffeau A. Outwitting multidrug resistance to antifungals. *Science*. 2008;321(5887):367-9.

Monteoliva L, Sanchez M, Pla J, Gil C, Nombela C. Cloning of *Candida albicans* SEC14 gene homologue coding for a putative essential function. *Yeast*. 1996;12(11):1097-105.

Nakano M, Fukuda M, Kudo T, Endo H, Handa T. Determination of interbilayer and transbilayer lipid transfers by time-resolved small-angle neutron scattering. *Phys Rev Lett*. 2007;98(23):238101.

Narayan K, Lemmon MA. Determining selectivity of phosphoinositide-binding domains. *Methods*. 2006;39(2):122-33.

Nile AH, Bankaitis VA, Grabon A. Mammalian diseases of phosphatidylinositol transfer proteins and their homologs. *Clinical Lipidology*. 2010;5(6):867-97.

Nile AH, Tripathi A, Yuan P, Mousley CJ, Suresh S, Wallace IM, et al. PITPs as targets for selectively interfering with phosphoinositide signaling in cells. *Nature Chemical Biology*. 2014;10(1):76-84.

Oliveira DL, Freire-de-Lima CG, Nosanchuk JD, Casadevall A, Rodrigues ML, Nimrichter L. Extracellular vesicles from *Cryptococcus neoformans* modulate macrophage functions. *Infection and Immunity*. 2010;78(4):1601-9.

Ostrosky-Zeichner L, Casadevall A, Galgiani JN, Odds FC, Rex JH. An insight into the antifungal pipeline: selected new molecules and beyond. *Nat Rev Drug Discov*. 2010;9(9):719-27.

Pfaller MA, Jones RN, Castanheira M. Regional data analysis of *Candida* non-albicans strains collected in United States medical sites over a 6-year period, 2006-2011. *Mycoses*. 2014;57(10):602-11.

Ren J, Pei-Chen Lin C, Pathak MC, Temple BR, Nile AH, Mousley CJ, et al. A phosphatidylinositol transfer protein integrates phosphoinositide signaling with lipid droplet metabolism to regulate a developmental program of nutrient stress-induced membrane biogenesis. *Molecular Biology of the Cell*. 2014;25(5):712-27.

Ryan MM, Temple BR, Phillips SE, Bankaitis VA. Conformational dynamics of the major yeast phosphatidylinositol transfer protein sec14p: insight into the mechanisms of phospholipid exchange and diseases of sec14p-like protein deficiencies. *Molecular Biology of the Cell*. 2007;18(5):1928-42.

Schaaf G, Dynowski M, Mousley CJ, Shah SD, Yuan P, Winklbauer EM, et al. Resurrection of a functional phosphatidylinositol transfer protein from a pseudo-Sec14 scaffold by directed evolution. *Molecular Biology of the Cell*. 2011;22(6):892-905.

Schmiedel Y, Zimmerli S. Common invasive fungal diseases: an overview of invasive candidiasis, aspergillosis, cryptococcosis, and *Pneumocystis pneumonia*. *Swiss Med Wkly*. 2016;146:w14281.

Selmecki A, Forche A, Berman J. Aneuploidy and isochromosome formation in drug-resistant *Candida albicans*. *Science*. 2006;313(5785):367-70.

Sha B, Phillips SE, Bankaitis VA, Luo M. Crystal structure of the *Saccharomyces cerevisiae* phosphatidylinositol-transfer protein. *Nature*. 1998;391(6666):506-10.

Shao X, Li C, Fernandez I, Zhang X, Sudhof TC, Rizo J. Synaptotagmin-syntaxin interaction: the C2 domain as a Ca²⁺-dependent electrostatic switch. *Neuron*. 1997;18(1):133-42.

Smirnova TI, Chadwick TG, Voinov MA, Poluektov O, van Tol J, Ozarowski A, et al. Local polarity and hydrogen bonding inside the Sec14p phospholipid-binding cavity: high-field multi-frequency electron paramagnetic resonance studies. *Biophysical Journal*. 2007;92(10):3686-95.

Sugiura T, Ikeda K, Nakano M. Kinetic Analysis of the Methyl-beta-cyclodextrin-Mediated Intervesicular Transfer of Pyrene-Labeled Phospholipids. *Langmuir*. 2016;32(51):13697-705.

Wu WI, Routt S, Bankaitis VA, Voelker DR. A new gene involved in the transport-dependent metabolism of phosphatidylserine, PSTB2/PDR17, shares sequence similarity with the gene encoding the phosphatidylinositol/phosphatidylcholine transfer protein, SEC14. *The Journal of Biological Chemistry*. 2000;275(19):14446-56.

Xie Z, Hur SK, Zhao L, Abrams CS, Bankaitis VA. A Golgi Lipid Signaling Pathway Controls Apical Golgi Distribution and Cell Polarity during Neurogenesis. *Developmental Cell*. 2018;44(6):725-40 e4.

Zeng Q, Morales AJ, Cottarel G. Fungi and humans: closer than you think. *Trends Genet*. 2001;17(12):682-4.

CHAPTER II
STRUCTURAL ELEMENTS THAT GOVERN SEC14-LIKE
PHOSPHATIDYLINOSITOL TRANSFER PROTEIN SENSITIVITIES TO POTENT
SMALL MOLECULE INHIBITORS¹

Disclaimer for Chapter II

Chapter II is reprint of a publication, which I am the first author on. I performed all of the work presented in this chapter, except for molecular modeling studies, presented in Figure 2-1, Figure 2-3A and Figure 2-7 that were done by Dr. Ashutosh Tripathi. Summary section of this chapter is the abstract of the publication, rest are as in publication with minor editing.

¹Reprinted from “Structural Elements That Govern Sec14-like Phosphatidylinositol Transfer Protein Sensitivities to Potent Small Molecule Inhibitors” by Khan et al., 2016. Journal of Lipid Research, Vol. 57, 4, 650–662, Copyright © American Society For Biochemistry And Molecular Biology, Inc. (ASBMB) 2016. Published by ASBMB on behalf of Journal of Lipid Research.

Summary

Sec14-like phosphatidylinositol transfer proteins (PITPs) play important biological functions in integrating multiple aspects of intracellular lipid metabolism with phosphatidylinositol-4-phosphate signaling. As such, these proteins offer new opportunities for highly selective chemical interference with specific phosphoinositide pathways in cells. The first and best characterized small molecule inhibitors (SMIs) of the yeast PITP Sec14 are nitrophenyl(4-(2-methoxyphenyl)piperazin-1-yl) methanones (NPPMs), and a hallmark feature of NPPMs is their exquisite targeting specificities for Sec14 relative to other closely-related related Sec14-like PITPs. Present understanding of Sec14::NPPM binding interactions is based on computational docking and rational loss-of-function approaches. While these approaches have been informative, we still lack an adequate understanding of the basis for the high selectivity of NPPMs amongst closely related Sec14-like PITPs. Herein, we describe a Sec14 motif we term the VV-signature that contributes significantly to the NPPM sensitivity/resistance of Sec14-like PtdIns/PtdCho-transfer proteins. The data not only reveal previously unappreciated determinants that govern Sec14-like PITP sensitivities to NPPMs, but enable predictions of which Sec14-like PtdIns-/PtdCho-transfer proteins are likely to be NPPM-resistant or sensitive based on primary sequence considerations. Finally, these data provide independent evidence in support of previous studies highlighting the importance of Sec14 residue Ser173 in the mechanism by which NPPMs engage and inhibit Sec14-like PITPs.

Introduction

Phosphoinositides (PIPs) are phosphorylated derivatives of phosphatidylinositol (PtdIns), and the metabolism of these lipids constitutes a major membrane-associated signaling system in eukaryote cells (Zhang et al, 1997; Fruman et al., 1998; Ile et al., 2006; McLaughlin et al., 2005; Strahl et al., 2007). The chemical heterogeneity that distinguishes individual PIP species forms one basis for functionally compartmentalizing signaling platform identities on membrane surfaces (Balla et al., 2005; Lemmon et al., 2008). Yet while the chemical heterogeneity of PIP species is simple, it translates to an enormous diversity of biological outcomes that derive from PIP signaling. In that regard, recent studies demonstrate additional layers of functional specification for PIP signaling that are of such resolution that production of an individual PIP species by a specific PtdIns kinase yields multiple biological outcomes in the same cell (Bankaitis et al., 2010) We now appreciate that PtdIns-transfer proteins (PITPs) play critical roles in functional compartmentalization of PIP signaling reactions by channeling PtdIns to PtdIns-kinases and, subsequently, to distinct sets of effector proteins (Schaaf et al., 2008; Nile et al., 2010; Grabon et al., 2015). The Sec14-like PITPs are best studied in this regard, and the multiplicity of Sec14-like PITPs expressed in even simple unicellular eukaryotes highlights the high degree of functional specification for these proteins (Routt et al., 2005; Li et al., 2000).

Emerging evidence that PITPs instruct the biological outcomes of PtdIns kinase activities recommends these proteins as novel targets for chemical intervention with phosphoinositide signaling pathways in cells (Grabon et al., 2015; Nile et al., 2014). The advantages of targeting PITPs for this purpose are that such interventions can be imposed with selectivities superior to those possible by popular strategies that either target individual PtdIns-kinase isoforms or individual PIP species (Chang-Ileto et al., 2012; Keaney et al., 2014). Proof of concept is

exemplified by the identification and validation of several classes of small molecule inhibitors that target Sec14, the major PITP of yeast. Sec14 binds both PtdIns and phosphatidylcholine (PtdCho) *in vitro*, and it coordinates PtdIns-4-phosphate production with PtdCho metabolism so as to promote membrane trafficking through trans-Golgi network/and endosomal compartments *in vivo* (Cleves et al., 1991; Bankaitis et al. 1990; Hoon et al. 2008; Lee et al., 2014). Of the small molecule inhibitors that target Sec14 activity, the nitrophenyl(4-(2-methoxyphenyl) piperazin-1-yl) methanones (NPPMs), are best understood (Nile, et al., 2014; Hoon, et al., 2008; Lee, et al., 2014). These inhibitors inhibit Sec14 by loading into the phospholipid binding pocket of this PITP and preventing subsequent rounds of lipid-exchange (Nile et al., 2014).

An attractive property of NPPMs is their exquisite selectivity for Sec14 as target. Even though yeast express five other Sec14-like PITPs (Li et al., 2000), none of these proteins are at all sensitive to inhibition by NPPMs. Available data project that NPPM invades the hydrophobic lipid-binding pocket of Sec14 during a lipid-exchange cycle where the inhibitor engages both residues within PtdIns- and PtdCho-acyl chain space and residues essential for coordination of the PtdCho headgroup. Computational docking simulations, coupled with rational mutagenesis experiments, indicate the latter binding interactions are crucial. The NPPM activated aryl halide moiety is projected to engage residue Ser173, a key component of the PtdCho headgroup-coordinating substructure, via a halogen bond (Nile et al., 2014). Because 4 of the other 5 yeast Sec14-like PITPs (Sfh2-Sfh5) do not conserve this PtdCho-coordinating unit (Schaaf et al., 2008), the NPPM-resistance of those proteins is readily explained by their lacking the structural elements essential for NPPM binding.

The Sec14 specificity of NPPM remains completely obscure in other cases. For example, the Sec14-like PITP Sfh1 is highly homologous to Sec14. Sfh1 has both PtdIns- and PtdCho-

binding/transfer activities as it shares with Sec14 the same PtdIns-binding motif and, more strikingly, the same PtdCho-coordinating substructure that is critical for NPPM binding (Schaaf et al., 2008; Li et al., 2000; Schaaf et al., 2011). Yet, Sfh1 lipid exchange activities are impervious to NPPM challenge (Nile et al., 2014). Moreover, Sec14-like PtdIns-/PtdCho-transfer proteins from other fungal pathogens are even more similar to Sec14 than is Sfh1 but are similarly resistant to inhibition by NPPMs (see Results). These exceptional cases indicate that, despite a detailed and experimentally well-supported description for how NPPMs dock into the Sec14 lipid-binding pocket (Nile et al., 2014), there remain substantial gaps in our knowledge regarding the mechanism of Sec14 inhibition by NPPMs. Herein, we exploit unbiased approaches to identify a new Sec14 motif, the VV-signature, that contributes to NPPM sensitivity. The data empower prediction of which Sec14-like PtdIns-/PtdCho-transfer proteins are likely to be NPPM-resistant or sensitive by extending our understanding of the underlying mechanisms that govern the sensitivities of Sec14-like PITPs to NPPMs.

Results

Comparisons of NPPM 6748-481 docking poses in Sec14 vs Sfh1

We sought to capitalize on high resolution Sfh1 crystal structures, and a detailed computational model for how Sec14 binds NPPM 6748-481, to produce an NPPM-sensitive Sfh1 for the purpose of direct structural analysis of an Sfh1::NPPM complex. This approach was recommended by the fact that the modeled NPPM-binding pose in the Sec14 hydrophobic pocket is experimentally supported by rational mutagenesis and chemical structure-activity relationship data (Nile, et al., 2014), that the Sfh1 and Sec14 binding pockets share 79% primary sequence identity and 89% similarity in the residues that form the boundaries of their respective phospholipid binding cavities,

and that those two PITPs share essentially identical phospholipid binding properties (Schaaf et al., 2008). The high degree of structural conservation between these two cavities is further emphasized by the 1.06 Å RMSD calculated after superposition of the two cavity structures. In those comparative analyses, the binding pockets were defined by the binocular criteria of Sfh1 vs Sec14 structural alignments and residues of interest falling within 4.5 Å of bound 6748-481 (as represented by the experimentally favored Sec14::NPPM 6748-481 pose previously described) (Nile et al., 2014).

To query why Sfh1 is naturally resistant to inhibition by NPPMs, 6748-481 was docked into the phospholipid-binding cavity of Sfh1 (see Materials and Methods), and those results were compared to the model pose for 6748-481 bound in the Sec14 hydrophobic pocket. First, the Sfh1 crystal structure was superposed on Sec14 coordinates and the respective phospholipid-binding cavities were related by defining a reference centroid within the superposed cavity environments. As had previously been done with Sec14 (Nile et al., 2014), the Sfh1 pocket environment was defined as the sampling space in 6748-481 docking simulations. The reference centroid ensured that the Sec14 and Sfh1 interaction grids shared relatable spatial coordinates, thereby allowing direct comparisons of Sfh1 and Sec14 6748-481 docking results. Comparison of the highest-scoring 6748-481 dock pose indicated the Sfh1 solution shared the same coordinate space within the hydrophobic pocket, and a similar conformation, as that calculated for Sec14. That is, the chloro-nitrophenyl group of 6748-481 was oriented towards the polar sub-region of pocket (Figure 2-1A). However, unlike the case of the Sec14::6748-481 complex, where the chloro-nitrophenyl headgroup coordinates with the S₁₇₃ –OH group, the Sfh1::6748-481 complex has the NPPM headgroup rotated 180° around the single phenyl-acyl rotatable bond that links the chloro-nitrophenyl headgroup moiety with ketone functional group of the NPPM. This same rotamer was

also represented in potential docking solutions for NPPM 6748-481 with Sec14, and it was initially considered a plausible binding mode pending experimental test (Nile et al., 2014). Short MDS runs (10ns) showed the rotamer readily flips its headgroup orientation to adopt the 6748-481 pose in the Sec14 cavity supported by experiment. Nonetheless, the Sec14 and Sfh1 6748-481 docking poses remain significantly different (RMSD > 3Å Figure 2-1B). Of particular note, the distal fluoro-benzyl moiety of 6748-481 is wedged in a deep hydrophobic cleft of the Sec14 lipid-binding cavity where it engages in stacking interactions with residues F₂₂₈ and F₂₁₂. In the Sfh1 case, these hydrophobic interactions are not evident (Figure 2-1B), and this disparity reflects the fact that the Sec14 and Sfh1 pocket residues diverge most significantly along this sub-region of their respective lipid-binding cavities.

Rational structure-based engineering of the Sfh1 pocket is insufficient to produce an NPPM-sensitive Sfh1

We sought to use the structural and 6748-481 docking information to design an Sfh1 with a Sec14-like pocket with the expectation that such an Sfh1 variant would now acquire NPPM sensitivity. To that end, structural and primary sequence alignments of Sfh1 and Sec14 identified six divergent residues in the cohort of amino acids that line the binding pocket and lie within 4.5Å of the “bound” 6748-481. Except for F₁₅₆ (as numbered in Sfh1) most of the non-conserved residues are positioned towards the hydrophobic sub-region of the proposed NPPM binding site (Figure 2-2A). Those six residues were converted en bloc to the cognate residues in Sec14 (F₁₅₃V, L₁₇₆M, I₁₉₃V, V₁₉₆A, A₁₉₇S, V₂₂₇F) to generate what we term the Sfh1^{6X} mutant. Computational docking experiments were then run using the same parameters and settings as those employed in the Sfh1/Sec14 comparative docking experiments. Gratifyingly, the highest ranked docking solution was much more similar to the favored Sec14::6748-481 pose (RMSD = 1.0Å), and the distal fluoro-benzyl

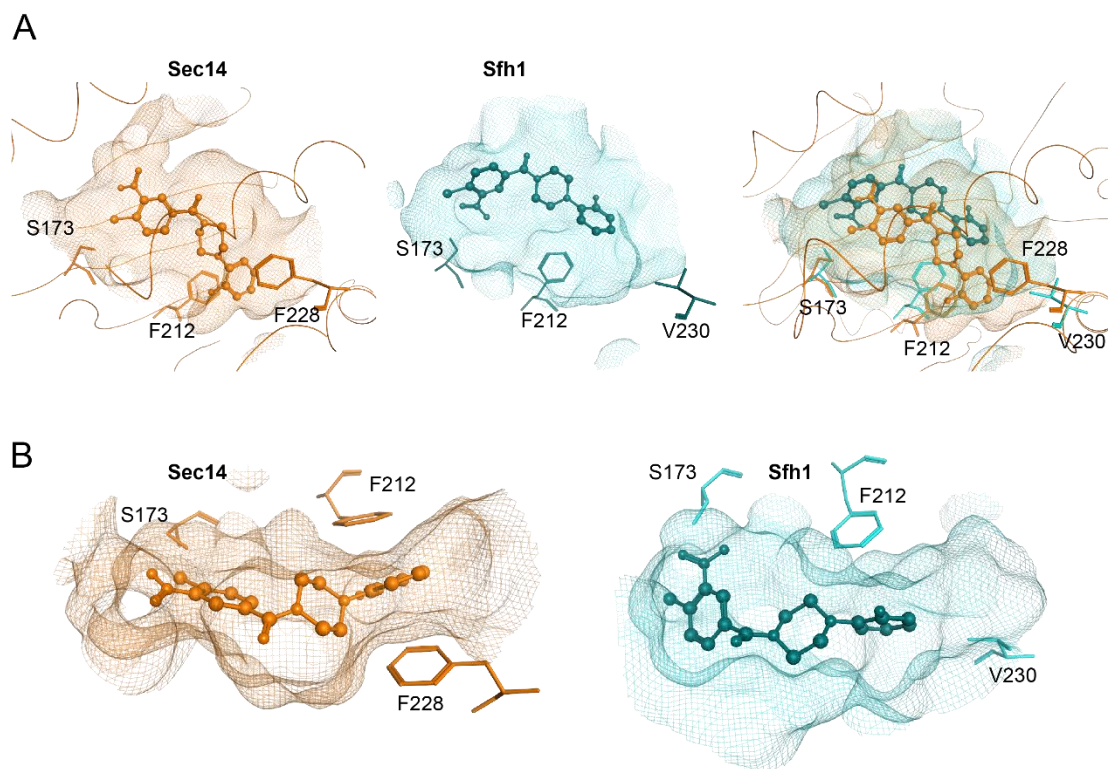


Figure 2-1. Comparisons of NPPM 6748-481 docking poses in the hydrophobic pockets of Sec14 and Sfh1.

(A) Modeled NPPM 6748-481 poses within the hydrophobic pockets of Sec14 (left panel, orange) and Sfh1 (middle panel, teal) are shown. Residues of interest are labeled. The right panel shows a superposition of the binding modes in the two distinct pocket environments and highlights the differences between the two binding modes. Sec14 residue F₂₂₈ is projected to stabilize NPPM binding via stacking interactions, and these interactions are not available in the Sfh1 context.

(B) Top views of NPPM-481 docked to Sec14 (left panel) and Sfh1 (right panel) are shown. The protein pocket is rendered in surface mesh with residues of interest highlighted in ball and stick representation.

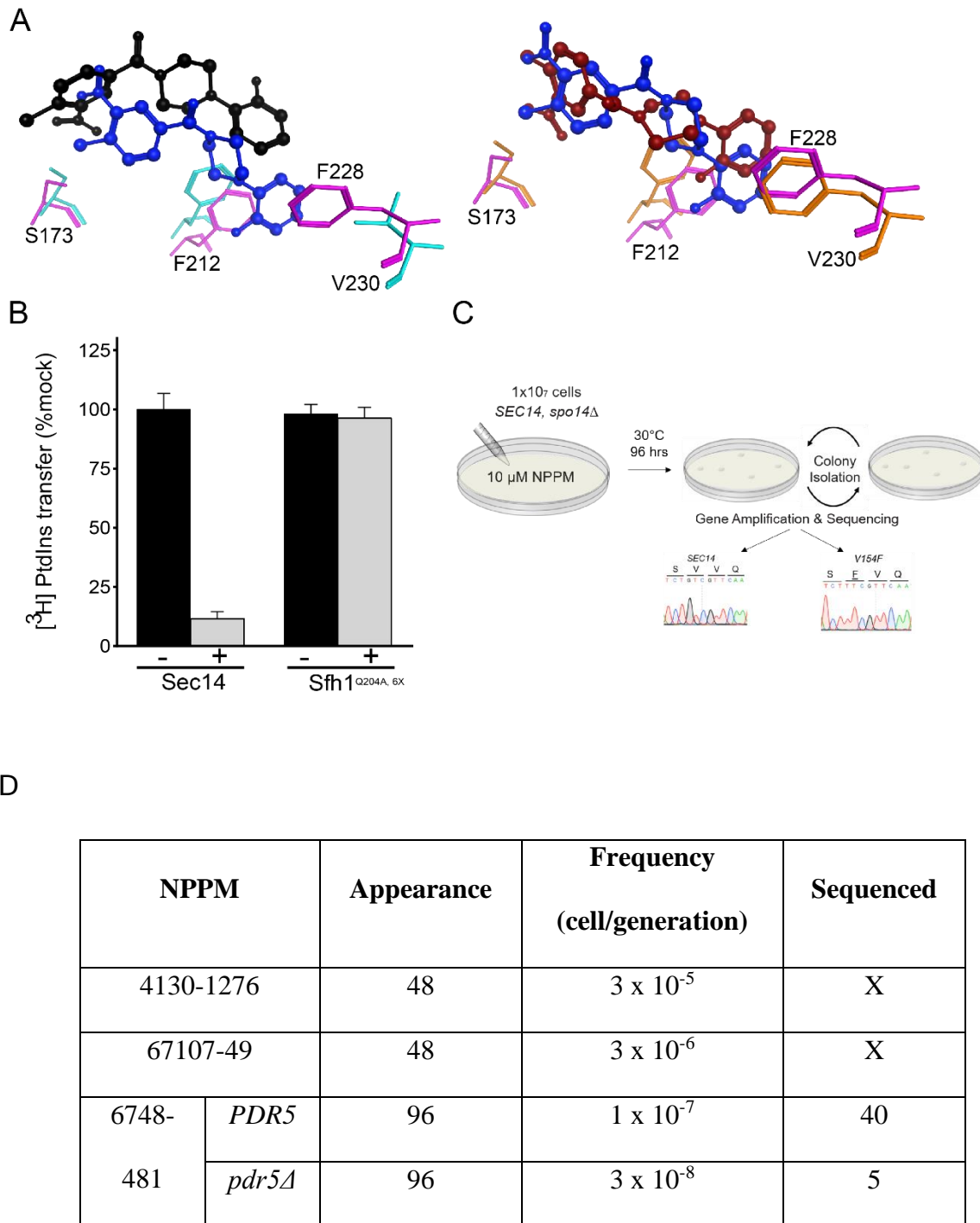


Figure 2-2. A rational approach for engineering Sfh1 sensitivity to NPPM 6748-481.

(A) Superposition of the 6748-481 poses in Sec14 (blue) and Sfh1 (black) binding pockets is shown in ball and stick representation (left panel). This is to be compared with the improved superposition of 6748-481 poses in Sec14 (blue, ball and stick) versus Sfh1^{6X} (red, ball and stick) binding pockets (right panel). Key residues in the Sfh1 and Sfh1^{6X} binding pockets are represented in orange and magenta, respectively.

(B) Biochemical characterization of purified recombinant proteins is shown. Sec14/Sfh1^{Q204A,6X} activity was measured in *in vitro* [³H]PtdIns transfer assays, in the absence (black bars) and presence (gray bars) of 6748-481. The proteins were preincubated with DMSO or 20 μ M 6748-481 in the presence of PtdCho liposomes, as appropriate, prior to assay (see Materials and Methods). The values reported for assays with inhibitor are related to mock DMSO vehicle controls. Average values and standard deviations are given (n = 3). The intrinsic PtdIns-transfer activities measured for Sec14 and Sfh1^{Q204,6X} were 18-26% and 22-25% respectively. Total input was 8915-10863 c.p.m. of [³H]PtdIns and the background was 645-955 c.p.m.

(C) A schematic representation of the unbiased genetic screen for NPPM-resistant Sec14 proteins is illustrated. Approximately 10⁷ cells were seeded onto each individual YPD agar plate supplemented with the appropriate NPPM (10 μ M final concentration). After the indicated period of incubation, NPPM^R colonies were purified by two rounds of streaking for isolated colonies on NPPM-containing agar plates. The corresponding *SEC14* genes were amplified by PCR from genomic DNA prepared isolated NPPM^R clones using the appropriate oligonucleotide primers (see Materials and Methods). Nucleotide sequences for each *SEC14* amplicon were determined and analyzed for missense substitutions.

(D) Documents that the frequency of colony generation was inversely proportional to the inhibitor potency. Decreased potency of the challenge NPPM came with more rapidly arising NPPM^R colonies. To reduce screen background (i.e. occurrence of NPPM^R mutations that did not map to *SEC14*), a *pdr5* Δ strain that shows increased NPPM-sensitivity was used in a parallel genetic screen.

group now intercalated into the hydrophobic cleft where it engaged in stacking interaction with the newly converted F₂₃₀ (Figure 2-2A). While, the chloro-nitrophenyl headgroup of 6748-481 still adopted the 180° rotamer conformation relative to the Sec14::6748-481 pose, we considered this a conformer that could rotate the activated aryl-halide functional group to a pose nearly identical to that which we predict describes bound 6748-481 in the Sec14 lipid-binding cavity (Nile et al., 2014). To test whether the re-engineered protein was sensitive to inhibition by NPPM, a Q_{204A} missense substitution was incorporated into the Sfh1^{6X} protein. This was done because Q_{204A} endows Sfh1 the desirable properties of stimulated lipid exchange activity *in vitro* and enhanced Sec14-like properties *in vivo* (Nile et al., 2014; Schaaf et al., 2011).

Those features made it an ideal experimental scaffold for manipulating, and subsequently monitoring, the NPPM-resistance/sensitivity properties of Sfh1 and its variants. Surprisingly, while purified recombinant Sfh1^{Q204A,6X} exhibited robust [³H]-PtdIns transfer activity *in vitro*, this activity remained indifferent to a high concentration of 6748-481 (20μM, ~ 100X Sec14 IC₅₀; Figure 2-2B).

Genetic screen for Sec14 variants resistant to NPPM.

The inadequacy of the working Sec14::NPPM 6748-481 docking solution in guiding successful engineering of an NPPM-sensitive version of Sfh1 indicated that our understanding of the inhibitor binding mechanism was incomplete. We therefore sought to gain additional insight regarding mechanisms of NPPM-binding by Sec14 (and NPPM-resistance for Sfh1) via an approach that did not rely on the necessarily targeted logic inherent to structure-based regimes. To that end, an unbiased genetic screen was performed that selected for mutant Sec14s ablated for NPPM sensitivity while at the same time demanding maintenance of biologically sufficient levels of protein activity. One important consideration in designing the screen was limiting re-isolation of

previously characterized ‘bypass Sec14’ mutations that represent loss-of-function mutations in structural genes of the CDP-choline pathway for PtdCho biosynthesis (Cleves et al., 1991), the *SAC1* gene which encodes the major yeast PtdIns-4-P phosphatase (Cleves, et al., 1989, Guo et al., 1999, Rivas et al., 1999), and the sterol- and PtdIns-4-P-binding protein Kes1/Osh4 (Li, et al., 2002, Fang et al., 1996, Im et al., 2005, de Saint-Jean et al., 2011) . These bypass Sec14 mutations occur spontaneously at high frequencies [$\sim 5 \times 10^{-5}$ per cell per generation; (Cleves et al., 1991, Cleves et al., 1989)], would pass selection by conferring viability to yeast cells deficient in normally essential Sec14 activities (Nile et al., 2014, Lee et al., 2014) and would overwhelm the results of the screen. We therefore took advantage of the fact that all known bypass Sec14 mechanisms require activity of the normally non-essential phospholipase D enzyme encoded by the *SPO14* gene to alleviate the cellular Sec14 requirement, and *spo14Δ* yeast fail to yield spontaneously occurring bypass Sec14 mutants at all [$< 10^{-10}$ /cell/generation; (Xie et al., 1998)]. Thus, the NPPM^R screen was conducted using an otherwise wild-type *spo14Δ* yeast mutant as parental strain to preclude any background of known bypass Sec14 mutants.

Parental cells were seeded onto YPD agar plates individually supplemented with NPPMs 6748-481, 4130-1276, or 67170-49 to final concentrations of 10 μ M (Figure 2-2C). While these NPPMs vary in their potencies as Sec14 inhibitors (6748-481 > 67170-49 > 4130-1276), all three NPPMs strongly inhibited yeast cell proliferation when incorporated in growth medium at this concentration. After incubation at 30°C for 96 h, the frequencies of emerging NPPM^R colonies were scored. As expected, those frequencies were inversely proportional to NPPM potency as Sec14 inhibitor. Colonies resistant to 4130-1276 or 67179-49 intoxication arose at frequencies of $\sim 3 \times 10^{-5}$ and 10^{-6} per cell per generation, respectively, and those resistant clones started appearing within 48h of incubation. By contrast, colonies resistant to the most potent inhibitor 6748-481

appeared only after approximately 96 h of incubation, and those colonies emerged at much lower frequencies ($\sim 10^{-7}$ per cell per generation) (Figure 2-2D). A parallel 6748-481 resistance selection was also performed in an isogenic *pdr5Δ* genetic background where the structural gene for the major yeast drug pump was deleted (Katzmann et al., 1994). In that version of the screen, the 6748-481 concentration for selection was lowered to $2\mu\text{M}$ as the *pdr5Δ* parental strain is approximately five times more sensitive to the inhibitor (unpublished observations). The frequencies of 6748-481^R colonies obtained in this sensitized selection regime were reduced even further ($\sim 3 \times 10^{-8}$ per cell per generation). As existing Sec14::NPPM docking poses were built using 6748-481 as ligand (Nile et al., 2014), subsequent analyses were restricted to yeast isolates resistant to NPPM 6748-481. A total of 45 independently isolated 6748-481-resistant clones were recovered from the two parallel screens, these clones were purified by at least two rounds of single colony isolation, and were analyzed in further detail.

Sec14 missense substitutions that confer NPPM resistance.

The *SEC14* gene was amplified from each of the isolates by PCR using genomic DNA as template. Of the genes so analyzed, 35 exhibited wild-type *SEC14* sequence while the remaining 10 carried single missense mutations in *SEC14*. Those 10 mutant *SEC14* genes represented a total of 7 unique *SEC14* missense mutations that resulted in the following single amino acid changes to the Sec14 protein sequence: P₁₂₀Q, V₁₅₄F, V₁₅₅F, S₁₇₃P, R₂₀₈L, G₂₁₀V, and F₂₁₂L. Superposition of the NPPM^R missense substitutions onto high resolution Sec14 structural models demonstrated that, consistent with our previous in silico docking solution (Nile et al., 2014), all substitutions involved residues positioned in the immediate vicinity of the Sec14 lipid binding pocket (Figure 2-3A). Indeed, we had previously identified S₁₇₃ and F₂₁₂ in Sec14::NPPM interaction fingerprint analyses where those two residues engaged the activated aryl halide and fluoro-benzyl moieties of NPPM

6748-481 via polar and hydrophobic/ π - π stacking interactions, respectively (Nile et al., 2014). Recovery of Sec14^{S173P} was particularly satisfying as this variant was altered for the very residue identified by our previous docking simulations and rational mutagenesis studies as essential for the halogen-bonding mechanism that we propose governs Sec14::NPPM binding interactions (Nile et al., 2014). By contrast, the remaining five residues exhibited either weak scores in these analyses (V₁₅₄ and R₂₀₈), or were excluded from the interaction fingerprint list entirely (P₁₂₀, V₁₅₅ and G₂₁₀).

To verify that these 7 missense substitutions were sufficient to confer NPPM 6748-481 resistance to Sec14, each corresponding mutation was individually incorporated into the genome of the naïve parental strain and resistance to NPPM 6748-481 was subsequently queried as an unselected phenotype. Survey of NPPM^R as an unselected phenotype circumvented the possibility of mistaking that phenotype for a bypass Sec14 phenotype. In every case, the mutation of interest was sufficient to render the recipient yeast strain resistant to the NPPM 6748-481 concentration used as selection filter in the NPPM^R screen irrespective of whether the naïve recipient was of a *SPO14*⁺ (Figure 2-3B) or a *spo14Δ* genetic background. However, in both genetic backgrounds we noted that the NPPM^R phenotype of Sec14^{F212L} allele was very weak. Each *SEC14^R* allele held the added feature of conferring an unselected NPPM 4130-1276 and 67170-49 resistance to naïve yeast cells and when interrogated in the context of these NPPMs, the resistance phenotype associated with the *SEC14^{F212L}* allele was clear (Figure 3C). We inferred from these collective data that the mutant Sec14^R were rendered insensitive to challenge with any of these three NPPMs.

SEC14^R gene products exhibit NPPM^R lipid exchange activities.

As Sec14 is required for yeast cell viability (Cleves et al., 1991; Bankaitis et al., 1989; Cleves et al., 1989) the NPPM^R screen demanded that any Sec14^R proteins passing through the screen must retain sufficient PtdIns- and PtdCho-exchange activities for biological function, but that those

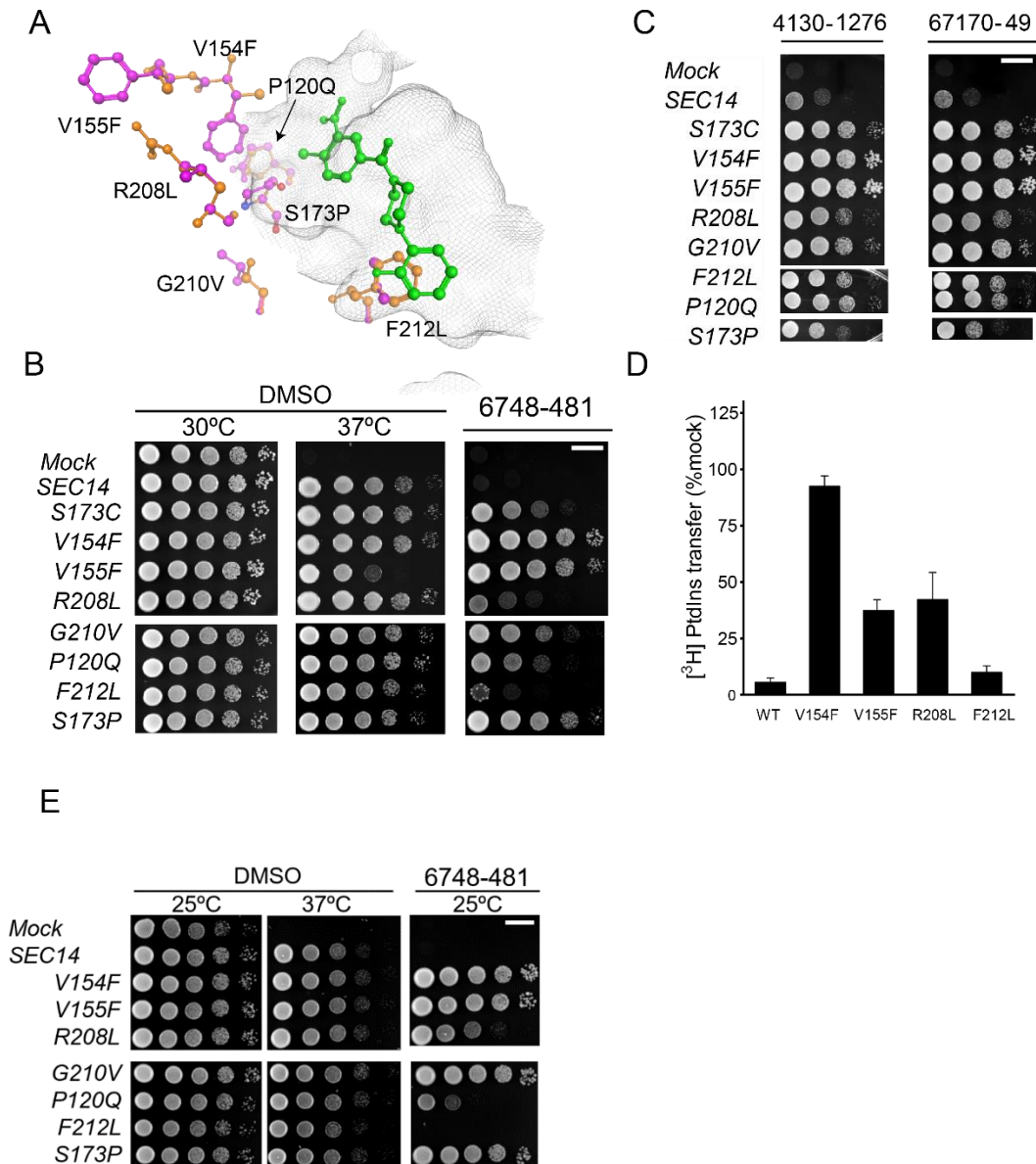


Figure 2-3. Functional characterization of NPPM-resistant Sec14 proteins.

(A) The seven independently isolated Sec14 missense substitutions identified in NPPM^R isolates are highlighted in ball and stick representation with mutant residues depicted in magenta and the corresponding wild-type residues in orange. The positions of the corresponding side chains are related to the NPPM 6748-481 pose depicted in green ball and stick. The surface of the Sec14 hydrophobic pocket is rendered as a gray wire-mesh.

(B) The indicated *SEC14* genes were integrated into the *LEU2* locus of a *sec14-1^{ts}* strain and expressed under the control of the *S. cerevisiae* *SEC14* promoter to generate strains exhibiting “physiological” levels of each Sec14 variant. The integrants were subsequently dilution spotted onto YPD plates supplemented with vehicle control DMSO or 20 μ M NPPM, as indicated at top, and incubated for 48 h at the indicated temperatures. The mock condition documents the phenotype of an isogenic strain where a *SEC14*-less integration cassette was transplanted into the *LEU2* locus. That expression of each Sec14 protein was sufficient to rescue *sec14-1^{ts}* growth defects at the restrictive temperature of 37°C is demonstrated by comparison of the growth profiles in the left (30°C) and center (37°C) panels of the integrants relative to mock controls. The NPPM^R phenotypes are displayed in the right panel. The plates were incubated for 48 h at the indicated temperatures before imaging. The NPPM481-resistance phenotypes were scored at 30°C. Note that R208L and F212L were weak mutants. Scale bar, 1 cm.

(C) Indicates that spontaneous mutants generated in response to 6748-481 confer pan-NPPM resistance to Sec14. The experiment is the same as above in (B) except that the plates were supplemented with NPPMs 4130-1276 and 67170-49, as indicated (20 μ M final concentration). The mock condition documents the phenotype of an isogenic strain where a *SEC14*-less integration cassette was transplanted into the *LEU2* locus. Scale bar, 1 cm.

(D) NPPM^R Sec14 proteins were expressed and purified as recombinant proteins and [³H]PtdIns transfer activities were measured *in vitro* in the presence of 20 μ M NPPM. Protein concentration was clamped at 287 nM. Inhibition was normalized to the DMSO vehicle control. Values are representative of mean \pm SEM; triplicate measurements from three independent experiments. The intrinsic PtdIns-transfer activities measured for each Sec14^R and other assay statistics are provided in supplementary Table 4.

(E) The indicated *SEC14* genes were integrated into the *MET17* locus of a *sec14-1^{ts} spo14 Δ* strain and expressed under the control of the *S. cerevisiae* in the same manner as in (B). The figure organization is also as in (B). Expression of each Sec14 protein was sufficient to rescue *sec14-1^{ts}* growth defects at the restrictive temperature of 37°C was demonstrated by comparison of the growth profiles in the left (25°C) and center (37°C) panels of the integrants relative to mock controls. The NPPM^R phenotypes are displayed in the right panel. The plates were incubated for 48 h at the indicated temperatures before imaging. The NPPM481-resistance phenotypes were scored at 25°C. Scale bar, 1cm.

Table 2-1. Intrinsic PtdIns-transfer activities for NPPM^R Sec14

| Protein | Activity (Transfer as % of input [³H]-PtdIns) | Total Input [³H]-PtdIns (c.p.m.) | Background (c.p.m.) |
|--------------------|---|--|--------------------------------|
| Sec14 | 16-28 | 7410-10100 | 530-570 |
| P120Q [*] | - | - | - |
| V154F | 13-18 | 8510-12125 | 780-1630 |
| V155F | 10-20 | 7400-10915 | 570-870 |
| S173P [*] | - | - | - |
| R208L | 6-10 | 8500-12125 | 570-1630 |
| G210V [*] | - | - | - |
| F212L | 13-21 | 7805-10400 | 590-870 |

*Insufficient activity for confident assessment (<3% transfer)

activities would be intrinsically resistant (at least to a substantial degree) to inhibition by NPPM. To examine those biochemical properties directly, representative Sec14^Rs were produced as recombinant protein in bacteria, purified, and the NPPM-resistance properties tested *in vitro*. We were unable to analyze Sec14^{S173P} or Sec14^{P120Q} in this manner because those two mutant proteins exhibited insufficient activity for confident analysis when purified from the bacterial host (unpublished observations). As expected, the Sec14^R proteins exhibited a range of basal PtdIns transfer activities (Table 2-1).

Given previous analyses of Sec14^{S173C} and Sec14^{S173A} substitutions whose design was guided by the Sec14::NPPM 6748-481 docking pose (Nile et al., 2014), the Sec14^{V154F} was of particular interest as it was impervious to challenge with 20 μ M NPPM 6748-481 *in vitro* (Figure 2-3D). Indeed, it exhibited an essentially complete resistance to NPPM 6748-481 challenge at near saturating aqueous concentrations of inhibitor (100 μ M; data not shown) even though V₁₅₄ was not identified by our working Sec14::NPPM 6748-481 pose as a residue critical to the mechanism by which the NPPM is coordinated within the Sec14 lipid-binding cavity (Nile et al., 2014). As shown in Figure 2-3D, the [³H]PtdIns transfer activities of Sec14^{V155F} and Sec14^{R208L} were also significantly more resistant to 6748-481 challenge compared with Sec14 in transfer assays spiked with 20 μ M NPPM, but all those proteins nevertheless retained measurable sensitivities to the NPPM at this concentration [\sim 100 times IC₅₀ Sec14; (Nile et al., 2014)]. Sec14^{F212L} was least resistant to inhibition by NPPM481 at this concentration of inhibitor, and the PtdIns transfer activity of this mutant exhibited an IC₅₀ (642.7 \pm 1.2 nM) that was only modestly increased relative to that of wild-type Sec14 protein (287.8 \pm 1.1 nM).

A VV signature correlated with NPPM sensitivity.

Of the seven Sec14 residues identified in the unbiased NPPM-resistance screen, we noted that P₁₂₀, S₁₇₃, R₂₀₈, G₂₁₀, and F₂₁₂ are precisely conserved between Sec14 and Sfh1. However, V₁₅₄ and V₁₅₅ are not conserved at all (Figure 2-4A). The Sec14 V₁₅₄V₁₅₅ motif is diverged to F₁₅₄A₁₅₅ in Sfh1 and, strikingly, this very V₁₅₄F substitution conferred upon Sec14 an essentially complete resistance to inhibition by NPPMs (see above). We therefore investigated the possibility that the Sec14 V₁₅₄V₁₅₅ motif is a signature of NPPM-sensitive Sec14-like PtdIns-/PtdCho-transfer proteins. To that end, primary sequence alignments highlighting residues which line the Sec14 and Sfh1 phospholipid-binding pockets were generated. Those alignments were subsequently compared with the corresponding residues projected to line the phospholipid-binding cavities of Sec14 orthologs from *Candida albicans* (Sec14_{CA}), *Candida glabrata* (Sec14_{CG}) and *Kluyveromyces lactis* (Sec14_{KL}). The essentially complete conservation, across this set of proteins, of the distinct substructures that coordinate PtdIns- and PtdCho-binding, emphasizes yet again the close similarities of the various pocket architectures (Figures 2-4A). Even in this extended analysis, five out of seven residues identified in the NPPM^R screen (P₁₂₀, S₁₇₃, R₂₀₈, G₂₁₀ and F₂₁₂) are absolutely preserved across this cohort of Sec14-like PITPs. By contrast, while the Sec14 V₁₅₄V₁₅₅ motif is conserved between *Saccharomyces cerevisiae* and *C. glabrata* (V₁₅₂V₁₅₃ in the latter), *K. lactis* exhibits an F₁₅₂V₁₅₃ version whereas the motif is diverged to M₁₅₄C₁₅₅ in *C. albicans*. (Figures 2-4A). Although the Sec14 V₁₅₄V₁₅₅ motif is not predicted to directly with bound NPPM 6748-481 (Figure 2-4B), we noted that the cognate V₁₅₄ polymorphisms in *K. lactis* and *C. albicans* Sec14 proteins (F and M, respectively) had the effect of extending hydrophobic side chains deeper into the hydrophilic microenvironment that defines the PtdCho-headgroup coordination substructure of Sec14 (Figure 2-4C).

To test the predictive power of the VV signature for NPPM sensitivity of a Sec14 protein, the corresponding *SEC14* genes were amplified from genomic DNAs of the corresponding fungal species, the amplified products were sub-cloned into the appropriate transplacement cassettes, and the genes of interest were individually integrated into the *S. cerevisiae* genome. All of those Sec14 orthologs scored as functional proteins when expressed in yeast as judged by their abilities to rescue growth of *sec14-1^{ts}* mutants on YPD agar at a restrictive temperature of 37°C (Figure 2-5A). When these yeast strains were challenged with 20µM NPPM 6748-481, the Sec14- and Sec14_{CG} – expressing strains failed to proliferate, whereas yeast expressing Sec14^{KL} and Sec14^{CA} were indifferent to the chemical challenge. We inferred from those results that Sec14_{CG} was sensitive to NPPM 6748-481 whereas Sec14_{KL} and Sec14_{CA} were not (Figure 1-5A). As control, the Sfh1^{E126A} protein was similarly analyzed, and proliferation of yeast expressing this protein was insensitive to inhibition by NPPM 6748-481 (Figure 2-5A). The inferences derived from *in vivo* data were confirmed by *in vitro* biochemical experiments where [³H]PtdIns transfer-assays that directly assessed the intrinsic sensitivities of these Sec14 proteins to NPPM 6748-481. Whereas Sec14_{CG} activity was strongly inhibited by NPPM 6748-481 to an extent similar to that observed for *S. cerevisiae* Sec14, activities of the Sec14_{CA} and Sfh1^{E126A} proteins were completely impervious to challenge with this compound. Sec14_{KL}, which has an incomplete VV signature (FV), was also resistant to inhibition by NPPM 6748-481 *in vitro* (Figure 2-5B). These collective data report a strong correlation between the VV signature and NPPM sensitivity in closely related Sec14 proteins.

Reconstitution of a VV signature sensitizes Sec14-like PITPs to NPPM

The second approach for examining the relationship between the VV signature and NPPM sensitivity of Sec14-like PtdIns-/PtdCho-transfer proteins interrogated whether transplacement of

a VV signature into a naturally NPPM^R Sec14-like P1TP sensitizes the protein to this class of inhibitor. To that end, the divergent M₁₅₄C₁₅₅ and F₁₅₆A₁₅₇ motifs of Sec14_{CA} and Sfh1^{E126A} respectively, were each converted to VV signatures. The NPPM-resistance properties of the mutant proteins were subsequently examined *in vitro* and *in vivo*. [³H]PtdIns transfer assays demonstrated that purified Sec14_{CA}^{M154V, C155V} had now acquired a significant sensitivity to NPPM 6748-481. While this sensitivity was not as marked as that of Sec14, it was dramatic nonetheless when gauged against the complete resistance of the parental Sec14_{CA} to inhibitor. Similarly, whereas partial reconstitution of a VV motif in Sfh1^{E126A} (by incorporation of the single F₁₅₆V substitution) endowed a modest NPPM sensitivity, full reconstitution of a VV signature further enhanced the sensitivity of Sfh1^{E126A, F156V, A157V} to inhibition by NPPM 6748-481 (Figure 2-5C). Consistent results were also obtained when the F₁₅₂V substitution was transplanted into Sec14^{KL} to reconstitute a VV signature in that protein. Although Sec14_{CG}^{V152F, V153F} also showed a reduced sensitivity to NPPM inhibition, as expected, those data came with the caveat that this mutant protein exhibited poor PtdIns- and PtdCho-transfer activity *in vitro* (unpublished observation). Thus, these substitutions come with a structural cost and, as described above, the mutant Sec14 variants exhibited a range of basal PtdIns-transfer activities *in vitro* (Table 2-2).

The biochemical results were supported by *in vivo* experiments where *S. cerevisiae* strains individually expressing Sec14_{CA}^{M154V, C155V} or Sec14_{KL}^{F152V} were tested for sensitivity to intoxication with NPPM 6748-481. Whereas proliferation of yeast cells expressing the WT versions of these Sec14 proteins was resistant to inclusion of this NPPM (20μM) in the culture medium, the growth of cells expressing these same proteins with reconstituted VV signatures was arrested in the presence of inhibitor (Figure 2-5D). The same result was observed in the case of Sfh1^{E126A}, where full reconstitution of a VV signature rendered the Sfh1^{E126A, F156V, A157V} sensitive

Table 2-2. Intrinsic PtdIns-transfer activities for Sec14-like PITPs and VV-motif variants

| Protein | Basal Activity (%) | Total Input (c.p.m.) | Background (c.p.m.) |
|---|---------------------------|-----------------------------|----------------------------|
| Sec14 | 18 – 26 | 8915 - 10863 | 645 – 955 |
| Sec14 _{CA} | 24 – 27 | 10243 – 11080 | 810 – 1054 |
| Sec14 _{CA} ^{M154V, C155V} | 12 – 18 | 8955 – 10470 | 960 – 1105 |
| Sec14 _{CG} | 22 – 24 | 10787 – 11113 | 1547 – 1669 |
| Sec14 _{KL} | 20 – 23 | 10585 – 11240 | 1460 – 1517 |
| Sec14 _{KL} ^{F152V} | 25 – 27 | 9421 – 11133 | 1226 – 1330 |
| Sfh1 E126A | 18 – 26 | 8716 – 8976 | 645 – 955 |
| Sfh1 ^{E126A, F156V} | 19 – 24 | 9220 – 10878 | 825 – 980 |
| Sfh1 ^{E126A, F156V A157V} | 13 – 16 | 10510 – 11285 | 834 – 1060 |

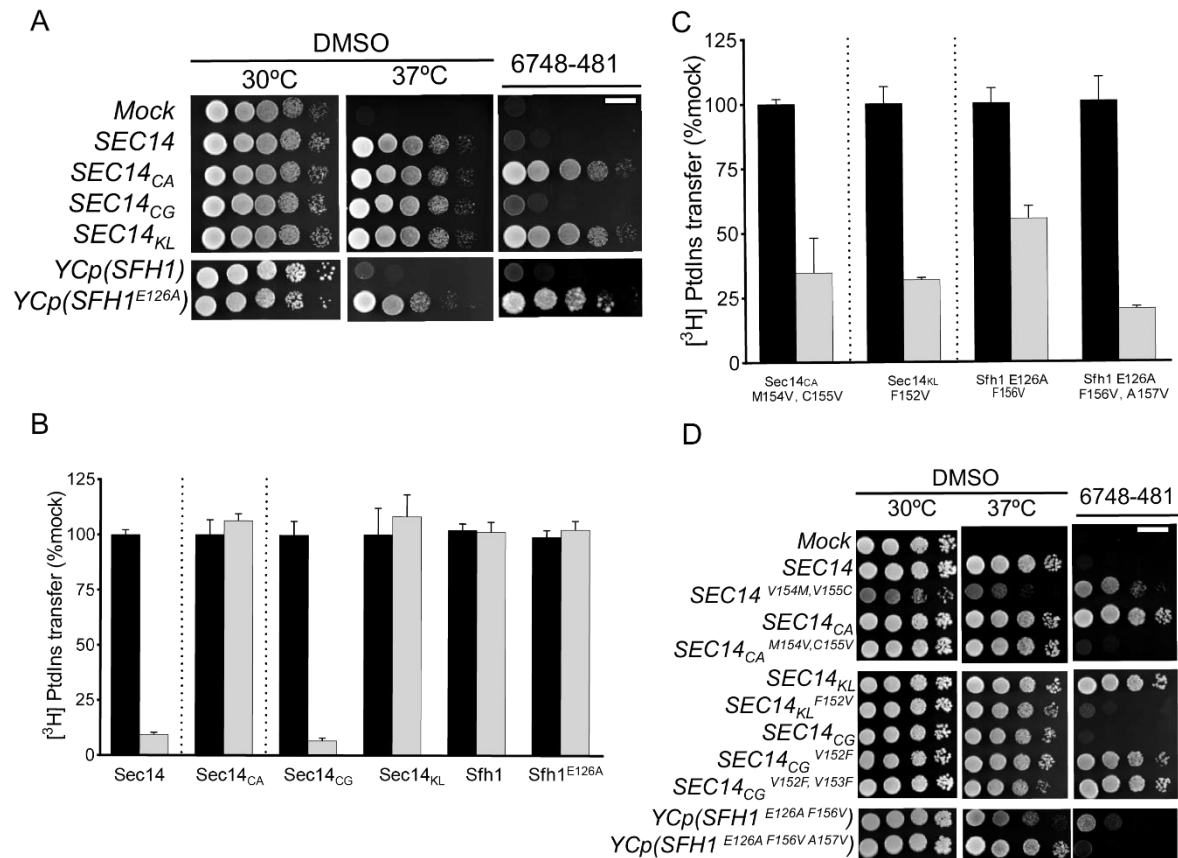


Figure 2-5. The VV motif is a signature of NPPM-sensitive yeast Sec14-like PtdIns/PtdCho-transfer proteins.

(A) *SEC14* genes from the indicated fungal species were integrated into the *LEU2* locus of a *sec14-I^{ts}* strain and expressed under the control of the *S. cerevisiae* *SEC14* promoter to generate strains exhibiting physiological levels of Sec14_{CA}, Sec14_{CG}, and Sec14_{KL}. The integrants were subsequently dilution spotted onto YPD plates supplemented with vehicle control DMSO or NPPM, as indicated at top, and incubated for 48 h at the indicated temperatures. The mock condition documents the phenotype of an isogenic strain where a *SEC14*-less integration cassette was transplanted into the *LEU2* locus. That expression of each heterologous Sec14 protein was sufficient to rescue *sec14-I^{ts}* growth defects at the restrictive temperature of 37°C is demonstrated by comparison of the growth profiles in the left (30°C) and center (37°C) panels of the integrants relative to mock controls. A (right panel): NPPM 6748-481 resistance or sensitivity of the corresponding integrants was scored by spotting cells on YPD plates supplemented with 20μM 6748-481 and incubating at 30°C for 48 h, at which time images were taken. The mock condition documents the phenotype of an isogenic strain where a *SEC14*-less integration cassette was transplanted into the *LEU2* locus. The *SFH1* control (little Sec14-like function *in vivo*) and the test *SFH1^{E126A}* (enhanced Sec14-like function *in vivo*) were expressed from low-copy centromeric plasmids (YCp) as ectopic expression of this sort was required for visualization of the enhanced Sec14-like properties of Sfh1^{E126A}.

(B) Characterization of the *in vitro* sensitivities of purified recombinant Sec14/Sec14-like proteins and the indicated mutant variants is shown. Protein concentrations were clamped at 287 nM throughout and NPPM 6748-481 concentrations were fixed at 20 μ M. Values represent the mean \pm SEM of triplicate measurements from three independent experiments. The intrinsic PtdIns-transfer activities measured for each Sec14 P1TP and other assay statistics are provided Table 2-2

(C) Characterization of the *in vitro* sensitivities of purified recombinant Sec14/Sec14-like proteins with transplaced VV motifs is shown. Protein concentrations were clamped at 287 nM and NPPM 6748-481 concentrations were fixed at 20 μ M. Values represent the mean \pm SEM of triplicate assay determinations from three independent experiments. The intrinsic PtdIns-transfer activities measured for each Sec14 P1TP, the indicated variants, and other assay statistics are provided in Table 2-2.

(D) Figure organization and experimental conditions are as described for (A). The abilities of the indicated *SEC14* and *SFH1* variants to complement *sec14-1^{ts}* growth defects at 37°C (middle panels) and to endow naïve yeast with resistance to NPPM challenge (right panels) were tested. Left panels represent vehicle growth controls under nonchallenge conditions (30°C), whereas the NPPM challenge plates were also incubated at 30°C. Images were taken after 48 h. The mock condition documents the phenotype of an isogenic strain where a *SEC14* -less integration cassette was transplanted into the *LEU2* locus.

to inhibition by NPPM 6748-481. Reciprocally, conversion of the *Saccharomyces* Sec14 VV-motif to that of the *Candida* PITP (Sec14^{V154M} and Sec14^{V154M,V155C}) yielded mutant Sec14s that were resistant to NPPM 6748-481. (Figure 2-5D). Taken together, the data indicate the VV signature is not only a strong predictor of NPPM-sensitivity in Sec14-like PITPs, but that transplacement of a VV signature into a naturally NPPM-resistant Sec14-like PtdIns-/PtdCho-transfer protein is sufficient to confer NPPM sensitivity to that PITP.

Degrees of freedom in the Sec14 VV signature

Given that divergence from the VV signature exerted significant effects of the sensitivity of Sec14-like PtdIns-/PtdCho-transfer proteins to NPPM 6748-481, we wished to better assess the degrees of freedom permitted in the VV-motif associated with NPPM-sensitivity of the PITP. To that end, a series of single missense substitutions was incorporated into the Sec14 V₁₅₄V₁₅₅ motif, and the NPPM-sensitivities of the individual mutants were tested by integrating the mutant *SEC14* alleles into the genome of a naïve yeast strain and subjecting the transplacement mutants to an NPPM challenge. Yeast expressing the Sec14^{V154F}, Sec14^{V154E}, Sec14^{V154Y}, Sec14^{V155F}, Sec14^{V155A} or Sec14^{V155Y} proteins were completely resistant to NPPM 6748-481 – indicating these polypeptides were functional PITPs with the property of being NPPM^R (Figure 2-6A). The former property was demonstrated in *sec14-1^{ts}* growth rescue experiments at 37°C, and in plasmid shuffle experiments where rescue of the lethal *sec14Δ* allele was scored (Figure 2-6B). By contrast, expression of the Sec14^{V154A} and Sec14^{V155E} mutants failed to confer an NPPM^R phenotype to yeast cells (Figure 2-6B), and this failure was not the trivial consequence of these proteins having been inactivated for PITP activity, as both proteins scored as active by the *sec14-1^{ts}* complementation assay (Figure 2-6B). These collective results indicate that Sec14 tolerates non-conservative changes in its VV-motif from both a protein structure and protein function point of view, and with regard to its NPPM

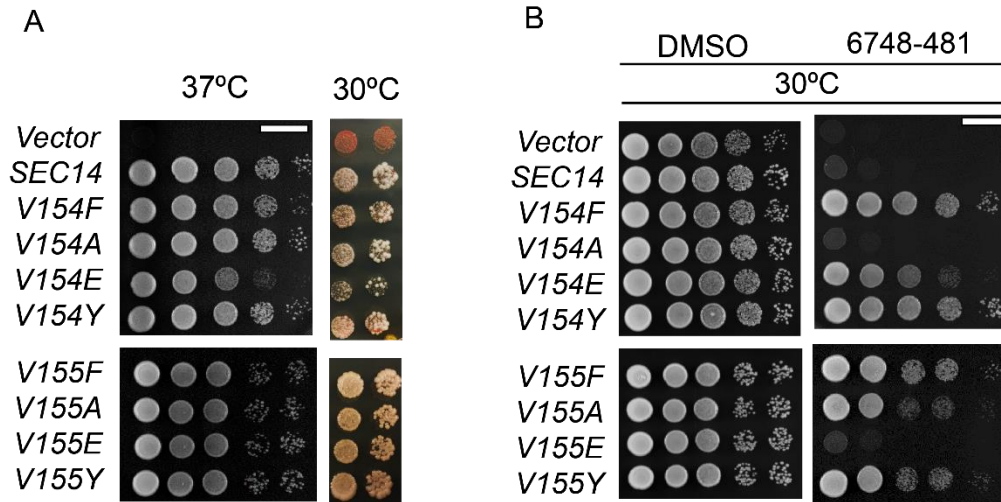


Figure 2-6. Functional analysis of the VV motif in Sec14.

(A) *SEC14* genes carrying the indicated for V154 and V155 missense substitutions (Phe, Ala, Glu, Tyr) were integrated into the *LEU2* locus of a *sec14-1^{ts}* strain. The mock condition documents the phenotype of an isogenic strain where a *SEC14*-less integration cassette was transplanted into the *LEU2* locus. Integrants were interrogated for *in vivo* function by scoring rescue of *sec14-1^{ts}* growth defects at the restrictive temperature of 37°C (left panel) or complementation of the normally lethal *sec14Δ* allele (right panel). Left panel: The YPD plates upon which the cells were spotted were incubated at 37°C for 48 h and images taken. Right panel: A colony color-based plasmid shuffle assay was used for determining whether the mutant Sec14 proteins could fulfil all biological functions of Sec14. Each mutant *SEC14* gene was integrated into the *MET17* locus of an *ade2 ade3 sec14Δ* strain carrying a Yep (*SEC14*, *LEU2*, *ADE3*) plasmid [strain CTY558 (Schaaf et. al, 2008)]. The mock condition documents the phenotype of an isogenic strain where a *SEC14*-less integration cassette was transplanted into the *MET17* locus. Plates were incubated at 30°C for 48 h and images were taken. The ability of mutant Sec14 expression to rescue lethality of the *sec14Δ* allele is recognized by loss of the Yep (*SEC14*, *LEU2*) plasmid upon relief of nutritional selection for *LEU2* selection by spotting cells onto YPD agar. Plasmid loss is recognized by appearance of white colony segregants from the background of red plasmid-bearing colonies. All mutant proteins retained biological activity in this assay.

(B) Integrants expressing the indicated mutant Sec14 proteins in *sec14-1^{ts}* genetic background were examined for NPPM 6748-481 sensitivity by dilution spotting on DMSO and drug supplemented YPD agar. Plates were incubated at 30°C for 48 h and images taken. For both panels, the mock condition documents the phenotype of an isogenic strain where a *SEC14*-less integration cassette was transplanted into the *LEU2* locus.

sensitivity properties. However, Sec14 does not tolerate incorporation of residues with side-chains bulkier than Val, or of charged residues, at those positions from the standpoint of maintaining sensitivity to inhibition by NPPM.

Discussion

A sophisticated appreciation of how NPPMs bind and inhibit Sec14 activity is essential for further progress in several important areas, including rational design of Small Molecule Inhibitors (SMIs) with desirable properties, e.g. increased potency and a suitably broadened range of activity among closely-related Sec14-like PITPs, etc. Our previous efforts to understand Sec14::NPPM binding interactions relied on rational loss-of-function approaches. That is, functional properties of Sec14 and of the NPPM were altered, using computational docking model-guided logic, with a view towards compromising protein::inhibitor interactions (Nile et al., 2014). Herein, we exploit an unbiased NPPM-resistance genetic screen to identify a new Sec14 motif, termed the VV signature, that contributes to NPPM sensitivity. We further demonstrate that suitable transplacement of a VV-signature into naturally NPPM-resistant Sec14-like PtdIns-/PtdCho-transfer proteins confers an NPPM-sensitivity onto those PITPs. The collective data both extend our appreciation of the determinants that govern Sec14-like PITP sensitivities to NPPMs, and facilitate primary sequence predictions of which Sec14-like PtdIns-/PtdCho-transfer proteins are likely to be NPPM-resistant or sensitive. Moreover, these data further emphasize the importance of S₁₇₃ in the mechanism by which NPPMs engage and inhibit Sec14-like PITPs.

A hallmark feature of NPPMs as PITP-inhibitors is their exquisite specificity. Even very closely related Sec14-like PITPs exhibit differential sensitivities to these inhibitors, and the detailed structural pose for NPPM-binding to Sec14 does not offer a satisfactory structural basis

for explaining these variable sensitivities. The Sec14-like Sfh1 makes a case in point. Unlike Sec14, this protein is completely resistant to NPPM challenge even though it preserves all obvious structural features required for NPPM-binding as defined by the model Sec14::NPPM pose (Nile et al., 2014). As described herein, attempts to capitalize on the proposed Sec14::NPPM 6748-481 pose to engineer an NPPM-sensitive Sfh1 failed. In those analyses, we presumed that the NPPM pose closely approximates the stably bound configuration of the inhibitor within the Sec14 lipid-binding cavity.

There are several potential mechanisms by which a Sec14-like PITP can be intrinsically resistant to NPPM inhibition, however. First, the PITP may simply fail to bind the SMI. Such defects could be manifested anywhere along the NPPM binding trajectory from initial association of SMI with the protein's surface to assumption of its resting pose within the PITP lipid-binding cavity. In such cases, the computed Sec14::NPPM pose would be of limited utility in deciphering mechanisms of resistance. Alternatively, NPPM binding might occur, but could be of sufficiently reduced affinity that the inhibitor becomes an exchangeable ligand (like PtdIns and PtdCho) so that SMI binding is readily reversible. In such circumstances, subtle differences in Sec14-like PITP pocket geometries could determine NPPM sensitivity/resistance. Subtle differences of this nature might be difficult to recognize when examination of the problem relies strictly on a dock model in the absence of a high resolution Sec14::NPPM crystal structure.

Unbiased genetic screens cast a wider net in terms of what types of NPPM-resistant Sec14 variants one might recover, and these strategies powerfully complement structural approaches. Using such screens, we uncovered 7 unique missense substitutions (P₁₂₀Q, V₁₅₄F, V₁₅₅F, S₁₇₃P, R₂₀₈L, G₂₁₀V, F₂₁₂L) that confer varying degrees of NPPM-resistance to Sec14. This set is noteworthy on several counts. First, the S₁₇₃P substitution involves the very Ser residue essential

for the proposed halogen-bonding interaction required for stable binding of NPPM-481 (Nile et al., 2014). Second, five of the seven substitutions do not involve residues previously highlighted for rational mutagenesis on the basis of the proposed NPPM-481 binding pose (S_{173} and F_{212} are the exception). Third, while S_{173} is the only one of these seven residues projected to contact bound NPPM directly, six of the seven substitutions lie within 4.5\AA of NPPM-481 as it is configured in the proposed Sec14::NPPM binding pose (V_{155} is the exception). Interpretation of the NPPM resistance phenotypes associated with these missense substitutions provides detailed new insights into what properties determine NPPM resistance/sensitivity in Sec14-like PITPs.

Taken together, the results from the genetic screen, while highlighting new residues for consideration, nonetheless strongly support the proposed Sec14::NPPM docking pose (Nile et al., 2014). What is striking is that, contrary to the structure-based logic that drove engineering of the Sfh1^{6X} variant, all but one of the residues identified in the screen lie in the sub-region of the Sec14 lipid-binding cavity projected to coordinate binding of the NPPM-481 activated aryl-halide headgroup. Only one (F_{212}) lies in the hydrophobic region of the cavity proposed to coordinate the distal fluorobenzene moiety of bound NPPM-481, and the $F_{212}L$ substitution is the weakest of the substitutions recovered in terms of conferring NPPM resistance to Sec14. Residue F_{212} resides on the cavity floor and is projected to engage in π - π stacking interactions with the NPPM fluorobenzene moiety as the NPPM intercalates into the narrow hydrophobic cleft bounded by residues F_{212} , M_{177} (also on the cavity floor), and F_{228} (on the helical gate). We suggest the $F_{212}L$ substitution disorders that hydrophobic cleft and thereby weakens NPPM binding by interfering with its normal intercalation into this substructure. It is a plausible notion that this substitution results in NPPM becoming an exchangeable ligand and therefore a poor inhibitor of Sec14^{F212L}.

Of the remaining six missense substitutions, five can be interpreted in the context of the previously proposed Sec14::NPPM docking pose that is anchored by a strong halogen bond interaction between the headgroup halide and residue S₁₇₃ (Nile et al., 2014). Obviously, recovery of S₁₇₃P in the unbiased genetic screen is particularly satisfying in that regard, and this mutant is essentially indifferent to NPPM challenge. However, the strong NPPM-resistance phenotypes associated with the R₂₀₈L, G₂₁₀V and P₁₂₀Q missense substitutions can be interpreted in terms of a highly conserved “S₁₇₃ coordination envelope” that governs the essential nature of the S₁₇₃ interaction with NPPM (Figure 2-7). The R₂₀₈ backbone engages in an H-bond with the backbone amide group of S₁₇₃ whereas the G₂₁₀ backbone amide coordinates with the S₁₇₃ backbone carbonyl oxygen. Similarly, the S₁₇₃ backbone amide is coordinated with the carbonyl oxygen of P₁₂₀ (Figure 2-7). Thus, these 3 residues not only reside within 4.5Å of the NPPM binding site, but make direct contacts with residue S₁₇₃ and contribute to the spatial positioning of its side-chain. Even subtle conformational perturbations in this ‘S₁₇₃ coordination envelope’ are expected to be sufficient to upset the strict geometric requirements for formation of the critical S₁₇₃-NPPM halogen bond and thereby compromise NPPM-binding – even though PtdCho-binding is not catastrophically affected as these remain functional proteins in cells.

The remaining two Sec14 residues V₁₅₄ and V₁₅₅ are of particular interest on several counts. First, these represent divergent residues amongst the Sec14-like PtdIns/PtdCho-transfer proteins, in contrast to the other five residues identified in the screen, which are highly conserved. Second, Sec14^{V154F} resembles Sec14^{S173P} in its complete indifference to NPPM-481, and Sec14^{V155F} is also significantly resistant to NPPM challenge. Third, and most strikingly, NPPM sensitivity amongst Sec14-like PITPs tracks closely with this VV signature and transplacement of this signature into resistant Sec14-like PITPs confers significant NPPM sensitivity to those

otherwise naturally NPPM-resistant PITPs. Residues V₁₅₄V₁₅₅ reside at the conserved kink in the long α -helix A₈ that frames one side of the hydrophobic cavity of Sec14-like proteins (Schaaf et al., 2008, Sha et al., 1998, Ren et al., 2014). Both residues are positioned in proximity to S₁₇₃, and V₁₅₄ lies within the S₁₇₃ coordination envelope. Although neither V₁₅₄ nor V₁₅₅ are projected to make any direct contacts with bound NPPM, one reasonable interpretation of NPPM^R substitutions at these positions is these perturb the S₁₇₃ coordination envelope. In support of this, structural modeling experiments show the V₁₅₄F, V₁₅₄M and V₁₅₄E substitutions, associated with NPPM-resistance, intrude into the hydrophilic microenvironment of the lipid binding pocket that coordinates the S₁₇₃::NPPM interaction (Figure 2-7). Consistent with this idea, substitution of V₁₅₄ with a small non-polar residue (Ala) does not perturb the S₁₇₃ coordination envelope in this manner and does not compromise NPPM binding by Sec14. Why bulky amino acid substitutions for V₁₅₅ can endow NPPM-resistance to Sec14 is less obvious, but indirect perturbation of the S₁₇₃ coordination envelope is a tenable possibility given the close proximity of this residue to the coordination envelope. Another possibility is that the VV-motif directly binds NPPM during the binding trajectory of the SMI into its most stable configuration within the hydrophobic cavity. Polymorphisms within the VV-motif may thereby sufficiently weaken Sec14 affinity for the NPPM to render it an easily exchangeable ligand and therefore an ineffectual inhibitor.

A detailed understanding of how NPPMs bind and inhibit Sec14 activity requires high resolution crystal structures of those complexes, and such information is essential for progress in rational design of NPPMs with increased potencies and suitably broadened ranges of activity among closely-related Sec14-like PITPs. The latter goal is desirable as it would provide new avenues for crystallization of PITP::NPPM complexes. That is, the engineering of NPPM binding activity to mutant versions of naturally NPPM-resistant Sec14-like PITPs which efficiently

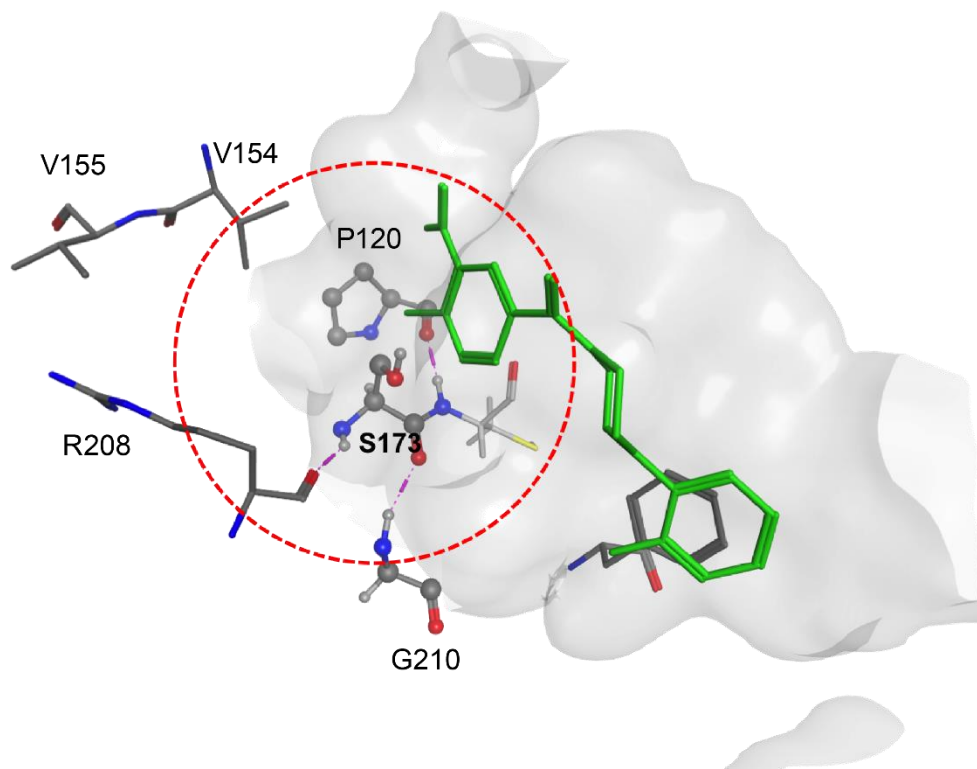


Figure 2-7. The Ser173 coordination envelope.

The boundaries of the Sec14 S173 coordination envelope are defined by the dotted circle (red). Residues that coordinate S173 via H-bond interactions (purple) are shown in stick render with carbon atoms in gray, oxygen in red and nitrogen in blue. The NPPM::6748481 pose is shown in green and the binding pocket surface is rendered in gray.

crystallize with bound ligands (e.g. Sfh1; (Schaaf et al., 2008). High resolution structures of such complexes are required for understanding how NPPMs inhibit Sec14-like PITPs, and directly determining whether the proposed S₁₇₃-NPPM halogen-bonding interaction precisely describes the mechanism by which NPPMs inhibit Sec14-like PtdIns/PtdCho-transfer proteins.

Materials and Methods

Yeast media and methods.

Yeast complex and minimal media and genetic methods followed standard procedures (Ito et al., 1983, Rothstein et al., 1983, Sherman et al., 1983). Yeast strains used in this study included the wild-type strain CTY182 (*MATa ura3-52 lys2-801 his3Δ-200*) and its isogenic *sec14-1^{ts}* and *spo14Δ* derivatives CTY1-1A (*MATa ura3-52 lys2-801 his3Δ-200 sec14-1^{ts}*) and CTY1092 (*MATa ura3-52 lys2-801 his3 his3Δ-200 spo14Δ*), respectively (Xie et al., 1998, Bankaitis et al., 1989). An isogenic *pdr5Δ* derivative of strain CTY1079 was designated YKM03 (*MATa ura3-52 lys2-801 his3Δ-200 spo14Δ pdr5Δ*) (this study). The gene replacement cassette plasmids used are listed in Table 2-3.

Small-molecule inhibitors.

Small molecules of interest were purchased from ChemBridge Chemical Store (San Diego, CA.), dissolved in DMSO to a final stock concentration of 20mM, and stored in the dark at -20°C.

Unbiased cell-based screen.

Spontaneous NPPM resistant (NPPM^R) mutants were generated using yeast strain CTY1079 (*MATa ura3-52 lys2-801 his3Δ-200 spo14Δ SEC14*) or the isogenic *pdr5Δ* strain YKM03 and seeded onto YPD plates individually supplemented with the appropriate NPPM at a concentration

of 10 μ M and 2 μ M, respectively. Approximately 1x10⁷ cells from 45 independent overnight cultures were each seeded onto a YPD agar plate, and the seeded plates were incubated at 30°C for 96 hours. One colony was picked from each plate and purified by two rounds of dilution streaking for isolated colonies. The NPPM^R phenotype of each mutant colony was verified on YPD agar supplemented with NPPM and the colonies were expanded to generate individual frozen stocks.

Amplification and DNA sequencing of SEC14 genes from isolated NPPM^R yeast isolates.

Genomic DNA from each independently-isolated NPPM^R mutant was prepared and the *SEC14* gene amplified via PCR using the DKO98 and 99 primer pair (Table 2-4). The *SEC14* nucleotide sequences were determined in both directions (Eton), and aligned using the multiple sequence alignment program Clustal Omega with wild-type *SEC14* as query sequence (Bankaitis et al., 1989; Engel et al., 2014).

Protein expression construct generation

NPPM^R missense mutations and VV-bar code mutants were generated by site-directed mutagenesis using pET28b (*His₈-SEC14*) as mutagenesis substrate. Site-directed mutations were generated using QuikChange II (Stratagene) and confirmed by nucleotide sequencing. *SEC14_{CA}* was amplified from genomic DNA via two rounds of PCR using the DKO1, 2 and DKO14,15 primer sets (Table 2-4), and subcloned into pET28b taking advantage of plasmid *NcoI* and *SacI* restriction sites. *SEC14_{KL}* was amplified using oligonucleotides KL100,101 and subcloned into the *SacI* and *SphI* restriction sites of plasmid pVB16. An internal *NcoI* restriction site in *SEC14_{KL}* was destroyed by incorporating a sense mutation using the KL92,93 mutagenic primer pair followed by a second round of amplification using primers KL90, 91 to incorporate an N-terminal His₈ tag. That PCR product was subcloned as an *NcoI-SacI* restriction fragment. Primer sequences are listed in Table 2-4. Protein expression plasmids used in study are listed in Table 2-5.

Table 2-3. Gene replacement cassette plasmids

| Plasmid | Description | Origin |
|----------------|---|---------------|
| pVB9 | pBSK(<i>pdr5Δ::GFP, KanMX</i>) | This study |
| pVB16(mock) | pBSK(<i>leu2Δ::HIS3</i>) | This study |
| pVB18 | pBSK(<i>leu2Δ::SEC14,HIS3</i>) | This study |
| pVB70 | pVB18(<i>leu2Δ::SEC14 S173C,HIS3</i>) | This study |
| pKM16 | pVB18(<i>leu2Δ::SEC14 P120Q,HIS3</i>) | This study |
| pDK154 | pVB18(<i>leu2Δ::SEC14 V154F,HIS3</i>) | This study |
| pDK155 | pVB18(<i>leu2Δ::SEC14 V155F,HIS3</i>) | This study |
| pKM14 | pVB18(<i>leu2Δ::SEC14 S173P,HIS3</i>) | This study |
| pDK156 | pVB18(<i>leu2Δ::SEC14 R208L,HIS3</i>) | This study |
| pDK157 | pVB18(<i>leu2Δ::SEC14 G210V,HIS3</i>) | This study |
| pKM17 | pVB18(<i>leu2Δ::SEC14 F212L,HIS3</i>) | This study |
| pDK257 | pVB18(<i>leu2Δ::SEC14 V154M, V155C ,HIS3</i>) | This study |
| pDK9 | pVB18(<i>leu2Δ::SEC14CA, HIS3</i>) | This study |
| pDK265 | pVB18(<i>leu2Δ::SEC14CA M154V, C155V, HIS3</i>) | This study |
| pDK248 | pVB18(<i>leu2Δ::SEC14KL, HIS3</i>) | This study |
| pDK266 | pVB18(<i>leu2Δ::SEC14KL F152V, HIS3</i>) | This study |
| pDK247 | pVB18(<i>leu2Δ::SEC14CG, HIS3</i>) | This study |
| pDK267 | pVB18(<i>leu2Δ::SEC14CG V152F, HIS3</i>) | This study |
| pDK268 | pVB18(<i>leu2Δ::SEC14CGV152F, V153F, HIS3</i>) | This study |
| pDK80 | pBSK(<i>met17Δ::URA3</i>) | This study |
| pDK81 | pBSK(<i>met17Δ::SEC14,URA3</i>) | This study |
| pDK239 | pDK81(<i>met17Δ::SEC14 V154F,URA3</i>) | This study |
| pDK240 | pDK81(<i>met17Δ::SEC14 V154A,URA3</i>) | This study |
| pDK241 | pDK81(<i>met17Δ::SEC14 V154E,URA3</i>) | This study |
| pDK242 | pDK81(<i>met17Δ::SEC14 V154Y,URA3</i>) | This study |
| pDK243 | pDK81(<i>met17Δ::SEC14 V155F,URA3</i>) | This study |
| pDK244 | pDK81(<i>met17Δ::SEC14 V155A,URA3</i>) | This study |
| pDK245 | pDK81(<i>met17Δ::SEC14 V155E,URA3</i>) | This study |
| pDK246 | pDK81(<i>met17Δ::SEC14 V155Y,URA3</i>) | This study |
| pDK280 | pDK81(<i>met17Δ::SEC14 F212L,URA3</i>) | This study |
| pDK281 | pDK81(<i>met17Δ::SEC14 S173P,URA3</i>) | This study |
| pDK282 | pDK81(<i>met17Δ::SEC14 P120Q,URA3</i>) | This study |
| pDK283 | pDK81(<i>met17Δ::SEC14 R208L,URA3</i>) | This study |

Table 2-3. Continued

| Plasmid | Description | Origin |
|----------------|--------------------------------------|---------------|
| pCTY1716 | YCp(<i>SFH1, URA3</i>) | (22) |
| pCTY1727 | YCp(<i>SFH1 E126A, URA3</i>) | (22) |
| pDK252 | YCp(<i>SFH1 F156V, URA3</i>) | This study |
| pDK255 | YCp(<i>SFH1 F156V A157V, URA3</i>) | This study |

Table 2-4. Primer sequences

| Name | Purpose | Sequence |
|-------------|---|--|
| DKO98 | To subclone <i>SEC14</i> into pVB16 at <i>SacII</i> , <i>SphI</i> sites | aaaccgcgatgggttacagtatgtgtgc |
| DKO99 | | tttgcattgctcatttcacgaaaggcttcgg |
| DKO107 | To generate <i>SEC14</i> V154F by mutagenesis | cttggttgggaatacgaatcttctgcaatacagattacctg |
| DKO108 | | ggcaggtaattctgtattgaacgaagattcgtattcccaaccaag |
| DKO105 | To generate <i>SEC14</i> V155F by mutagenesis | ggttgggaatacgaatctgtcttcaatacagattacctgcctg |
| DKO106 | | caggcaggtaattctgtattgaaagacagattcgtattcccaaac |
| DKO201 | To generate <i>SEC14</i> S173P by mutagenesis | ctggcaccatg gaaactccatgtacaattat ggattgaaa g |
| DKO202 | | cttcaaatccataattgtacatggagttccactagtgaccag |
| DKO109 | To generate <i>SEC14</i> R208L by mutagenesis | cataagtcaaaactattacccgaacttatgggtaaatftacatcatc |
| DKO110 | | gatgatgtaaaattaccataagttcgggtaatagtttgacttatg |
| DKO111 | To generate <i>SEC14</i> G210V by mutagenesis | caaaactattacccgaacgtatggttaaatftacatcatcaacgcgcc |
| DKO112 | | ggcgcggtgatgatgtaaaatcaaccatcgttcgggtaatagtttg |
| KMO104 | To generate <i>SEC14</i> P120Q by mutagenesis | cataaaaccgataaagatggccgc caa gtatatttgaagaattaggtg |
| KMO105 | | cacctaattctcaaaataacttggcggccatcttatcggtttatg |
| KMO106 | To generate <i>SEC14</i> F212L by mutagenesis | ctattacccgaacgtatgggtaaacftttacatcatcaacgcgccattc |
| KMO107 | | gaatggcgcggtgatgatgtaaaaagttaccatcgttcgggtaatag |
| DKO189 | To generate <i>SEC14</i> V155A by mutagenesis | ggttgggaatacgaatctgtcgtcaatacagattacctgcctgtc |
| DKO190 | | gaacaggcaggtaattctgtattgagcgacagattcgtattcccaaac |
| DKO191 | To generate <i>SEC14</i> V155E by mutagenesis | ggttgggaatacgaatct gtcgaacaata cagattacct gcctgttc |
| DKO192 | | gaacaggcaggtaattctgtattgttcgacagattcgtattcccaaac |

Table 2-4. Continued

| Name | Purpose | Sequence |
|-------------|---|--|
| DKO193 | To generate SEC14 V155Y by mutagenesis | ggtttgggaatacgaatctgtctatcaata cagattacct gcctgttc |
| DKO 194 | | gaacaggcaggaatctgtattgatagacagattcgtattcccaaacc |
| DKO195 | To generate SEC14 V154A by mutagenesis | cttggttgggaatacgaatctgccgttcaata cagattacct gcctg |
| DKO196 | | caggcaggaatctgtattgaacggcagattcgtattcccaaaccaag |
| DKO197 | To generate SEC14 V154E by mutagenesis | cttggttgggaatacgaatctgaagtcaata cagattacct gcctg |
| DKO198 | | caggcaggaatctgtattgaactcagattcgtattcccaaaccaag |
| DKO199 | To generate SEC14 V154Y by mutagenesis | cttggttgggaatacgaatcttactgtcaata cagattacct gcctg |
| DKO200 | | caggcaggaatctgtattgaacgtaagattcgtattcccaaaccaag |
| DKO335 | To generate SEC14 V154M by mutagenesis | gaaaaacttggttgggaatacgaatctatggttcaatacagattacctgc |
| DKO336 | | gcaggaatctgtattgaacatagattcgtattcccaaaccaagttttc |
| DKO337 | To generate SEC14 V154M, V155C by mutagenesis | gaaaaacttggttgggaatacgaatct atg tgt caatacagattacctgcctgttc |
| DKO338 | | gaacaggcaggaatctgtattgacacatagattcgtattcccaaaccaagttttc |
| DKO1 | To amplify SEC14 _{CA} from gDNA and sub-clone into pVB16 at <i>SacII</i> , <i>SphI</i> sites | aaaccgcgatgactacgatgactactgaagaaatattggc |
| DKO2 | | tttgcattgctaaatgttataagctctaggacattcacc |
| DKO14 | To sub-clone 8His-SEC14 _{CA} into pET28b at <i>NcoI</i> , <i>SacI</i> sites | aaccatgggtcatcatcatcatcatcatcatatgactacgatgactactgaa |
| DKO15 | | aagagctctta aatgttataagctctaggacattcacc |
| CA84 | To generate SEC14 _{CA} M154V, C155V by mutagenesis | cttggtatgggaatatgaagccgtggttcaatcgtttacctgcatgttc |
| CA85 | | gaacatgcaggtaaacgatattgaaccacggcttcatattcccataccaag |

Table 2-4. Continued

| Name | Purpose | Sequence |
|-------|--|--|
| KL100 | To amplify <i>SEC14_{KL}</i> from gDNA & subclone into pVB16 at <i>SacII</i> , <i>SphI</i> sites | aaccgcggtaggtaagtgaacaagaaatttag |
| KL101 | | ttgcatgcttacaattgaaaagccttggagcttc |
| KL90 | To sub-clone 8His- <i>SEC14_{KL}</i> into pET28b at <i>NcoI</i> , <i>SacI</i> sites | Aaccatgggtcatcatcatcatcatcatcatcatatggaagtgaacaagaaatttag |
| KL91 | | aagagctcttacaattgaaaagccttggagcttcaccttcaggtccaatgat |
| KL92 | To generate <i>SEC14_{KL}</i> without internal <i>NcoI</i> site by silent base-pair exchange and mutagenesis | ctatatctatccgatattggctcctggagagaggaggaatacattggacc |
| KL93 | | ggccaatgtattcctcctctctccagggaaccaatcggatagatag |
| KL 95 | To generate <i>SEC14_{KL}</i> F152V by mutagenesis | gaacttggctcgggaatacgaagctgtttagatacagattgctgcatttc |
| KL 96 | | gaacatgcaggcaatctgtatctaacaacagcttcgattccagaccaagttc |
| CG102 | To amplify <i>SEC14_{CG}</i> from gDNA and sub-clone into pVB16 at <i>SacII</i> , <i>SphI</i> sites | aaccgcggtaggtaggaagcggagttttg |
| CG103 | | ttgcatgcttatttcatggaaaacatctc |
| CG88 | To sub-clone 8His- <i>SEC14_{CG}</i> into pET28b at <i>NcoI</i> , <i>SacI</i> sites | aaccatgggtcatcatcatcatcatcatcatcatatggttaggaagcggagttttggc |
| CG89 | | ttgagctcttatttcatggaaaacatctctggggcttcaccttc |
| CG104 | To generate <i>SEC14_{CG}</i> without internal <i>NcoI</i> site by silent base-pair exchange and mutagenesis | cctgtacttgcgacatcggcccctggagagacgccaagtacatc |
| CG105 | | gatgtacttggcgtctctccagggccgatgtcggacaagtacagg |

Table 2-4. Continued

| Name | Purpose | Sequence |
|-------------|---|---|
| CG112 | To generate <i>SEC14_{CG}</i> F152V by mutagenesis | gaacttggtgtgggagtacgagtcc ttt gtcaactacagactgctgcttgctc |
| CG113 | | gagcaagcaggcagctctgtagttgacaaaggactcgtactcccacaccaagttc |
| CG114 | To generate <i>SEC14_{CG}</i> F152V, F153V by mutagenesis | gaacttggtgtgggagtacgagtccttttcaactacagactgcctgcttgctc |
| CG115 | | gagcaagcaggcagctctgtagttcaaaaaggactcgtactcccacaccaagttc |
| DKO94 | To sub-clone <i>SFH1</i> into pVB16 at <i>SacII</i> , <i>SphI</i> sites | aaaccgcggtatgacaaccagcatactc |
| DKO95 | | tttgcattgcttagctggtaacagtaaatttac |
| DKO163 | To generate <i>SFH1</i> F156V by mutagenesis | gaaacttagtcaaggagtacgaattagttgccacgtaccgggtcccagcgtgttcg |
| DKO164 | | cgaacacgctgggacccgggtacgtggcaactaattcgtactccttgactaagtttc |
| DKO147 | To generate <i>SFH1</i> F156V, A157V by mutagenesis | cttagtcaaggagtacgaattagttgtcacgtaccgg gtcccagcgt gttcg |
| DKO148 | | cgaacacgctgggacccgggtacgtgacaactaattcgtactccttgactaag |

Table 2-5. Protein expression plasmids

| Plasmid | Description | Origin |
|----------------|--|-----------------------|
| pRE1201 | pET28b (His8- <i>SEC14</i>) | (Schaaf et al., 2008) |
| pDK221 | pET28b (His8- <i>SEC14 P120Q</i>) | This study |
| pDK150 | pET28b (His8- <i>SEC14 V154F</i>) | This study |
| pDK152 | pET28b (His8- <i>SEC14 V155F</i>) | This study |
| pRE1270 | pET28b (His8- <i>SEC14 S173C</i>) | (Nile et al., 2014) |
| pDK171 | pET28b (His8- <i>SEC14 S173P</i>) | This study |
| pDK151 | pET28b (His8- <i>SEC14 R208L</i>) | This study |
| pDK153 | pET28b (His8- <i>SEC14 G210V</i>) | This study |
| pDK222 | pET28b (His8- <i>SEC14 F212L</i>) | This study |
| pDK31 | pET28b (His8- <i>SEC14CA</i>) | This study |
| pDK212 | pET28b (His8- <i>SEC14CA M154V,C155V</i>) | This study |
| pDK262 | pET28b (His8- <i>SEC14KL</i>) | This study |
| pDK269 | pET28b (His8- <i>SEC14KL F152V</i>) | This study |
| pDK261 | pET28b (His8- <i>SEC14CG</i>) | This study |
| pDK270 | pET28b (His8- <i>SEC14CG V152F</i>) | This study |

Table 2-5. Continued

| Plasmid | Description | Origin |
|----------------|---|---------------------------|
| pDK271 | pET28b (His8- <i>SEC14CG V152F, V153F</i>) | This study |
| pRE1227 | pET28b (His8- <i>SFHI</i>) | (Schaaf, et al., 2008) |
| pRE1234 | pET28b (His8- <i>SFHI E126A</i>) | (Schaaf, et al., 2011) |
| pDK77 | pET28b (His8- <i>SFHI F153V, L176M, I193V, V196A, A197S, Q204A, V227F</i>) | This study |
| pDK149 | pET28b (His8- <i>SFHI E126A, F156V</i>) | This study |
| pDK126 | pET28b (His8- <i>SFHI E126A, F156V, A157V</i>) | This study |

Protein purification

Recombinant proteins were purified essentially as described (Schaaf et al., 2008). Briefly, *E. coli* BL21 (DE3) cells carrying the appropriate expression plasmids were incubated at 37°C with shaking until cultures reached the desired cell densities ($A_{600}=0.8$). Recombinant protein expression was induced with 60 μ M isopropyl β -D-1-thiogalactopyranoside and cultures were incubated for an additional 18 hours at 16°C. Cells were pelleted, resuspended in 300mM NaCl, 25mM Na₂HPO₄, 1mM phenylmethanesulfonylfluoride (pH 7.8), and subsequently disrupted by two successive passages through a French press at 10,000 p.s.i. Cell-free lysates were clarified by serial centrifugations at 2800g (20 min) and 27,000g (60 min). Clarified lysates were incubated with Co²⁺ TALON metal affinity beads overnight at 4°C with agitation, and washed exhaustively with 300mM NaCl, 25mM Na₂HPO₄, 5mM 2-mercapthoethanol, 5mM imidazole (pH 7.8). Bound proteins were eluted with a continuous 10-200mM imidazole gradient in 300mM NaCl, 25mM Na₂HPO₄, 5mM 2-mercapthoethanol (pH 7.8). Peak fractions were pooled, dialyzed against 300mM NaCl, 25mM Na₂HPO₄ (pH 7.8), 5mM 2-mercapthoethanol, and concentrated by using Amicon Ultra filter centrifugation (EMD Millipore). Protein concentrations were estimated by SDS-PAGE and visual comparisons to BSA titration series, and by A₂₈₀ measurements.

PtdIns-transfer assays

Assays were performed by previously established methods (Schaaf et al., 2008, Nile et al., 2014). Recombinant Sec14 proteins were pre-incubated with acceptor membranes in 300mM NaCl, 25mM Na₂HPO₄, pH 7.5 and small molecule inhibitor or DMSO (vehicle control), as appropriate, for 30 minutes at 37°C. Donor membranes (rat-liver microsomes) were added to initiate the assay, and reactions were incubated for an additional 30 minutes at 37°C. [³H]-PtdIns transfer activities in the presence of small molecule inhibitors were normalized to mock DMSO controls.

Preparation of structural files for docking simulations

A homology model for the closed Sec14 conformer was generated based on structural templates for both the open Sec14 conformer (PDB ID 1AUA) and the closed conformer of Sfh1 bound to PtdIns (PDB ID 3B7N). Proteins were prepared for docking using the *Protein Preparation Wizard* panel in Schrodinger Suite and complete structure was optimized to relieve all atom and bond constraints after adding all side chains and missing atoms (Schrödinger, 2015).

Docking simulations

Two independent docking platforms were used. Computational docking used the genetic algorithm-based ligand docking program GOLD (version 5.2.1) which exhaustively explores ligand conformations and provides limited flexibility to protein side chains with -OH groups by reorienting the H-bond donor and acceptor moieties. The GOLD scoring function is based on favorable conformations documented in the Cambridge Structural Database, and on empirical results of weak chemical interactions. The active site was defined by a single solvent accessible point near the center of the protein active site, a radius of ~ 10 Å, and the GOLD cavity detection algorithm. To maintain consistency in docking Sfh1 crystal structure was superposed on Sec14 coordinates and the binding cavity was defined using the same centroid that was used to define the Sec14 binding pocket. This ensured the binding site interaction grids generated before docking shared reliable spatial coordinates and allowed direct comparisons of Sfh1 and Sec14 6748-481 docking results. GOLD docking was unconstrained to obtain unbiased results and to explore all possible ligand binding modes. Ligand was docked in independent runs, the ten best solutions were produced for each run, and early termination of ligand docking was switched off. All other parameters used default settings (Jones et al., 1997).

For Glide docking routines, proteins and ligands were prepared using Protein Preparation Wizard and the LigPrep module of Maestro 10.1 Interface of Schrodinger Suite (Schrodinger Suite 2015; Glide version 6.6). Receptor grids were generated without constraints and with standard settings. Docking was performed using XP scoring function. No similarity, torsional and inter-molecular interaction (hydrogen bonding or hydrophobic) constraints were used. Ligand was docked flexibly with nitrogen inversions and ring sampling turned on with post-docking minimization (Freisner et al., 2006).

MM-GBSA

Molecular **M**echanics with **G**eneralized **B**orn and **S**urface **A**rea solvation is widely applied method to calculate the free energy of binding of ligands to proteins. MM-GBSA approach was applied to calculate ligand binding energies and ligand strain energies in wild type and mutant protein-ligand complexes. The docked solutions generated from GOLD and Glide ligand docking were used for calculating ligand binding energies of complexes. Residues within a 10Å radius from the ligand were included in the flexible region with implicit solvent. MM-GBSA is implemented in Prime module of the Schrodinger software package (Schrödinger, 2015). Structural coordinates of Sec14::NPPM complexes overlayed on model Sec14 structures from *C. albicans*, *C. glabrata*, *K. lactis* in PDB format are available upon request.

References

- Balla T, Inositol-lipid binding motifs: signal integrators through protein-lipid and protein-protein interactions. *J. Cell Sci.* 2010;118:2093 – 2104 .
- Bankaitis VA, Malehorn DE, Emr SD, Greene R. The *Saccharomyces cerevisiae* SEC14 gene encodes a cytosolic factor that is required for transport of secretory proteins from the yeast Golgi complex. *The Journal of Cell Biology.* 1989;108(4):1271-81.
- Bankaitis VA, Malehorn DE, Emr SD, Greene R. The *Saccharomyces cerevisiae* SEC14 gene encodes a cytosolic factor that is required for transport of secretory proteins from the yeast Golgi complex. *The Journal of Cell Biology.* 1989;108(4):1271-81.
- Bankaitis VA, Mousley CJ, Schaaf G. The Sec14 superfamily and mechanisms for crosstalk between lipid metabolism and lipid signaling. *Trends in Biochemical Sciences.* 2010;35(3):150-60.
- Chang-Ileto B, Frere SG, Di Paolo G. Acute manipulation of phosphoinositide levels in cells. *Methods Cell Biol.* 2012;108:187-207.
- Cleves AE, Novick PJ, Bankaitis VA. Mutations in the SAC1 gene suppress defects in yeast Golgi and yeast actin function. *The Journal of Cell Biology.* 1989;109(6 Pt 1):2939-50.
- de Saint-Jean M, Delfosse V, Douguet D, Chicanne G, Payraastre B, Bourguet W, et al. Osh4p exchanges sterols for phosphatidylinositol 4-phosphate between lipid bilayers. *The Journal of Cell Biology.* 2011;195(6):965-78.
- Engel SR, Dietrich FS, Fisk DG, Binkley G, Balakrishnan R, Costanzo MC, et al. The reference genome sequence of *Saccharomyces cerevisiae*: then and now. *G3 (Bethesda).* 2014;4(3):389-98.
- Fang M, Kearns BG, Gedvilaite A, Kagiwada S, Kearns M, Fung MK, et al. Kes1p shares homology with human oxysterol binding protein and participates in a novel regulatory pathway for yeast Golgi-derived transport vesicle biogenesis. *The EMBO journal.* 1996;15(23):6447-59.
- Friesner RA, Murphy RB, Repasky MP, Frye LL, Greenwood JR, Halgren TA, et al. Extra precision glide: docking and scoring incorporating a model of hydrophobic enclosure for protein-ligand complexes. *J Med Chem.* 2006;49(21):6177-96.
- Fruman DA, Meyers RE, Cantley LC. Phosphoinositide kinases. *Annu Rev Biochem.* 1998;67:481-507.
- Grabon A, Khan D, Bankaitis VA. Phosphatidylinositol transfer proteins and instructive regulation of lipid kinase biology. *Biochimica et Biophysica Acta.* 2015;1851(6):724-35.

Guo S, Stolz LE, Lemrow SM, York JD. SAC1-like domains of yeast SAC1, INP52, and INP53 and of human synaptojanin encode polyphosphoinositide phosphatases. *The Journal of Biological Chemistry*. 1999;274(19):12990-5.

Hoon S, Smith AM, Wallace IM, Suresh S, Miranda M, Fung E, et al. An integrated platform of genomic assays reveals small-molecule bioactivities. *Nature Chemical Biology*. 2008;4(8):498-506.

Ile KE, Schaaf G, Bankaitis VA. Phosphatidylinositol transfer proteins and cellular nanoreactors for lipid signaling. *Nature Chemical Biology*. 2006;2(11):576-83.

Im YJ, Raychaudhuri S, Prinz WA, Hurley JH. Structural mechanism for sterol sensing and transport by OSBP-related proteins. *Nature*. 2005;437(7055):154-8.

Ito H, Fukuda Y, Murata K, Kimura A. Transformation of intact yeast cells treated with alkali cations. *Journal of Bacteriology*. 1983;153(1):163-8.

Jones G, Willett P, Glen RC, Leach AR, Taylor R. Development and validation of a genetic algorithm for flexible docking. *Journal of Molecular Biology*. 1997;267(3):727-48.

Katzmann DJ, Burnett PE, Golin J, Mahe Y, Moye-Rowley WS. Transcriptional control of the yeast PDR5 gene by the PDR3 gene product. *Mol Cell Biol*. 1994;14(7):4653-61.

Keaney EP, Connolly M, Dobler M, Karki R, Honda A, Sokup S, et al. 2-Alkyloxazoles as potent and selective PI4KIIIbeta inhibitors demonstrating inhibition of HCV replication. *Bioorg Med Chem Lett*. 2014;24(16):3714-8.

Lee AY, St Onge RP, Proctor MJ, Wallace IM, Nile AH, Spagnuolo PA, et al. Mapping the cellular response to small molecules using chemogenomic fitness signatures. *Science*. 2014;344(6180):208-11.

Lemmon MA. Membrane recognition by phospholipid-binding domains. *Nature Reviews Molecular Cell Biology*. 2008;9(2):99-111.

Li X, Rivas MP, Fang M, Marchena J, Mehrotra B, Chaudhary A, et al. Analysis of oxysterol binding protein homologue Kes1p function in regulation of Sec14p-dependent protein transport from the yeast Golgi complex. *The Journal of Cell Biology*. 2002;157(1):63-77.

Li X, Routt SM, Xie Z, Cui X, Fang M, Kearns MA, et al. Identification of a novel family of nonclassic yeast phosphatidylinositol transfer proteins whose function modulates phospholipase D activity and Sec14p-independent cell growth. *Molecular Biology of the Cell*. 2000;11(6):1989-2005.

McLaughlin S, Murray D. Plasma membrane phosphoinositide organization by protein electrostatics. *Nature*. 2005;438(7068):605-11.

Ren J, Pei-Chen Lin C, Pathak MC, Temple BR, Nile AH, Mousley CJ, et al. A phosphatidylinositol transfer protein integrates phosphoinositide signaling with lipid droplet metabolism to regulate a developmental program of nutrient stress-induced membrane biogenesis. *Molecular Biology of the Cell*. 2014;25(5):712-27.

Rivas MP, Kearns BG, Xie Z, Guo S, Sekar MC, Hosaka K, et al. Pleiotropic alterations in lipid metabolism in yeast *sac1* mutants: relationship to "bypass Sec14p" and inositol auxotrophy. *Molecular Biology of the Cell*. 1999;10(7):2235-50.

Routt SM, Ryan MM, Tyeryar K, Rizzieri KE, Mousley C, Roumanie O, et al. Nonclassical PITPs activate PLD via the Stt4p PtdIns-4-kinase and modulate function of late stages of exocytosis in vegetative yeast. *Traffic*. 2005;6(12):1157-72.

Rothstein RJ. One-step gene disruption in yeast. *Methods Enzymol*. 1983;101:202-11.

Schaaf G, Dynowski M, Mousley CJ, Shah SD, Yuan P, Winklbauer EM, et al. Resurrection of a functional phosphatidylinositol transfer protein from a pseudo-Sec14 scaffold by directed evolution. *Molecular Biology of the Cell*. 2011;22(6):892-905.

Schaaf G, Dynowski M, Mousley CJ, Shah SD, Yuan P, Winklbauer EM, et al. Resurrection of a functional phosphatidylinositol transfer protein from a pseudo-Sec14 scaffold by directed evolution. *Molecular Biology of the Cell*. 2011;22(6):892-905.

Schrödinger Release 2015-3: Prime version 4.1, Schrödinger, LLC, New York, NY.

Schrödinger Release 2015-3: Schrödinger Suite 2015-3 Protein Preparation Wizard; Epik version 3.3, Schrödinger, LLC, New York, NY; Impact version 6.8, Schrödinger, LLC, New York, NY.

Sha B, Phillips SE, Bankaitis VA, Luo M. Crystal structure of the *Saccharomyces cerevisiae* phosphatidylinositol-transfer protein. *Nature*. 1998;391(6666):506-10.

Sherman, F., G. R. Fink, and J. B. Hicks. 1983. *Methods in Yeast Genetics: A Laboratory Manual*. Cold Spring Harbor Press, Cold Spring Harbor, NY.

Strahl T, Thorner J. Synthesis and function of membrane phosphoinositides in budding yeast, *Saccharomyces cerevisiae*. *Biochimica et Biophysica Acta*. 2007;1771(3):353-404.

Xie Z, Fang M, Rivas MP, Faulkner AJ, Sternweis PC, Engebrecht JA, et al. Phospholipase D activity is required for suppression of yeast phosphatidylinositol transfer protein defects. *Proceedings of the National Academy of Sciences of the United States of America*. 1998;95(21):12346-51.

Zhang X, Loijens JC, Boronenkov IV, Parker GJ, Norris FA, Chen J, et al. Phosphatidylinositol-4-phosphate 5-kinase isozymes catalyze the synthesis of 3-phosphate-containing phosphatidylinositol signaling molecules. *The Journal of Biological Chemistry*. 1997;272(28):17756-61.

CHAPTER III

TARGET IDENTIFICATION AND MECHANISM OF ACTION OF PICOLINAMIDE AND BENZAMIDE BASED CHEMOTYPES WITH ANTIFUNGAL PROPERTIES²

Disclaimer for Chapter III

Chapter III is reprint of a publication, which I am a co-first author on along with Verena Pries (Hoepfner Lab), Christina Nöcker (Waldmann Lab), Philipp Johnen (Schaaf Lab), Zebin Hong (Bono Lab) and Ashutosh Tripathi (Bankaitis Lab). This work was done principally in collaboration with Dominic Hoepfner's group at Novartis Institutes of Biomedical Research, Switzerland. Members from Herbert Waldmann's group at Max Planck Institute for Molecular Physiology, Dortmund, Germany, Fulvia Bono's group at Max Planck Institute for Developmental Biology, Tübingen, Germany and Gabriel Schaaf's group at Institute of Crop Science and Resource Conversation, Bonn, Germany, contributed to the work. I performed genetic and biochemical experiments presented in Figure 3-1E, Figure 3-3, Figure 3-4C and Figure 3-5. The Summary section of this chapter is the abstract of the publication, while the rest are as in publication with minor editing.

²Reprinted with permission from "Target Identification and Mechanism of Action of Picolinamide and Benzamide Chemotypes with Antifungal Properties" by Pries et al., 2018. Cell Chemical Biology, Vol. 25, 1-12, Copyright © Elsevier Ltd. Published by Cell Press on behalf of Cell Chemical Biology.

Summary

Invasive fungal infections are accompanied by high mortality rates that range up to 90%. At present, only three different compound classes are available for use in the clinic, and these often suffer from low bioavailability, toxicity, and drug resistance. These issues emphasize an urgent need for novel antifungal agents. Herein, we report the identification of chemically versatile benzamide and picolinamide scaffolds with antifungal properties. Chemogenomic profiling and biochemical assays with purified protein identified Sec14p, the major phosphatidylinositol/phosphatidylcholine transfer protein in *Saccharomyces cerevisiae*, as the sole essential target for these compounds. A functional variomics screen identified resistance-conferring residues that localized to the lipid-binding pocket of Sec14p. Determination of the X-ray co-crystal structure of a Sec14p-compound complex confirmed binding in this cavity and rationalized both the resistance-conferring residues and the observed structure-activity relationships. Taken together, these findings open new avenues for rational compound optimization and development of novel antifungal agents.

Introduction

Invasive fungal infections (IFIs) are associated with high morbidity and mortality rates (Schmiedel and Zimmerli, 2016). Moreover, the incidence of fungal infections is rapidly escalating as the numbers of premature infants, patients receiving immunosuppressive therapy, and patients afflicted with AIDS, neoplastic disease, and advanced age increase (Pfaller et al., 2006). Although the incidence of IFIs is rising, the launch of initiatives aimed at antifungal drug discovery is lagging (Schmiedel and Zimmerli, 2016). Only three compound classes (i.e., azoles, polyenes, and echinocandins) are currently in therapeutic use (Prasad et al., 2016; Roemer and Krysan, 2014), and these act on the fungal plasma membrane, its biosynthetic pathways, and cell wall components, respectively. However, these drugs are only modestly effective in reducing the high mortality rates associated with IFIs because of: (1) restrictions in route of administration, (2) limited spectrum of activity, (3) poor bioavailability in target tissues, (4) significant toxicities that result from undesirable drug interactions, and (5) the emergence of drug-resistant pathogens (Brown et al., 2012). All of these factors highlight the acute demand for the discovery and development of novel classes of small-molecule inhibitors (SMIs) against a wider range of targets.

Genome-wide fitness profiling approaches using the surrogate model fungus *Saccharomyces cerevisiae* are proving themselves as powerful tools for identifying novel antifungal agents and developing hypotheses for their cellular target (Hoepfner et al., 2012; Richie et al., 2013). Haploinsufficiency profiling (HIP) identifies candidate pathways for direct inhibition by the compound as genes are identified in which one functional copy, compared with two, confers hypersensitivity to inhibition by that compound. In homozygous profiling (HOP), both gene copies are deleted so that information on synthetic lethal gene interactions and compensating pathways is accessed (Giaever et al., 1999; Hoon et al., 2008; Lee et al., 2014; Lum et al., 2004; Parsons et al.,

2006; Roemer et al., 2011). Using the HIP-HOP approach, we identified compounds with benzamide and picolinamide scaffolds as inhibitors of Sec14p, the major phosphatidylinositol-transfer protein (PTP) in *S. cerevisiae*, whose activity is essential for cell viability (Bankaitis et al., 1989, 1990).

A battery of genetic and biochemical assays corroborated the target hypothesis. Finally, we report the first crystal structure for a Sec14p::SMI complex, - thus providing a detailed mechanism of inhibition. Taken together, these findings outline a path for rationale synthesis of the next generation of small-molecule Sec14p inhibitors with optimized antifungal properties.

Results

Chemogenomic profiling

Screening of the Novartis compound archive for SMIs with antifungal activity (Richie et al., 2013) identified the picolinamide-containing compound 1 (Table 3-1) as a novel inhibitor of *S. cerevisiae* growth with a half maximal inhibitory concentration (IC₅₀) value of 13.5 μM. Lack of potent cytotoxicity against mammalian HCT116 cells (Table 3-1) led us to initiate follow-up studies on this chemotype. To identify the target protein of compound 1, HIP and HOP experiments were performed. For data analysis, the strain sensitivity was plotted against the Z score, which relates the sensitivity score of a strain in the compound profile to the variability in sensitivity of that strain across all the >3,000 compounds tested in the dataset (Hoepfner et al., 2014).

Execution of the HIP-HOP assay at a sub-lethal compound concentration (20 mM) identified a single strain to be significantly hypersensitive to compound 1: the strain carrying a heterozygous deletion for *SEC14* (Figure 3-1A). *SEC14* encodes an essential phosphatidylinositol transfer protein that plays a crucial role in protein transport from the trans-Golgi network (TGN)

Table 3-1. Structures and IC₅₀ values for active compounds

| Cpd | Structure | IC ₅₀ (μM) <i>S. cerevisiae</i> Wildtype | Fold IC ₅₀ shift <i>S. cerevisiae</i> Wildtype/ WildtypeΔ8 | IC ₅₀ (μM) <i>S. cerevisiae</i> <i>SEC14/sec14</i> | IC ₅₀ (μM) HCT116 | IC ₅₀ (μM) lipid transfer |
|-----|-----------|---|---|---|------------------------------------|---|
| 1 | | 13.5 | 13.8x | 5.9 | 30.4 | ND |
| 2 | | 18.5 | 2.7x | 9.4 | >100 | 8.5 |
| 3 | | 6.6 | 2.8x | 1.7 | >100 | 2.3 |
| 4 | | 134.9 | 2.3x | 99.4 | >100 | 29.4 |
| 5 | | 42.9 | 2.7x | 32.6 | >100 | 30.7 |
| 6 | | >200 | ND | >200 | >100 | 129 |
| 7 | | >200 | ND | ND | ND | >200 |
| 8 | | >200 | ND | ND | ND | ND |

Table 3-1. Continued

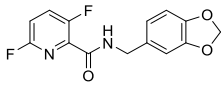
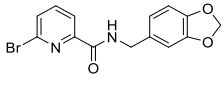
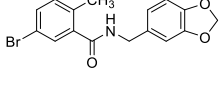
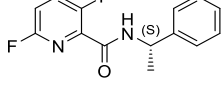
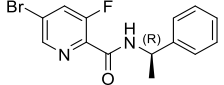
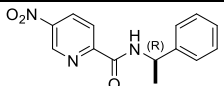
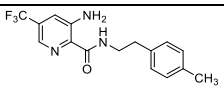
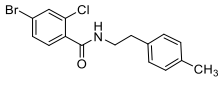
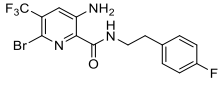
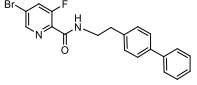
| Cpd | Structure | IC ₅₀ (μM) <i>S. cerevisiae</i> Wildtype | Fold IC ₅₀ shift <i>S. cerevisiae</i> Wildtype/ WildtypeΔ8 | IC ₅₀ (μM) <i>S. cerevisiae</i> <i>SEC14/sec14</i> | IC ₅₀ (μM) HCT116 | IC ₅₀ (μM) lipid transfer |
|-----|---|---|---|---|------------------------------------|---|
| 9 |  | >200 | ND | ND | ND | ND |
| 10 |  | >200 | ND | ND | ND | ND |
| 11 |  | >200 | ND | ND | ND | ND |
| 14 |  | >200 | ND | ND | ND | ND |
| 15 |  | >200 | ND | ND | ND | ND |
| 17 |  | >200 | ND | ND | ND | ND |
| 34 |  | >200 | ND | ND | ND | ND |
| 36 |  | >200 | ND | ND | ND | ND |

Table 3-1. Continued

| Cpd | Structure | IC₅₀ (μM) <i>S. cerevisiae</i> Wildtype | Fold IC₅₀ shift <i>S. cerevisiae</i> Wildtype/ WildtypeΔ8 | IC₅₀ (μM) <i>S. cerevisiae</i> <i>SEC14/sec14</i> | IC₅₀ (μM) HCT116 | IC₅₀ (μM) lipid transfer |
|------------|---|---|---|---|--|--|
| 38 |  | >200 | ND | ND | ND | ND |
| 46 |  | >200 | ND | ND | ND | ND |

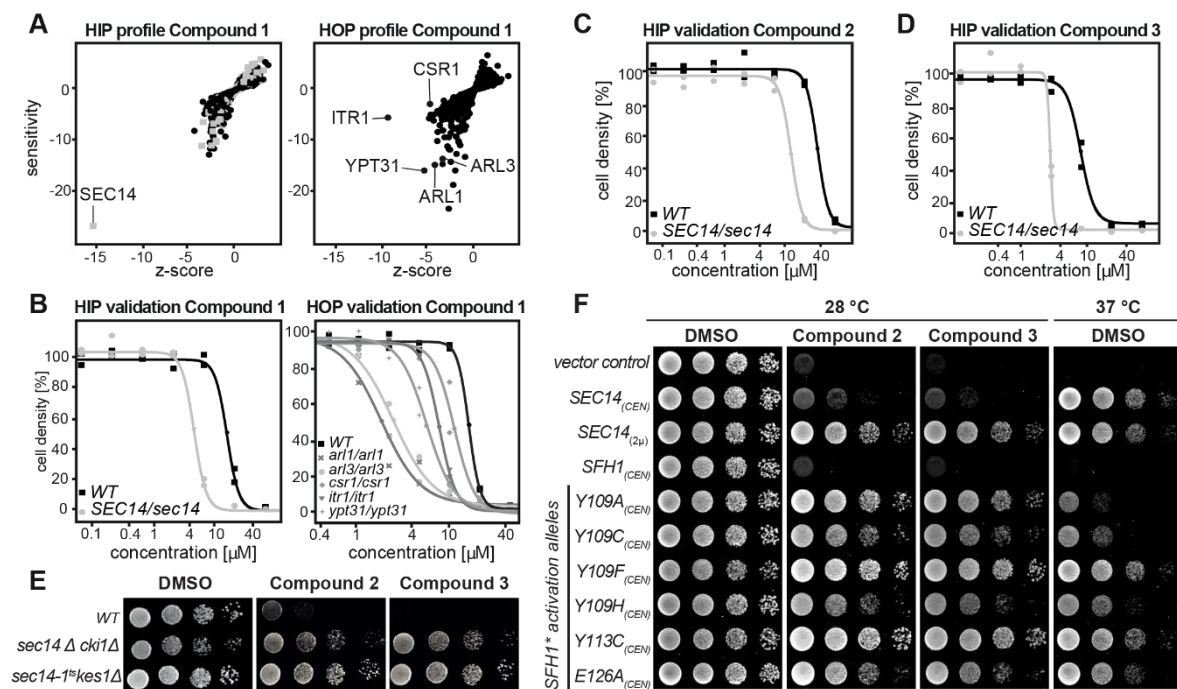


Figure 3-1. Chemogenomic Profiling and Hypersensitivity Validation

(A) Calculated profiles of the chemogenomic profiling experiment. HIP outlines hits directly affected by the test compound. HOP identifies synthetic interactions with the target. Essential genes are depicted by gray boxes, non-essential genes by black dots.

(B) Single-strain validation of hits from the chemogenomic profiling experiments as recorded in duplicates.

(C and D) Confirmation of hypersensitivity of the *Sec14/sec14* HIP strain against compounds 2 and 3 as recorded in duplicates.

(E) The wild-type and two ‘bypass *Sec14p*’ strains were spotted on rich medium (YPD) supplemented with DMSO or 20 μM of compounds 2 and 3 and incubated at 30°C for 48 hr.

(F) Transformants of the temperature-sensitive *sec14-1^{ts}* yeast strain harboring centromeric (*CEN*) plasmids carrying either *SFH1* or the designated *SFH1* activation alleles (*SFH1*^{*}) were spotted on minimal medium supplemented with 120 μM of compound 2, 30 μM of compound 3, or DMSO, as indicated and incubated at permissive (left) or restrictive (right) temperature. Transformants harboring YCplac33 (empty vector), or *SEC14* expressed from a centromeric (*CEN*) or a multi-copy plasmid (2 μ) served as controls.

and endosomal system. As such, Sec14p function is essential for yeast cell viability (Bankaitis et al., 1990). HOP (Figure 3-1A) identified strains deleted for *ITRI* (Nikawa et al., 1991), encoding a myo-inositol transporter, *YPT31* (Benli et al., 1996), encoding a Rab GTPase essential for Golgi function, *ARL1* (Lee et al., 1997), and *ARL3* (Huang et al., 1999) encoding two ARF-like GTPases that are involved in TGN/endosomal membrane traffic and *SFH2/CSRI* (Li et al., 2000), a non-classical PITP, to be synthetic lethal. The significance of the HOP screen gene set was that it recapitulated independent screens that previously revealed genetic interactions between *SEC14* and *ARL1*, *ARL3*, *YPT31* and *CSRI/SFH2* (Fairn et al., 2007; Mousley et al., 2008). Hypersensitivities of the strains identified in the genome-wide, pooled experiment, were validated by recording individual growth curves with the specific single strains picked from the HIP and HOP collection (Figure 3-1B). Taken together, the data from the genome-wide fitness profiling suggested that compound 1 exerts its antifungal action through Sec14p.

Chemical derivatization

Sec14p is an attractive antifungal target as it has been shown to be druggable (Filipuzzi et al., 2016; Nile et al., 2014), it executes essential functions in several pathogenic fungi and it is required for efficient secretion of pathogenicity factors (Chayakulkeeree et al., 2011). We therefore sought to delineate structure-activity relationships (SARs) by producing and testing a small compound collection generated by coupling different carboxylic acids and amines via established chemical synthesis methods (El-Faham and Albericio, 2010; El-Faham et al., 2009) (Figure 3-2). All derivatives were tested for their activity against wild-type *S. cerevisiae* cells (Table 3-1). To ensure that the SMIs still acted at the level of Sec14p, hypersensitivity against the heterozygous *SEC14* deletion strain, as observed in the HIP assay for compound 1, was verified. For compounds 2 and 3 (Figures 3-1C and 3-1D), and 4 and 5 (Table 3-1), decreased fitness of the *SEC14/sec14Δ*

heterozygote was observed relative to the isogenic wild-type. Of this SMI series, the benzamide compound 3 was the most potent with an IC_{50} of 6.6 μ M. These data indicated that the nitrogen of the picolinamide moiety was not essential for the Sec14p-targeted inhibition of these compounds. Compound 3, however, had much reduced solubility in pure aqueous solutions at pH 7.4 (data not shown), thereby hampering subsequent testing by requiring careful handling when diluting into a variety of fungal and mammalian culture medium. Substituting the benzodioxole with benzene, biphenyl, fluorobenzene, pyridine, or pyrazine functional groups either reduced potency or ablated inhibitory activity entirely (Table 3-1). Similarly, exchange of bromine and fluorine on the benzamide/picolinamide moiety was also incompatible with inhibitor activity. One desirable property of the bioactive derivatives was that all active compounds of the collection showed reduced cytotoxicity for HCT116 cells compared with compound 1 (Table 3-1).

Validation of Sec14p as Cellular Target Several independent approaches were taken to establish Sec14p as the direct target of the most bioactive benzamide (compound 3) and picolinamides (compounds 1, 2, 4, 5, and 6). First, we exploited the fact that the otherwise essential Sec14p activity is rendered dispensable in mutant cells deleted for structural genes of the cytidine diphosphate-choline pathway (e.g., *CKII*; Cleves et al., 1991) or the structural gene for the oxysterol binding protein homolog Kes1p (Fang et al., 1996). In these “bypass Sec14p” mutants, a functional and Sec14p-independent balance of lipid metabolism and PtdIns-4-phosphate signaling for exocytic membrane trafficking from the yeast TGN/endosomal system is restored (Cleves et al., 1991; Fang et al., 1996; Li et al., 2002). It was previously shown that the growth-inhibitory activity of highly specific Sec14p-targeted SMIs is alleviated in genetic backgrounds carrying loss-of-function *cki1* or *kes1* alleles (Nile et al., 2014). Thus, the *cki1* and *kes1* bypass Sec14p mutants were spotted on agar plates supplemented with compounds 2 and 3 to a final

concentration of 20 μ M (Figure 3-1E). Indeed, growth of the bypass Sec14p mutants was indifferent to challenge by these compounds. To further investigate target specificity, we assessed the inhibitory effects of compounds 2 and 3 on Sfh1p, the closest Sec14p homolog (Schaaf et al., 2011) in *S. cerevisiae*. Sfh1p is a nonessential protein and therefore cannot be identified as a drug target by HIP profiling. In these experiments, we adopted the previously described strategy of assessing the inhibitory effects of compounds 2 and 3 on Sfh1p activation mutants that were identified by a directed evolution approach (Khan et al., 2016; Nile et al., 2014), and for which single-residue substitutions endow this pseudo-Sec14p with robust Sec14p-like PITP activities *in vivo* and *in vitro* (Schaaf et al., 2011). All *SFHI* activation alleles (*SFHI**) expressed from a single-copy plasmid endowed resistance to both compounds 2 and 3, even when the SMI was used at concentrations sufficiently high (120 and 30 μ M, respectively) that even an additional copy of wild-type *SEC14* failed to restore cell growth (Figure 3-1F). Rather, the *SFHI**-associated SMI-resistance phenotype resembled that of yeast expressing a multi-copy episomal *SEC14* expression plasmid or yeast carrying *cki1* or *kes1* “bypass Sec14p” mutations. Taken together, these results strongly suggest that Sec14p is the sole essential target for these compounds in the yeast cell.

SMIs inhibit Sec14p lipid-transfer activity in vitro

Based on the knowledge gained from the cell-based growth inhibition tests, a subset of 15 compounds was chosen for direct analysis of their inhibitory effect on Sec14p-mediated phospholipid transfer in a purified *in vitro* system (Khan et al., 2016; Nile et al., 2014; Schaaf et al., 2008) (Figure 3A). To exclude the possibility that compound activity was due to non-specific membrane-active effects, the selected scaffolds were tested in parallel in phospholipid transfer assays reconstituted with the structurally unrelated mammalian PtdIns/PtdCho-transfer protein PITP α (Figure 3-3B).

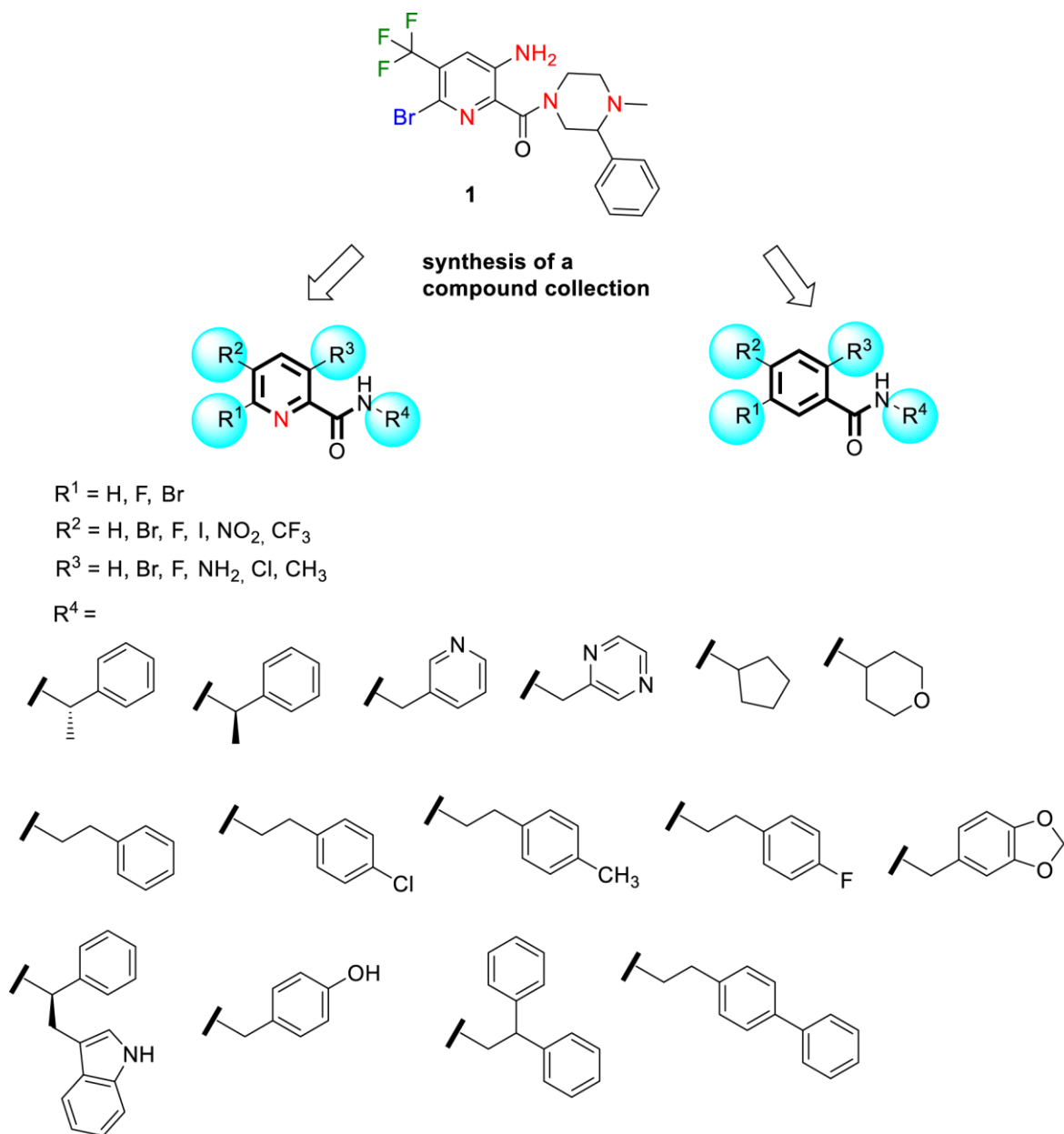


Figure 3-2. Synthesis of a collection of benz- and picolinamides for structure-activity relationship study.

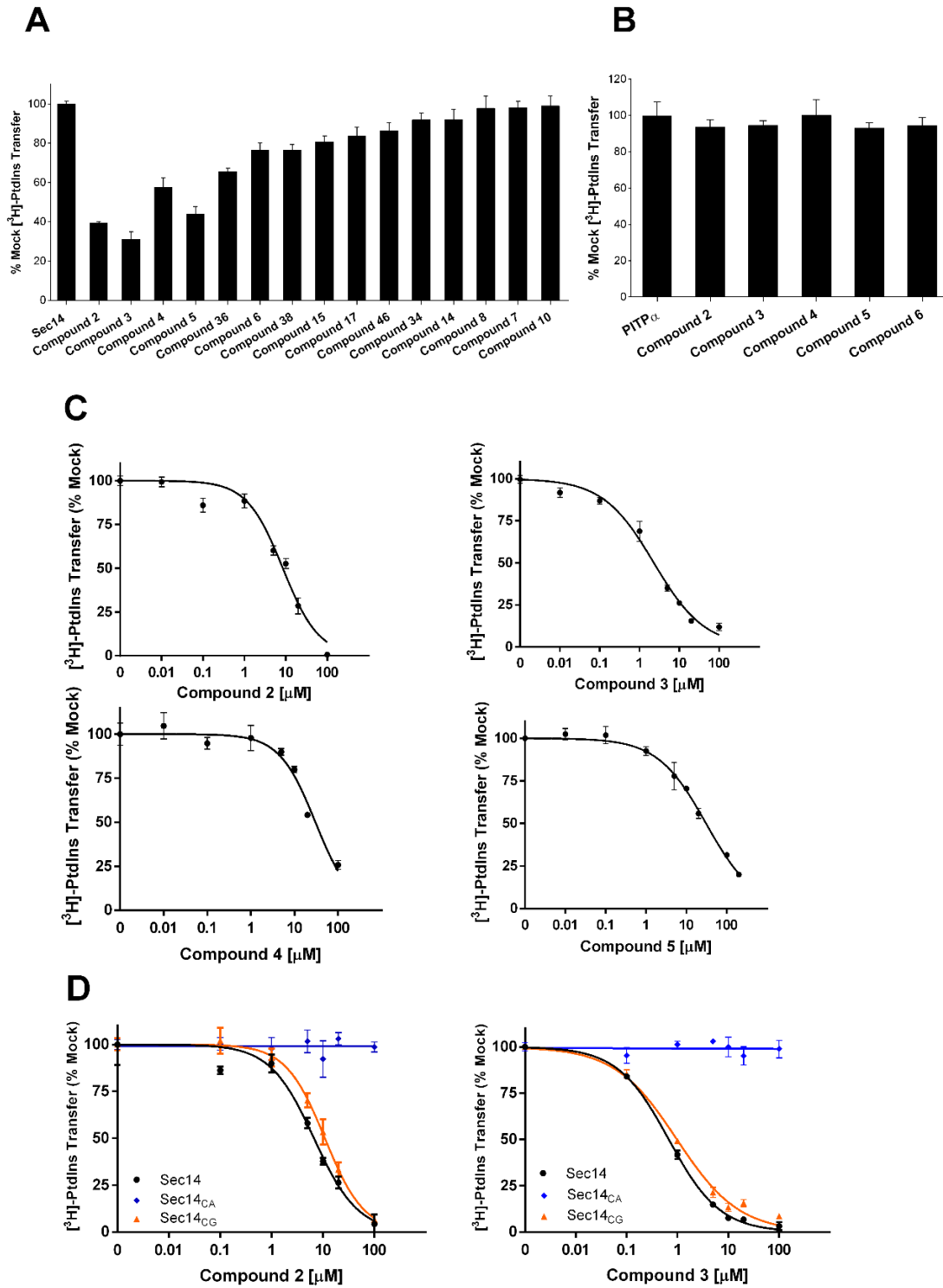


Figure 3-3. Analysis of Lipid-Transfer Inhibition with Recombinant Sec14p

(A) Fifteen compounds were tested for inhibition of Sec14p-mediated [³H]PtdIns transfer at a fixed concentration of 20 μM SMI. Values represent mean ± SEM of triplicate assay determinations from two independent experiments. Total radiolabel inputs per assay ranged from 8,356 to 9,604 cpm, backgrounds from 436 to 489 cpm, and the transfer efficiency from 14% to 16% of total input [³H]PtdIns. Activities were normalized against the mock condition set at 100%.

(B) The five small molecules that inhibited Sec14p [³H]PtdIns transfer by ≥ 30% in the endpoint assays in (A) were tested for inhibition of the structurally unrelated mammalian PITPα. [³H]PtdIns input for these assays ranged from 10,703 to 11,202 cpm, assay background from 403 to 415 cpm, and [³H]PtdIns-transfer efficiencies ranged from 10% to 11% of total input radiolabel. Values represent mean ± SEM of triplicate assay determinations from two independent experiments.

(C) IC₅₀ values for Sec14p-active compounds. Small-molecule inhibitors of Sec14p were titrated into PtdIns-transfer assays to determine IC₅₀ values. [³H]PtdIns input into these assays varied from 9,649 to 11,034 cpm, backgrounds ranged from 243 to 648 cpm, and transfer efficiencies as functions of total [³H]PtdIns input ranged from 12% to 18%.

(D) IC₅₀ curves for compounds 2 and 3 tested against Sec14p of *S. cerevisiae*, *C. albicans*, and *C. glabrata*. IC₅₀ values represent a 95% confidence interval from two independent experiments, with triplicate determinations for each data point.

Recombinant Sec14p was pre-incubated with acceptor membranes and compounds for 30 min at 37°C, the assay was initiated by the addition of radiolabeled rat liver microsomes, and the reaction was terminated after incubation of the assay for 30 min at 37°C. The [³H]PtdIns-transfer activities in the presence of test compounds were normalized to DMSO (mock) controls. Compounds 2, 3, 4, 5, and 6 showed clear inhibition of PtdIns transfer mediated by Sec14p, whereas no such inhibitory effects were observed when PtdIns transfer was catalyzed by the mammalian PITP α . Furthermore, IC₅₀ values were determined for active compounds in subsequent titration experiments (Figure 3-3C; Table 3-1). In agreement with the growth inhibition data, compound 3 again scored as the most potent inhibitor of Sec14p PtdIns-transfer activity, with an IC₅₀ of 0.7 μ M (IC₅₀ = 7 μ M *S. cerevisiae*). To assess if compounds 2 and 3 also inhibited the Sec14p of pathogenic species we recorded IC₅₀ curves as described above on the purified proteins of *C. albicans* and *C. glabrata*. In this experiment both compounds scored similar activity on *S. cerevisiae* and *C. glabrata* but did not inhibit PtdIns transfer by the *C. albicans* protein in the tested concentration range (Figure 3-3D). Activity on at least one other important fungal pathogen, and the absence of any measurable inhibition of PtdIns transfer by the mammalian PITP α , not only indicated that the Sec14p-directed inhibitory effect of compound 3 was fungal specific (and not the result of non-specific membrane-active effect), but it further emphasized the potential of this chemotype as antifungal lead.

Single-amino acid substitutions render Sec14p resistant to inhibition by compounds 2 and 3

The genetic and biochemical data strongly supported Sec14p as the sole essential cellular target of this SMI series. To obtain additional resolution for how this chemotype engages its target, and to identify amino acids mediating interaction and selectivity for these compounds, a functional variomics screen was deployed (Huang et al., 2013; Pries et al., 2016). This assay exploited a

library of plasmid-encoded *SEC14* genes mutagenized by error-prone PCR and screens for genetically dominant resistance of respective yeast transformants against the compound of interest. BY4743 wild-type cells (5×10^6) transformed with library DNA previously identified to be of a complexity above 2×10^5 (Huang et al., 2013) were plated onto 20 cm plates with synthetic defined media lacking uracil and containing growth-inhibitory concentrations of compound 2 (250 μ M) or compound 3 (100 μ M). Distinct colonies appeared after 72 hr, and 96 fast-growing colonies were selected from both SMI-resistance screens. The plasmid-encoded *SEC14* genes were then subjected to nucleotide sequence analysis and SNPs were identified. For both compounds, single-amino acid substitutions involving Tyr₁₅₁, Val₁₅₄, Val₁₅₅, and Ser₂₀₁ were recovered. Among the 96 clones picked against each compound, the frequencies of mutations identified with unambiguous sequences were as follows: Tyr₁₅₁ substitutions were identified 51 and 30 times in compounds 2 and 3 selections respectively, Val₁₅₄ was recovered 1 and 3 times, Val₁₅₅ 21 and 14 times, and Ser₂₀₁ 6 and 25 times, respectively. Furthermore, the compound 2 resistance screen identified a missense substitution of Ser₁₇₃ to Leu in four resistant clones (Figure 3-4A). Genotype-phenotype linkage of the most prominent SNPs, was verified by reintroduction of the plasmid-encoded mutant *SEC14* genes into the BY4743 Δ 8 *MATa*/ α strain, which is deleted for eight genes involved in drug resistance. Resistance phenotypes were subsequently assessed by dose-response experiments (Figure 3-4B). Integration of an additional *SEC14* wild-type allele already yielded a 5-fold IC₅₀ shift with compound 2 and a 3-fold IC₅₀ shift with compound 3 compared with wild-type cells. However, with the sole exception of *SEC14*^{V154G}, all mutant alleles tested endowed naive yeast cells with significantly increased, or effectively complete, resistance to SMI challenge. Next, these Sec14p variants were purified as recombinant proteins from *E. coli* and [³H]PtdIns-transfer activities were measured for each in SMI titrations *in vitro*. All of these mutant Sec14ps

exhibited substantially increased resistance to compounds 2- and 3-mediated inhibition of [³H]PtdIns transfer relative to wild-type Sec14p. With regard to compound 2, all mutant proteins exhibited IC₅₀ values that were some 7- to 30-fold higher than that of wild-type Sec14p (Figure 3-4C). Moreover, all mutant proteins but one were essentially indifferent to challenge with compound 3. That exception, Sec14p^{V155A}, exhibited a more modest 17-fold increase in IC₅₀ relative to wild-type Sec14p (Figure 3-4C). In general, the IC₅₀ values for each mutant protein were reflective of the levels of SMI resistance for the corresponding mutant yeast strains as measured by cell growth. These data unambiguously validate the identified resistance-conferring mutations by directly measuring PtdIns activities and demonstrating that the magnitude of intrinsic Sec14p resistance scaled proportionately to the SMI resistance of the corresponding yeast strain.

Mode of ligand binding

To identify the mechanism of inhibition, Sec14p was co-crystallized with picolinamide compound 2, and the crystal structure of the complex was determined at 2.6Å resolution. Compound 2 was prioritized for increased potency over compound 1 and better solubility than compound 3. The structure was solved by Molecular Replacement using Sec14p (PDB ID 1AUA; Sha et al., 1998) as input model in PHASER (Mccoy et al., 2007). The model was rebuilt and refined using PHENIX and COOT (Adams et al., 2010; Emsley and Cowtan, 2004). The final model exhibited an R_{factor} of 19.9% and an R_{free} of 22.5%, with good stereochemistry (Table 3-2). The asymmetric unit contained one molecule and Sec14p residues from 4 to 303 were identified in the final model. A discrete portion of the electron density in the 2mFo-DFc map (contoured at 1σ) revealed the presence of the ligand (Figure 3-4F). As expected, the protein exhibited a typical Sec14p fold consisting of a globular structure with an N-terminal tripod motif and a C-terminal lobe that

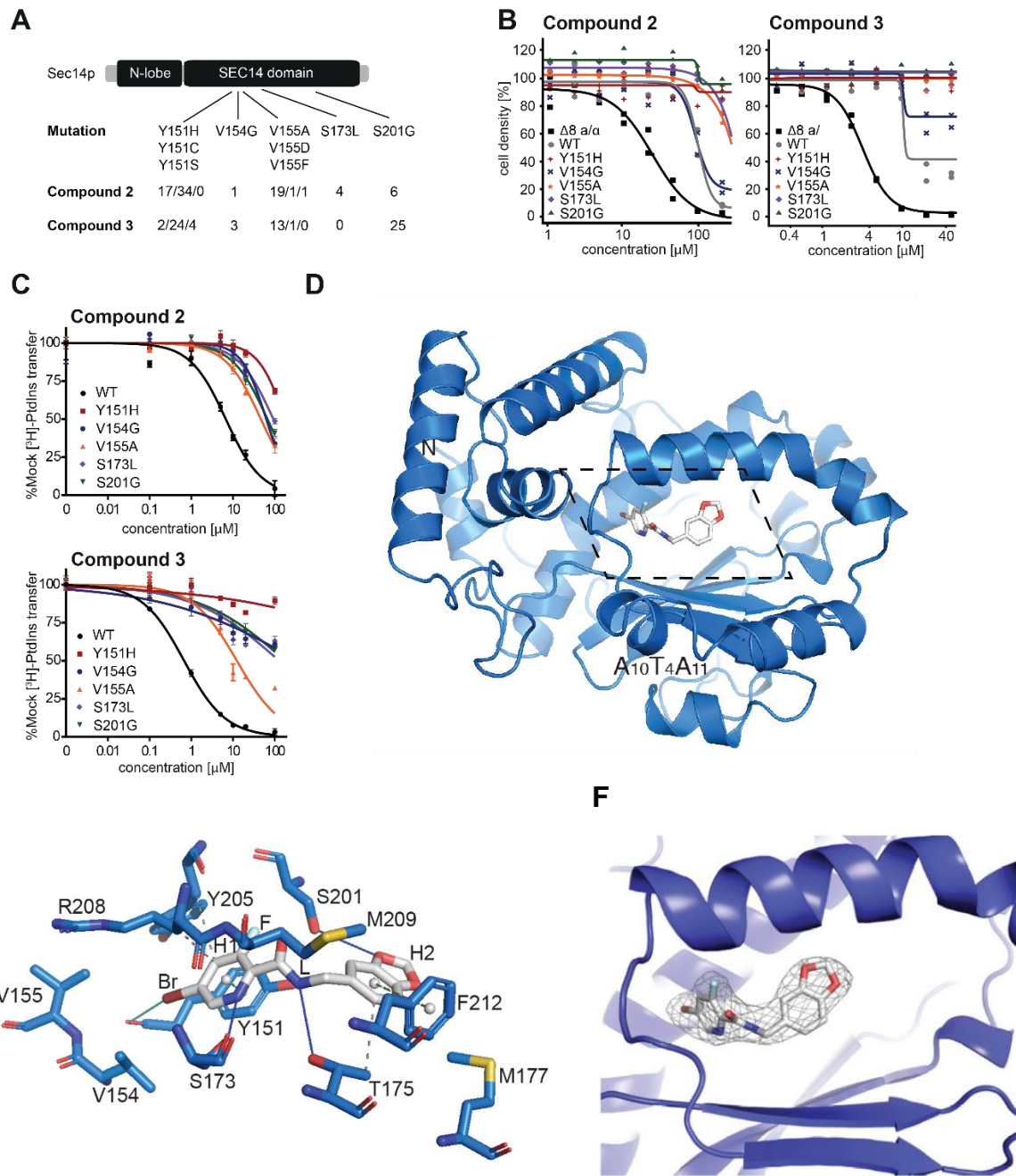


Figure 3-4. Structural and Functional Analysis of Sec14p-Compound Interactions

(A) SNPs and mutation frequency as identified by functional variomics for both tested compounds.

(B) Validation of identified mutations by integrative transformation of indicated SEC14 allele into cells.

(C) Validation of identified mutations by *in vitro* testing on recombinant protein. IC₅₀ values were determined at 95% confidence level from at least two independent experiments, each done in triplicate. [³H]-PtdIns input for Sec14, its mutant proteins ranged from 7111-11517 cpm per assay while the background ranged between 212-510 cpm per assay. The calculated IC₅₀s for compound 2 (μM) are as follows: Sec14 WT, 6.7; Sec14 Y151H, 177.2; Sec14 V154G, 62.5; Sec14 V155A, 46.5; Sec14 S173L, 92.5; Sec14 S201G, 66.6. For compound 3, the following IC₅₀ values (μM) were determined: Sec14 WT 0.68; Sec14 Y151H, >100; Sec14 V154G, >100; Sec14 V155A, >100; Sec14 S173L, >100; Sec14 S201G, >100. Error bars in (B and C) indicate 1 SD.

(D) Overview of the structure of Sec14p (as cartoon, in marine) in complex with compound 2 (in sticks representation, in gray). The section displayed in detail in (E) is outlined by dotted lines.

(E) Detailed view (rotated 45° along the x axis for clarity) of the binding pocket of Sec14p bound to compound 2 as identified by co-crystallization at 2.6 Å resolution. Interacting residues and relevant secondary structure elements of Sec14p are labeled; side chains are colored in marine and shown as sticks. H- and halogen-bonding are visualized as solid lines in blue and green, respectively, while hydrophobic interactions are shown as gray dashed lines. π-π stackings are depicted as green dashed lines (light green for parallel stacking; smudge green for perpendicular stacking), with aromatic ring centers as gray spheres. Functional groups of compound 2 are indicated.

(F) Stereo view of the electron density of the 2mFo-DFc map for the Sec14::compound 2 structure after refinement. The structure is shown in a similar view as in Figure 4C. Sec14p is colored in blue, the ligand in gray and the electron density contoured at 1σ is shown as a black mesh.

Table 3-2. Crystal structure model refinement parameters for Sec14-compound 2 complex

| | |
|------------------------------------|----------------------------|
| <i>Data collection</i> | |
| Wavelength (Å) | 0.9795 |
| Space group | <i>P</i> 3 ₂ 21 |
| <i>a</i> , <i>b</i> , <i>c</i> (Å) | 88.08, 88.08, 109.25 |
| α , β , γ (°) | 90, 90, 120 |
| Resolution (Å) | 50-2.6 (2.76-2.6) |
| <i>R</i> _{meas} | 0.227 (2.372) |
| <i>I</i> / σ <i>I</i> | 12.22 (1.12) |
| Completeness (%) | 99.9 (99.5) |
| Redundancy | 10.62 (10.87) |
| No. unique reflections | 29163 (4674) |
| CC(1/2) | 0.996 (0.385) |
| <i>Refinement</i> | |
| R-factor | 0.1993 |
| R-free | 0.2255 |
| Bond angles, rmsd (°) | 0.017 |
| Bond lengths, rmsd (Å) | 1.369 |
| <i>Ramachandran plot</i> | |
| Ramachandran favoured (%) | 98.32 |
| Ramachandran allowed (%) | 1.34 |
| Ramachandran outliers (%) | 0.34 |

included a large hydrophobic pocket of sufficient volume to accommodate a single phospholipid molecule (Schaaf et al., 2008; Sha et al., 1998) (Figures 3-4D and 3-4F). In the structure, Sec14p showed an open conformation, with the helical gate (helix A₁₀T₄A₁₁ [Bankaitis et al., 2010; Ryan et al., 2007; Schaaf et al., 2008]) displaced, as in the previously described detergent-bound Sec14p (Sha et al., 1998). Superposition with a known structure of Sec14p in the open conformation showed that the two structures were very similar overall, with a root-mean-square deviation of 0.336 Å over 1,917 atoms (PDB ID: 1AUA; Sha et al., 1998).

In the crystallized complex, compound 2 occupied the lipid binding pocket of Sec14p, where it was deeply buried in the cavity away from the solvent-exposed Sec14p surface (Figures 3-4D and 3-4E). The buried surface area of the ligand was 440.32 Å². The bromo-pyridine group (H1) of the picolinamide moiety pointed toward the core of the cavity, while the 1,3-benzodioxole ring (H2) was oriented toward solvent. The bromine was in van der Waals contact with Val₁₅₄ and Val₁₅₅ (range from 3.7 to 4.2 Å) and interacted with the carboxyl group of Tyr₁₅₁ (3.51 Å). The pyridine ring engaged in a π - π stacking interaction with Tyr₁₅₁ on one side, and in a hydrogen-bond (H-bond) interaction between the amine and the carboxyl of Ser₁₇₃ on the other. On this side, the Arg₂₀₈ side-chain and backbone atoms engaged in van der Waals interactions and further stabilized SMI binding. The fluorine atom interacted with Ser₂₀₁ and Tyr₁₅₁ and was in long-range interactions with Tyr₂₀₅. The linker (L) that connected rings H1 and H2 of compound 2 was stabilized by interactions with Ser₂₀₁ and Tyr₁₅₁ as well as with Met₂₀₉ and Thr₁₇₅. The 1,3-benzodioxole ring was positioned for H-bond interaction with Ser₂₀₁ and also engaged in van der Waals interactions with Phe₂₁₂, Thr₁₇₅, and Met₁₇₇ on the other side. These structural data were fully consistent with the results of the functional variomics screen described above, which

independently identified missense substitutions for Tyr₁₅₁, Val₁₅₄, Val₁₅₅, Ser₂₀₁, and Ser₁₇₃ as incompatible with SMI binding.

SAR analysis

SAR data assigned the relative importance of individual functional groups for the benz- and picolinamide analogs to their activities as Sec14p inhibitors. In that regard, an obligatory requirement for the para-Br on the phenyl ring (H1) and the H1 ring itself were notable, as demonstrated by compounds 2–6 showing inhibition of Sec14p PtdIns-transfer activity, while compounds 7–11 were ineffective inhibitors (Table 3-1). The crystal and in silico docking data rationalized these obligate requirements (Figures 3-4D, 3-4E, 3-4F). The hydrophobic planar ring system (H1) was critical for inhibitor activity as it: (1) acted as a scaffold to properly position the hydrophobic para-Br group for a functionally essential interaction with V₁₅₄V₁₅₅ and the backbone carboxyl of Tyr₁₅₁, and (2) provided a planar ring system for stacking interactions within the hydrophobic sub-pocket composed of residues Y₁₅₁, V₁₅₄, V₁₅₅, and R₂₀₈. Those latter stacking interactions lent significant stability to scaffold binding. The fluorine on Group R3 at the meta position of planar ring H1 contributed additional hydrophobicity (compounds 2, 3, 5, and 6). Polar substitutions (compounds 29, 34, and 38) and incorporation of larger moieties (e.g., CH₃, Cl, and Br; see compounds 7, 11, and 36) at that position were not well tolerated. Similarly, a halogen substitution on the R1 group (compounds 9, 10, and 11) also failed to enhance the inhibitory activities of these compounds. Nitrogen substitution in the hydrophobic planar ring H1 resulted in decreased activity, while inhibitory activity was enhanced when H1 was a hydrophobic phenyl ring system. The carboxyl oxygen (A) of the carboxamide group was required for the activity of the compounds as it favorably contributed to the polar amphipathic microenvironment of the PtdCho binding site. Similarly, the carboxamide amide nitrogen contributed to polarity of the

molecule and engaged residue Thr₁₇₅ in polar and/or H-bond interactions. The methylene group linker (L), which connects the carboxamide group and planar ring H1 with the proximal hydrophobic planar ring system (H2), also contributed to the activity of the picolinamide analogs. The SAR indicated the methylene group was well tolerated and oriented the benzodioxole planar ring H2 in a conformation favorable for docking to the amphipathic region of the binding cavity. However, extending the linker region (L), or substitution of methyl or phenyl group on the linker, was incompatible with inhibition of Sec14p activity. Several modifications of the hydrophobic planar ring system H2 were investigated and affect the potencies of active picolinamides. Alterations in size of that ring system, or modification of the ring system with polar substitutions, was also predicted to compromise SMI incorporation into the Sec14p hydrophobic cleft with the result that inhibitory activity was ablated.

Structure-based optimization of the benzamide/picolinamide series

Based on the Sec14p::compound 2 co-crystal structure, a medicinal chemistry transformation approach was applied to design novel chemical structures by structure-based transformation and optimization of existing ligands. van der Waals interaction maps of the Sec14p lipid-binding pocket were generated to identify steric incompatibility boundaries. For this purpose, we also generated an extended set of strains with mutations in the binding pocket (data not shown). These analyses suggest the availability of space between the respective C-terminal section of β strand B3 and the A9 helix, which might be productively exploited in alternative derivatizations of the benzodioxole planar ring H2 in further compound optimizations. Electrostatic maps and contact preference statistics were also created/applied to identify preferred energetically favorable locations for: (1) hydrophobic entities, and (2) hydrogen-bond donors and acceptors for potential ligand substitutions (Figure 3-4E). This model was used to screen fragment substitutions with

filters based on drug-like properties and favorable pharmacophoric features for optimal binding. Out of a total of ~41,000 fragments screened, 582 fragments were retrieved, and the top 15 were ranked and prioritized based on their estimated binding affinities. The novel designed compounds are devoid of chemically reactive groups, fulfill Lipinski's rule of five for bioavailable druglikeness (Lipinski et al., 2001), and are predicted to exhibit higher Sec14p binding affinities relative to compound 2. This strategy represents a prototypic approach comprising all structural and genetic data collected in this study for the design of second-generation, improved Sec14p SMIs as candidates for synthesis.

Importance of the VV motif in SMI sensitivity

Residues Val₁₅₄ and Val₁₅₅ constitute what is termed the VV motif, and it was previously recognized that: (1) this motif is a reliable predictor of sensitivity of fungal Sec14ps to NPPMs, and (2) that this motif is not conserved between the Sec14ps of *S. cerevisiae* and other pathogenic fungi (Khan et al., 2016) (Figure 3-5A). This observation took on added significance given that the Sec14ps of *S. cerevisiae* and *Candida glabrata* both naturally harbor a VV motif, and that the [³H]PtdIns-transfer activities of both proteins were sensitive to inhibition by compounds 2 and 3 *in vitro* (IC₅₀ values of 6.7 and 10.9 μM for compound 2, and 0.7 versus 1.0 μM for compound 3, respectively; Figure 3-3D). In contrast, the *Candida albicans* Sec14p, which is divergent at these positions was completely resistant to inhibition by both compounds 2 and 3 *in vitro*, even at concentrations that approached saturation in aqueous solution (IC₅₀ > 100 μM for each compound). The co-crystal data obtained in this study confirmed the VV motif to be involved in interactions with bioactive picolinamides and benzamides. Thus, we tested whether reconstitution of the VV motif sensitized otherwise resistant Sec14ps to these SMI chemotypes. To that end, Sec14p-deficient *S. cerevisiae* were reconstituted with the Sec14p of *C. albicans* and *C. glabrata* by the

previously described strategy (Khan et al., 2016), and those strains were spotted on rich medium (YPD) containing 20 μ M inhibitor. Only the strain expressing *C. glabrata* Sec14p (naturally harboring the VV motif) was sensitive to SMI challenge, whereas the strain reconstituted with *C. albicans* Sec14p was resistant to SMI challenge (Figure 3-5B). To further investigate whether reconstitution of the VV motif in a Sec14p that naturally lacks it sensitized the protein to SMI treatment, the VV motif was transplanted into the *C. albicans* Sec14p. However, unlike the case with NPPMs (Khan et al., 2016), transplacement of the VV motif into Sec14_{CA} (M₁₅₄V, C₁₅₅V double mutant) was insufficient to render the strain sensitive to challenge with compound 3 (Figure 3-5B). Why this is so remains an important and outstanding conundrum.

Antifungal activity

The initial aim of this study was to identify novel antifungal compounds. Identification of Sec14p as cellular target of the tested compounds by the methodologies described above motivated prioritization of the two optimized compounds, 2 and 3, for further antifungal testing. As Sec14ps play an important role in pathogenicity and virulence of pathogenic fungi (Chayakulkeeree et al., 2011), it was of interest to determine whether compounds 2 and 3 exerted activity beyond the *S. cerevisiae* P1TP. Thus, the inhibitory effects of compounds 2 and 3 were tested *in vitro* following the Clinical Laboratory Standards Institute guidelines against four diverse and clinically relevant pathogens (Wayne, 2008a, 2008b). These included two dimorphic fungi of the *Candida* genus (*C. albicans* and *C. glabrata*), one filamentous fungus (*Aspergillus brasiliensis*) and, as representative of the *Basidiomycota*, the yeast *Cryptococcus neoformans*. Posaconazole, a triazole compound, was used as positive control. For compound 2, a minimal inhibitory concentration (MIC) of 100 μ M was measured for *C. albicans* and *C. glabrata*, and an MIC of 50 μ M for *A. brasiliensis*.

Table 3-3. Growth inhibitory concentrations against pathogenic fungi.

| | <i>S. cerevisiae</i> BY4743 | <i>S. cerevisiae</i> BY4743Δ8 | <i>C. albicans</i> ATCC 10231 | <i>C. glabrata</i> ATCC 2001 | <i>C. neoformans</i> DSM 70219 | <i>Aspergillus brasiliensis</i> ATCC 16404 |
|--------------|---|----------------------------------|-------------------------------------|------------------------------------|-----------------------------------|--|
| | Minimal inhibitory concentration [μ M] | | | | | |
| Posaconazole | <0.3 | <0.3 | <0.3 | | <0.3 | <0.3 |
| Compound 2 | 200 | 100 | 100 | 100 | >200 | 50 |
| Compound 3 | >200 | 50 | >200 | 50 | >200 | >200 |

Minimal inhibitory concentrations on solid medium have been determined following the Clinical Laboratory Standards Institute reference in triplicates.

Compound 3 inhibited growth of *C. glabrata* with an MIC of 50 μ M, but residual growth was observed at higher concentrations (likely due to compound precipitation at higher dose). No growth inhibition was observed for *C. neoformans* (Table 3-3).

Discussion

This report describes the identification of a series of picolinamide- and benzamide-containing compounds as a novel class of SMIs of the *S. cerevisiae* PtdIns/PtdCho-transfer protein Sec14p. Although there are two previous reports of Sec14 inhibitors (Filipuzzi et al., 2016; Nile et al., 2014), this study presents the first Sec14p::SMI co-crystal structure. This structure, rationalized by both the functional variomics and SAR results of more than 40 generated analogs, supports strong structural fungal selectivity over the mammalian homolog and represents a quantum leap for rational design of the next generation of improved Sec14p inhibitors. The picolinamides and benzamides share some similarity with related inhibitors reported previously by Nile et al. (2014). However, they also differ considerable from these by the substituent patterns and the heteroatom in the aromatic acid part and by different amine substituents than reported before, thus opening up the chemical landscape for the design of novel Sec14p SMIs. Sec14p is the major PITP of the budding yeast *S. cerevisiae* and potentiates the efficient production of phosphoinositides, in particular PtdIns(4)P, whose signaling is specifically channeled to protein trafficking in the yeast TGN-endosomal system (Bankaitis et al., 1990) and for biogenesis of secretory vesicles from the TGN (Phillips et al., 2006). The sequence homology of Sec14p from *S. cerevisiae* with that of pathogenic fungi ranges from 45% to 86%, but amino acids that line the lipid-binding cavity surface are highly conserved. Although the role of Sec14p in other fungal species is less well characterized, it is reported to be involved in yeast dimorphism, sporulation, and in sustaining

mycelial growth, all prerequisites for the infectivity and pathogenicity of fungal pathogens (Chayakulkeeree et al., 2011; Lopez et al., 1994; Monteoliva et al., 1996; Phillips et al., 2006; Rudge et al., 2004). Compared with the *in vitro* potency measured on some fungal proteins, the recorded potencies on the tested pathogenic fungi were relatively low. But the used cell-based assay only recapitulated mitotic growth, but not any of the other functional aspects of Sec14p inhibition stated above. While the presented compounds need further evaluation to qualify as clinical candidates, the analytical platform and structural data identify a path for application of rational medicinal chemistry approaches. The fact that, at least in *S. cerevisiae*, SMI sensitivity is overcome by loss of function in any one of one of seven different genes (bypass Sec14p mutations [Bankaitis et al., 1990; Cleves et al., 1989; Fang et al., 1996]), or by single-amino acid substitutions in Sec14p itself, would seem to reduce enthusiasm for Sec14p as an attractive antifungal target. However, bypass Sec14p mutations derange lipid metabolism and are accompanied by pleiotropic effects that generally reduce the fitness of the organism, particularly under stress conditions (Cleves et al., 1989; Mousley et al., 2012). Sec14p amino acid substitutions that result in SMI resistance influence key residues required for optimal protein function and therefore are also likely to be deleterious under conditions of high Sec14p demand as in pathogenic settings. Specificity of target is always a primary issue in drug design.

The presented benz- and picolinamides, while toxic to fungi, were not cytotoxic to mammalian cells and failed to inhibit the structurally unrelated mammalian PtdIns-transfer proteins *in vitro*. The benz- and picolinamides reported here target the PtdCho head group coordination substructure of the Sec14p lipid-binding pocket. As none of the mammalian *SEC14L* proteins exhibit this substructure, it is highly unlikely that these activities will be targeted. Thus, the benz- and picolinamide compounds described herein represent privileged scaffolds that exhibit

exquisite specificity among fungal Sec14-like PtdIns/ PtdCho-transfer proteins. In summary, the structural and functional data gained by the experimental approach in this study, together with the experimental tools and data from previous studies (Filipuzzi et al., 2016; Khan et al., 2016; Nile et al., 2014), now provide the scientific community a robust roadmap to the design, synthesis, and validation of the next generation of Sec14p inhibitors aimed at treating severe fungal infections.

Significance

Due to increasing numbers of elderly or immunocompromised patients, severe antifungal infections are on the rise, and the mortality numbers are unacceptably high. Existing treatments suffer from emerging drug resistance against established pathogens and lack of efficacy as the spectrum of pathogenic fungi identified in patients today is much broader than a few decades ago. Despite this, the current pharmaceutical drug discovery pipeline lists less than a handful of compounds in clinical phases that modulate novel targets. This report describes benz- and picolinamide compounds with versatile and robust chemistry, which exert antifungal activity against the model organism *Saccharomyces cerevisiae*, but also against pathogenic *Candida* and *Aspergillus* species. Using a combination of genetic methodologies, the fungal lipid-transfer protein Sec14 was identified as the target of these compounds. Importantly, the tested benz- and picolinamides, while toxic to fungi, were not cytotoxic to mammalian cells and failed to inhibit the structurally diverged mammalian lipid-transfer proteins *in vitro*, further emphasizing their antifungal potential. A potent compound of the series was successfully co-crystallized with Sec14p, yielding the first high-resolution structural dataset for a phosphatidylinositol-transfer protein in complex with an inhibitor. The compound-protein data obtained by the structural approach was in full agreement with a series of genetic point mutants and the structure-activity

data derived from 48 compound derivatives. Combined, this dataset paves the way and provides the protocols for rational optimization of benz- and picolinamides as antifungal Sec14 inhibitors.

Materials & Methods

Microbial strain description, culture conditions and plasmids construction

Strains BY4743 (*MATa/a his3Δ1/his3Δ1 leu2Δ0/leu2Δ0 LYS2/lys2Δ0 met15Δ0/MET15 ura3Δ0/ura3Δ0*), BY4743Δ8 (as above but with *snq2Δ::KanMX4/snq2Δ::KanMX4, pdr3Δ::KanMX4/pdr3Δ::KanMX4, pdr5Δ::KanMX4/pdr5Δ::KanMX4, pdr1Δ::NatMX4/pdr1Δ::NatMX4, yap1Δ::NatMX4/yap1Δ::NatMX4, pdr2Δ/pdr2Δ, yrm1Δ/yrm1Δ, yor1Δ/yor1Δ*), CTY182 (*MATa ura3-52 lys2-801 his3Δ-200*) and its isogenic derivatives CTY1-1A (*MATa ura3-52 lys2-801 his3Δ-200 sec14-1^{ts}*), CTY159 (*MATa ura3-52 lys2-801 Δhis3-200 sec14-1^{ts} kes1 Δ*), and CTY303 (*MATa ura3-52 lys2-801 his3Δ-200 sec14Δ cki1Δ::HIS3*) (Cleves et al., 1991; Fang et al., 1996; Li et al., 2002). Gene replacement constructs were used to integrate *SEC14_{CG}*, *SEC14_{CA}* and *SEC14_{CA}^{M154V,C154V}* expression cassettes into the LEU2 locus as described by Khan et al., (Khan et al., 2016). Yeast strains were grown on YPD (yeast extract 1%, peptone 2%, dextrose 2%) plates or in liquid medium. If plasmid selection was necessary, the strains were grown on synthetic complete medium lacking uracil. Compound **1** was obtained from the Novartis compound store. All other reagents, chemicals, and buffer salts were purchased from Sigma-Aldrich Chemicals (St. Louis, MO), Fluka (Buchs, Switzerland), Alfa Aesar (Karlsruhe, Germany) and Acros Organics (Geel, Belgium). Centromeric YCplac33(*URA3*) plasmids carrying *SEC14*, *SFH1* and *sfh1* activation alleles under control of a *SEC14* promoter fragment (Schaaf et al., 2011) as well as episomal high-copy (*2μ*) plasmid pDR195-*SEC14* in which the *SEC14* ORF (without its intron) is expressed under control of a strong plasma membrane

ATPase (*PMA1*) promoter fragment (Schaaf et al., 2008) were described previously. Individual mutations were introduced in YCplac33-*SEC14* by site-directed mutagenesis (QuickChange, Stratagene).

Expression and purification of recombinant proteins

Recombinant *S. cerevisiae*, *C. glabrata* and *C. albicans* Sec14 proteins were purified as previously described (Khan et al., 2016, Schaaf et al., 2008). The murine PITP α structural gene was subcloned into pET28b(+) as an *NcoI*-*SacI* PCR fragment encoding an N-terminal octa-histidine epitope tag appended to the PITP α open reading frame. The construct was transformed in *E. coli* BL21 (DE3) cells and cultured in LB plus antibiotics at 37°C until an OD₆₀₀ of 0.6 was reached. Protein production was induced by adding IPTG to a final concentration of 60 μ M at which time the culture was shifted to 16°C and incubated overnight with shaking. Cells were pelleted, resuspended in buffer A (50 mM NaH₂PO₄ 300 mM NaCl pH 7.8) supplemented with PMSF and 2-mercaptoethanol (1 mM each, final concentration). Cells were disrupted by two successive passages through a French Press (10,000 p.s.i.), and crude lysates clarified by two successive rounds of centrifugation at 2800 g and 27,000 g for 30 minutes each. Clarified lysates were incubated with Co-TALON metal affinity beads for 3 hours at 4°C followed by exhaustive washing with buffer A. Bound proteins were eluted in a 20-200 mM imidazole gradient incremented in 1 ml steps of 20, 40, 60, 80, 100, 150, and 200 mM imidazole in buffer A and evaluated by SDS-PAGE using BSA mass standards to estimate PITP α yield.

Lipid transfer assays

Compounds of interest were maintained as 20 mM stock solutions in DMSO and stored at room temperature in the dark. *In vitro* sensitivities of Sec14p to the compounds was investigated as described by Nile et al. (Nile et al., 2014). Briefly, protein was incubated with DMSO/compound,

as applicable, in the presence of liposomes. Compound concentrations were fixed at 20 μ M throughout the experiments. Total [3 H]-PtdIns input per assay ranged from 8356-9604 c.p.m., background transfer from 436-489 c.p.m., and transfer efficiencies from 14-16%. Protein concentrations were clamped at 287 nM (\sim 10 μ g per assay).

For IC₅₀ determinations, % [3 H]PtdIns transfer (normalized to mock) was plotted as a function of log₁₀ of the compound concentration. The IC₅₀ was determined using GraphPad Prism Version 6 software. IC₅₀ values are determined at 95% confidence level from at least two independent experiments, each done in triplicate. [3 H]-PtdIns input for Sec14, its mutant proteins, Sec14_{CA} and Sec14_{CG}, ranged from 7111-11517 c.p.m. per assay; background ranged between 212-510 c.p.m. per assay. The transfer efficiencies are as follows: Sec14 (25-30%), Sec14_{CA} (39-43%), Sec14_{CG} (30-34%), Sec14^{Y151H} (32-35%), Sec14^{V154G} (15-18%), Sec14^{V155A} (26-31%), Sec14^{S201G} (40-43%) and Sec14^{S173L} (25-27%). Protein was clamped at 10 μ g per assay throughout these experiments.

Functional variomics

A functional variomics screen to isolate SMI-resistant Sec14p variants was performed (Huang et al., 2013; Pries et al., 2016). 6×10^7 *BY4743* yeast transformants harboring the *SEC14* variomic library (the *SEC14* ORF amplified by error-prone PCR and cloned under control of the endogenous promoter into a low-copy expression plasmid, at a pre-determined complexity above 2×10^5 primary alleles, (Huang et al., 2013)) were plated onto a 15 cm petridish containing uracil-free synthetic complete agar supplemented with either 250 μ M of compound 2 or 100 μ M of compound 3. The plates were incubated for four days at 30°C. Ninety-six resistant colonies were picked for each condition, the plasmids purified using the Wizard SV 96 plasmid DNA purification system (A2250, Promega,). The inserts were amplified by PCR Platinum Hot Start PCR Master Mix

(13000012, Invitrogen) using the oligonucleotides 5'CTGTTGGGAAGGGCGATC3' and 5'CCAGGCTTTACTTTATGCT3' respectively and performing the reaction as specified in Invitrogen's manual. Single nucleotide polymorphisms (SNPs) were then identified by Sanger sequencing.

Mutant Validation

To confirm the SNPs identified with the functional variomics screen, the isolated plasmids were cut with SacI and BamHI, ligated with a pBYInt-URA plasmid and transformed into BY4743D8 MATa/a strain, that is deleted for eight genes involved in drug resistance (efflux pumps SNQ2, PDR5, YOR1; transcription factors PDR1, PDR2, PDR3, YAP1, YRM1, detailed genotype is described in the Fungal Strains section above). This sensitized strain was chosen to open up the observable resistance window in the dose-response validation as testing of high compound concentrations were limited by solubility (Table S2). Growth curves were recorded over 24 hours as described in the growth curve section described above. *In vitro* validation with recombinant protein was performed as described above.

Protein Expression, Purification, and Crystallization

Octahistidine-tagged Sec14p was purified from BL21-CodonPlus (DE3)-RIL cells (Agilent Technologies) as described for Sfh1(Schaaf et al., 2006) with minor modifications. Protein expression was induced with 60 mM isopropyl-b-D-thiogalactoside at 16°C for 20 h, prior to harvesting cells and extracting protein in a modified lysis buffer (300 mM NaCl, 25 mM sodium phosphate pH 7.5 and 5mM β -mercaptoethanol). After purification with a Ni-NTA affinity resin (Macherey-Nagel), the protein was subjected to size exclusion chromatography (Superdex 75 16/600 column, GE Healthcare) at a flow rate of 1 mL/min in modified lysis buffer. Fractions of the second peak were pooled and concentrated to 5 mg/ml. Initial crystallization screens were

carried out manually by sampling an array of circa 1500 conditions that represent variations on crystallization conditions established for the Sec14 homolog Sfh1 (Schaaf et al., 2006, 2008). In this initial screen, His8-Sec14p was supplemented with 1 volume % compound 2 (30 mM in DMSO), and a sitting-drop geometry was employed in which drops consisted of 1 μ L protein/compound solution and 1 μ l well solution. After an incubation time of ca. 1 week at room temperature, crystals appeared in one condition where the solution consisted of 129.5 mM sodium acetate, 64.8 mM TRIS, 4.6 % (w/v) PEG 4000, and 11.9 % (v/v) glycerol adjusted to pH 7.0 (by acetic acid).

Crystallography

For data collection, crystals were transferred to a cryo solution (129.5 mM sodium acetate, 64.8 mM TRIS, 10 % (w/v) PEG 4000, 20 % (v/v) glycerol, pH 7.0) and flash frozen in liquid nitrogen. Diffraction data were collected at the Beamline PXII of the Swiss Light Source. Data scaling and processing was performed with XDS (Kabsch, 1993). The structure was solved by Molecular Replacement with PHASER (Mccoy et al., 2007) using the structure of Sec14p prior to removal of the detergent coordinates (pdb id.: 1aua (Sha et al., 1998)). Cycles of model building and restrained refinement were carried out in COOT and PHENIX (Adams et al., 2010; Emsley and Cowtan, 2004). Ligand restraints were generated with Jligand (Lebedev et al., 2012). Protein-ligand interaction was analysed with PLIP (Salentin et al., 2015). Protein structure figures were generated using PyMOL (<http://www.pymol.org>). The coordinates and structure factors have been deposited in the RSCB PDB database with ID code 6F0E.

Antifungal Testing

Fungal strains used for testing were as follows: *Candida albicans* (ATCC 10231), *Candida glabrata* (ATCC 2001), *Cryptococcus neoformans* (DSM 70219) *Aspergillus brasiliensis* (ATCC

16404). Antifungal susceptibility testing was performed in triplicates according to the Clinical and Laboratory Standards Institute (CLSI) guidelines for broth microdilution M27-A3 and M38-A2 (Wayne, 2008a, 2008b). By performing 1:2 serial dilutions, 10 concentrations in a range between 200 and 0.3 μM were tested for growth inhibitory activity on solid medium in 8 cm petridishes prepared with 15 ml Mueller-Hinton agar medium (2.0 g/L beef extract, 17.5 g/L casein hydrolysate, 1.5 g/L starch, 17 g/L agar), with pH adjusted to pH 7.2, in triplicates. 1 μl spore inoculi were spotted manually onto the plates and absence of growth was scored visually after 72 hours incubation at 30°C to determine the minimal inhibitory concentration.

References

Adams, P.D., Afonine, P.V., Bunkoczi, G., Chen, V.B., Davis, I.W., Echols, N., Headd, J.J., Hung, L.W., Kapral, G.J., Grosse-Kunstleve, R.W., et al. (2010). PHENIX: a comprehensive Python-based system for macromolecular structure solution. *Acta Crystallogr D* 66, 213-221.

Bankaitis, V.A., Aitken, J.R., Cleves, A.E., and Dowhan, W. (1990). An essential role for a phospholipid transfer protein in yeast Golgi function. *Nature* 347, 561-562.

Bankaitis, V.A., Malehorn, D.E., Emr, S.D., and Greene, R. (1989). The *Saccharomyces cerevisiae* SEC14 gene encodes a cytosolic factor that is required for transport of secretory proteins from the yeast Golgi complex. *The Journal of Cell Biology* 108, 1271-1281.

Bankaitis, V.A., Mousley, C.J., and Schaaf, G. (2010). The Sec14 superfamily and mechanisms for crosstalk between lipid metabolism and lipid signaling. *Trends Biochem Sci* 35, 150-160.

Benli, M., Döring, F., Robinson, D.G., Yang, X., and Gallwitz, D. (1996). Two GTPase isoforms, Ypt31p and Ypt32p, are essential for Golgi function in yeast. *The EMBO Journal* 15, 6460-6475.

Brown, G.D., Denning, D.W., Gow, N.A.R., Levitz, S.M., Netea, M.G., and White, T.C. (2012). Hidden Killers: Human Fungal Infections. *Science Translational Medicine* 4, 165rv113-165rv113.

Chayakulkeeree, M., Johnston, S.A., Oei, J.B., Lev, S., Williamson, P.R., Wilson, C.F., Zuo, X., Leal, A.L., Vainstein, M.H., Meyer, W., et al. (2011). SEC14 is a specific requirement for secretion of phospholipase B1 and pathogenicity of *Cryptococcus neoformans*. *Molecular Microbiology* 80, 1088-1101.

Cleves, A.E., McGee, T.P., Whitters, E.A., Champlon, K.M., Aitken, J.R., Dowhan, W., Goebel, M., and Bankaitis, V.A. (1991). Mutations in the CDP-choline pathway for phospholipid biosynthesis bypass the requirement for an essential phospholipid transfer protein. *Cell* 64, 789-800.

Cleves, A.E., Novick, P.J., and Bankaitis, V.A. (1989). Mutations in the SAC1 gene suppress defects in yeast Golgi and yeast actin function. *The Journal of Cell Biology* 109, 2939-2950.

El-Faham, A., and Albericio, F. (2010). COMU: a third generation of uronium-type coupling reagents. *J Pept Sci* 16, 6-9.

El-Faham, A., Subiros Funosas, R., Prohens, R., and Albericio, F. (2009). COMU: a safer and more effective replacement for benzotriazole-based uronium coupling reagents. *Chemistry* 15, 9404-9416.

Emsley, P., and Cowtan, K. (2004). Coot: model-building tools for molecular graphics. *Acta Crystallogr D* 60, 2126-2132.

Fairn, G.D., Curwin, A.J., Stefan, C.J., and McMaster, C.R. (2007). The oxysterol binding protein Kes1p regulates Golgi apparatus phosphatidylinositol-4-phosphate function. *Proceedings of the National Academy of Sciences of the United States of America* 104, 15352-15357.

Fang, M., Kearns, B.G., Gedvilaite, A., Kagiwada, S., Kearns, M., Fung, M.K., and Bankaitis, V.A. (1996). Kes1p shares homology with human oxysterol binding protein and participates in a novel regulatory pathway for yeast Golgi-derived transport vesicle biogenesis. *The EMBO Journal* 15, 6447-6459.

Filipuzzi, I., Cotesta, S., Perruccio, F., Knapp, B., Fu, Y., Studer, C., Pries, V., Riedl, R., Helliwell, S.B., Petrovic, K.T., et al. (2016). High-Resolution Genetics Identifies the Lipid Transfer Protein Sec14p as Target for Antifungal Ergolines. *PLoS Genet* 12, e1006374.

Giaever, G., Shoemaker, D.D., Jones, T.W., Liang, H., Winzeler, E.A., Astromoff, A., and Davis, R.W. (1999). Genomic profiling of drug sensitivities via induced haploinsufficiency. *Nature genetics* 21, 278-283.

Hoepfner, D., Helliwell, S.B., Sadlish, H., Schuierer, S., Filipuzzi, I., Brachat, S., Bhullar, B., Plikat, U., Abraham, Y., Altorfer, M., et al. (2014). High-resolution chemical dissection of a model eukaryote reveals targets, pathways and gene functions. *Microbiological Research* 169, 107-120.

Hoepfner, D., Karkare, S., Helliwell, S.B., Pfeifer, M., Trunzer, M., De Bonnechose, S., Zimmerlin, A., Tao, J., Richie, D., Hofmann, A., et al. (2012). An Integrated Approach for Identification and Target Validation of Antifungal Compounds Active against Erg11p. *Antimicrobial Agents and Chemotherapy* 56, 4233-4240.

Hoon, S., Smith, A.M., Wallace, I.M., Suresh, S., Miranda, M., Fung, E., Proctor, M., Shokat, K.M., Zhang, C., Davis, R.W., et al. (2008). An integrated platform of genomic assays reveals small-molecule bioactivities. *Nature Chemical Biology* 4, 498-506.

Huang, C.-F., Buu, L.-M., Yu, W.-L., and Lee, F.-J.S. (1999). Characterization of a Novel ADP-ribosylation Factor-like Protein (yARL3) in *Saccharomyces cerevisiae*. *Journal of Biological Chemistry* 274, 3819-3827.

Huang, Z., Chen, K., Zhang, J., Li, Y., Wang, H., Cui, D., Tang, J., Liu, Y., Shi, X., Li, W., et al. (2013). A Functional Variomics Tool for Discovering Drug-Resistance Genes and Drug Targets. *Cell Reports* 3, 577-585.

Kabsch, W. (1993). Automatic Processing of Rotation Diffraction Data from Crystals of Initially Unknown Symmetry and Cell Constants. *J Appl Crystallogr* 26, 795-800.

- Khan, D., McGrath, K.R., Dorosheva, O., Bankaitis, V.A., and Tripathi, A. (2016). Structural elements that govern Sec14-like P1TP sensitivities to potent small molecule inhibitors. *Journal of Lipid Research* 57, 650-662.
- Lebedev, A.A., Young, P., Isupov, M.N., Moroz, O.V., Vagin, A.A., and Murshudov, G.N. (2012). JLigand: a graphical tool for the CCP4 template-restraint library. *Acta Crystallogr D* 68, 431-440.
- Lee, A.Y., St Onge, R.P., Proctor, M.J., Wallace, I.M., Nile, A.H., Spagnuolo, P.A., Jitkova, Y., Gronda, M., Wu, Y., Kim, M.K., et al. (2014). Mapping the cellular response to small molecules using chemogenomic fitness signatures. *Science* 344, 208-211.
- Lee, F.-J.S., Huang, C.-F., Yu, W.-L., Buu, L.-M., Lin, C.-Y., Huang, M.-C., Moss, J., and Vaughan, M. (1997). Characterization of an ADP-ribosylation Factor-like 1 Protein in *Saccharomyces cerevisiae*. *Journal of Biological Chemistry* 272, 30998-31005.
- Li, X., Rivas, M.P., Fang, M., Marchena, J., Mehrotra, B., Chaudhary, A., Feng, L., Prestwich, G.D., and Bankaitis, V.A. (2002). Analysis of oxysterol binding protein homologue Kes1p function in regulation of Sec14p-dependent protein transport from the yeast Golgi complex. *The Journal of Cell Biology* 157, 63-78.
- Li, X., Routt, S.M., Xie, Z., Cui, X., Fang, M., Kearns, M.A., Bard, M., Kirsch, D.R., and Bankaitis, V.A. (2000). Identification of a Novel Family of Nonclassic Yeast Phosphatidylinositol Transfer Proteins Whose Function Modulates Phospholipase D Activity and Sec14p-independent Cell Growth. *Molecular Biology of the Cell* 11, 1989-2005.
- Lipinski, C.A., Lombardo, F., Dominy, B.W., and Feeney, P.J. (2001). Experimental and computational approaches to estimate solubility and permeability in drug discovery and development settings. *Adv Drug Deliv Rev* 46, 3-26.
- Lopez, M.C., Nicaud, J.M., Skinner, H.B., Vergnolle, C., Kader, J.C., Bankaitis, V.A., and Gaillardin, C. (1994). A phosphatidylinositol/phosphatidylcholine transfer protein is required for differentiation of the dimorphic yeast *Yarrowia lipolytica* from the yeast to the mycelial form. *The Journal of Cell Biology* 125, 113-127.
- Lum, P.Y., Armour, C.D., Stepaniants, S.B., Cavet, G., Wolf, M.K., Butler, J.S., Hinshaw, J.C., Garnier, P., Prestwich, G.D., Leonardson, A., et al. (2004). Discovering modes of action for therapeutic compounds using a genome-wide screen of yeast heterozygotes. *Cell* 116, 121-137.
- Mccoy, A.J., Grosse-Kunstleve, R.W., Adams, P.D., Winn, M.D., Storoni, L.C., and Read, R.J. (2007). Phaser crystallographic software. *J Appl Crystallogr* 40, 658-674.
- Monteoliva, L., Sánchez, M., Pla, J., Gil, C., and Nombela, C. (1996). Cloning of *Candida albicans* SEC14 gene homologue coding for a putative essential function. *Yeast* 12, 1097-1105.

Mousley, C.J., Tyeryar, K., Ile, K.E., Schaaf, G., Brost, R.L., Boone, C., Guan, X., Wenk, M.R., and Bankaitis, V.A. (2008). Trans-Golgi network and endosome dynamics connect ceramide homeostasis with regulation of the unfolded protein response and TOR signaling in yeast. *Molecular Biology of the Cell* 19, 4785-4803.

Mousley, C.J., Yuan, P., Gaur, N.A., Trettin, K.D., Nile, A.H., Deminoff, S.J., Dewar, B.J., Wolpert, M., Macdonald, J.M., Herman, P.K., et al. (2012). A sterol-binding protein integrates endosomal lipid metabolism with TOR signaling and nitrogen sensing. *Cell* 148, 702-715.

Nikawa, J., Tsukagoshi, Y., and Yamashita, S. (1991). Isolation and characterization of two distinct myo-inositol transporter genes of *Saccharomyces cerevisiae*. *Journal of Biological Chemistry* 266, 11184-11191.

Nile, A.H., Tripathi, A., Yuan, P., Mousley, C.J., Suresh, S., Wallace, I.M., Shah, S.D., Pohlhaus, D.T., Temple, B., Nislow, C., et al. (2014). PITPs as targets for selectively interfering with phosphoinositide signaling in cells. *Nat Chem Biol* 10, 76-84.

Parsons, A.B., Lopez, A., Givoni, I.E., Williams, D.E., Gray, C.A., Porter, J., Chua, G., Sopko, R., Brost, R.L., Ho, C.H., et al. (2006). Exploring the mode-of-action of bioactive compounds by chemical-genetic profiling in yeast. *Cell* 126, 611-625.

Pfaller, M.A., Pappas, P.G., and Wingard, J.R. (2006). Invasive Fungal Pathogens: Current Epidemiological Trends. *Clinical Infectious Diseases* 43, S3-S14.

Phillips, S.E., Vincent, P., Rizzieri, K.E., Schaaf, G., Bankaitis, V.A., and Gaucher, E.A. (2006). The Diverse Biological Functions of Phosphatidylinositol Transfer Proteins in Eukaryotes. *Critical Reviews in Biochemistry and Molecular Biology* 41, 21-49.

Pierce, S.E., Davis, R.W., Nislow, C., and Giaever, G. (2007). Genome-wide analysis of barcoded *Saccharomyces cerevisiae* gene-deletion mutants in pooled cultures. *Nat Protocols* 2, 2958-2974.

Prasad, R., Shah, A.H., and Rawal, M.K. (2016). Antifungals: Mechanism of Action and Drug Resistance. In *Yeast Membrane Transport*, J. Ramos, H. Sychrová, and M. Kschischo, eds. (Cham: Springer International Publishing), pp. 327-349.

Pries, V., Cotesta, S., Riedl, R., Aust, T., Schuierer, S., Tao, J., Filipuzzi, I., and Hoepfner, D. (2016). Advantages and Challenges of Phenotypic Screens: The Identification of Two Novel Antifungal Geranylgeranyltransferase I Inhibitors. *Journal of Biomolecular Screening* 21, 306-315.

Richie, D.L., Thompson, K.V., Studer, C., Prindle, V.C., Aust, T., Riedl, R., Estoppey, D., Tao, J., Sexton, J.A., Zabawa, T., et al. (2013). Identification and Evaluation of Novel Acetolactate Synthase Inhibitors as Antifungal Agents. *Antimicrobial Agents and Chemotherapy* 57, 2272-2280.

Roemer, T., and Krysan, D.J. (2014). Antifungal Drug Development: Challenges, Unmet Clinical Needs, and New Approaches. *Cold Spring Harbor Perspectives in Medicine* 4.

Roemer, T., Xu, D., Singh, S.B., Parish, C.A., Harris, G., Wang, H., Davies, J.E., and Bills, G.F. (2011). Confronting the challenges of natural product-based antifungal discovery. *Chemistry & Biology* 18, 148-164.

Rudge, S.A., Sciorra, V.A., Iwamoto, M., Zhou, C., Strahl, T., Morris, A.J., Thorner, J., and Engebrecht, J. (2004). Roles of Phosphoinositides and of Spo14p (phospholipase D)-generated Phosphatidic Acid during Yeast Sporulation. *Molecular Biology of the Cell* 15, 207-218.

Ryan, M.M., Temple, B.R.S., Phillips, S.E., and Bankaitis, V.A. (2007). Conformational dynamics of the major yeast phosphatidylinositol transfer protein Sec14p: Insight into the mechanisms of phospholipid exchange and diseases of Sec14p-like protein deficiencies. *Molecular Biology of the Cell* 18, 1928-1942.

Salentin, S., Schreiber, S., Haupt, V.J., Adasme, M.F., and Schroeder, M. (2015). PLIP: fully automated protein-ligand interaction profiler. *Nucleic Acids Research* 43, W443-447.

Schaaf, G., Betts, L., Garrett, T.A., Raetz, C.R.H., and Bankaitis, V.A. (2006). Crystallization and preliminary X-ray diffraction analysis of phospholipid-bound Sfh1p, a member of the *Saccharomyces cerevisiae* Sec14p-like phosphatidylinositol transfer protein family. *Acta Crystallogr F* 62, 1156-1160.

Schaaf, G., Dynowski, M., Mousley, C.J., Shah, S.D., Yuan, P., Winklbauer, E.M., de Campos, M.K.F., Trettin, K., Quinones, M.-C., Smirnova, T.I., et al. (2011). Resurrection of a functional phosphatidylinositol transfer protein from a pseudo-Sec14 scaffold by directed evolution. *Molecular Biology of the Cell* 22, 892-905.

Schaaf, G., Ortlund, E.A., Tyeryar, K.R., Mousley, C.J., Ile, K.E., Garrett, T.A., Ren, J., Woolls, M.J., Raetz, C.R.H., Redinbo, M.R., et al. (2008). Functional Anatomy of Phospholipid Binding and Regulation of Phosphoinositide Homeostasis by Proteins of the Sec14 Superfamily. *Molecular Cell* 29, 191-206.

Schmiedel, Y., and Zimmerli, S. (2016). Common invasive fungal diseases: an overview of invasive candidiasis, aspergillosis, cryptococcosis, and *Pneumocystis pneumonia*. *Swiss Med. Wkly.* 146, w14281.

Sha, B., Phillips, S.E., Bankaitis, V.A., and Luo, M. (1998). Crystal structure of the *Saccharomyces cerevisiae* phosphatidylinositol-transfer protein. *Nature* 391, 506-510.

Wayne, P. (2008a). Reference method for broth dilution antifungal susceptibility testing of filamentous fungi; approved standard - 2nd ed. CLSI document MA38-A2. In Reference method for broth dilution antifungal susceptibility testing of filamentous fungi; Approved Standard - Second Edition. CLSI Document MA38-A2 (Clinical and Laboratory Standards Institute).

Wayne, P. (2008b). Reference Method for Broth Dilution Antifungal Susceptibility Testing of Yeast; Approved Standard – Third Edition. CLSI Document M27-A3 (Clinical Laboratory Standards Institute).

CHAPTER IV

SFH5, A SEC14 HOMOLOG, IS A HEME BINDING PROTEIN

Summary

A Sec14-like protein from *S. cerevisiae*, Sfh5, was characterized for the first time. We show that recombinant Sfh5 is a heme binding protein which has never been observed for a PITP. Sfh5 binds to heme with a 1:1 stoichiometry. Using UV-vis, Electron Paramagnetic Resonance and Mössbauer spectroscopies, we elucidated the biophysical properties of the heme iron center. We determined the crystal structure of Sfh5 at 2.7Å resolution through X-Ray crystallography and discovered a novel mode of heme-binding. We analyzed specific mutant versions of Sfh5 that weaken or totally abolish heme binding. And discovered an antagonistic relationship between heme binding and phosphatidylinositol transfer abilities of the protein. Taken together these data expand our knowledge of phosphatidylinositol transfer proteins in eukaryotes.

Introduction

Fe-Protoporphyrin IX or heme has been implicated in a plethora of biological processes. As a cofactor of multiple proteins and enzymes, heme is essential to storage and transfer of gases, redox reactions, cell cycle regulation, microRNA processing etc (Schneider et al., 2007, Hamza et al., 2012, Shen et al., 2014). Yeast strains deficient in heme biosynthesis are non-viable unless supplied with exogenous heme or a relevant metabolic intermediate. At the same time, free heme within cells is toxic and so its production and utilization needs to be kept under tight regulation.

Amphipathic nature of heme affords it an easy ability to intercalate within lipid membranes. Through its peroxidase activity or by reacting with oxygen heme can generate harmful hydroxy radicals that attack cellular lipids and proteins alike. Under certain conditions, this may have protective effects on the cell too. Lipids rich in polyunsaturated fatty acids (PUFA) are prime targets of peroxidative attack by reactive oxygen species (ROS). Cytochrome *c*, a hemoprotein, uses its peroxidase activity to modify cardiolipin PUFAs in mitochondrial membranes, as well as other phospholipids such as PtdCho and PtdSer. Glutathione peroxidases use reduced glutathione to convert phospholipid-esterified polyunsaturated fatty acid hydroperoxides into hydroxyl species, thereby detoxifying membrane phospholipids. Heme has also been implicated in activating protein kinase C in mosquitoes, that serves to actively suppress ROS generation (Natarajan et. al., 2014, Oliviera et. al., 2011).

Biosynthesis of heme in *S. cerevisiae* consists of a series of well-studied steps that are distributed between the mitochondria and cytosol. HEM1 enzyme catalyzes the condensation of glycine and succinyl-CoA to form 5-aminolevulinic acid (ALA) in the mitochondrial matrix. ALA is exported to the cytoplasm where a series of reactions lead to the formation of coproporphyrinogen III which is then transported back to mitochondria. Coproporphyrinogen III

undergoes two rounds of oxidative decarboxylation to form porphyrinogen IX, a direct precursor of heme. HEM15/Ferrochelatase enzyme then catalyzes the insertion of ferrous ion into the porphyrinogen ring system to produce heme *b*. After its synthesis in mitochondria, heme is presumably delivered to other cellular compartments that need it (Hamza et. al., 2012, Korolnek et. al., 2014).

Many proteins have been posited to serve as “chaperones” that mop up freshly produced heme from mitochondria in mammalian cells. Congruency between the endocytic and secretory pathways of *S. cerevisiae* have led some to speculate the presence of porphyrin transfer proteins, analogous to lipid transfer proteins that may deliver heme to specific cellular compartments. Direct evidence for the same, however, is lacking (Korolnek et. al., 2014). This necessitates a detailed understanding of the mechanisms by which lipid transfer proteins execute their functions.

Eukaryotic lipid transfer proteins interface vital cell signaling events with metabolic processes. The yeast phosphatidylinositol transfer protein Sec14 has been recognized as key player in coupling PtdCho biogenesis with regulated production of PtdIns-4-P signaling molecules. It does so by regulating the accessibility of membrane PtdIns to interfacial kinases that produce PtdIns-4-P. By definition, all PITPs bind PtdIns and have been found to be capable of channeling PtdIns-4-OH kinase activity towards specific biological outcomes. In addition to PtdIns, the lipid binding domain of these proteins have been found to bind other amphipathic lipids. In addition to Sec14, yeast has five more Sec14-like proteins. Sfh1 has been crystallized with PtdEtn, in addition to PtdIns and PtdCho, whereas Sfh3 has been reported to bind ergosterol (Schaaf et. al., 2008, Holic et. al., 2014). Human Sec14-like proteins such as the α -tocopherol transfer protein has been crystallized with α -tocopherol, while Sec14L2 has been shown to bind squalene. However, the role

of such secondary ligands in potentiating lipid signaling activities that are mediated by a PITPs, is not well understood. (Min et al., 2003, Welti et al., 2007, Stocker et al., 2002).

Sfh5 is a non-classical Sec14-homolog that shares less than 30% identity with Sec14. Although non-essential for cell growth under laboratory conditions, studies have shown that Sfh5 can stimulate activation of phospholipase D in ‘bypass-Sec14’ strains that allow them to be viable in Sec14-null situations (Li et al., 2000). In a temperature sensitive strain of Sec14, overexpression of Sfh5 at restrictive temperature complemented the strain associated growth effects, albeit weakly. A homolog of Sfh5 has been also implicated in membrane trafficking processes of fungal pathogen, *Cryptococcus neoformans*, but its precise role is unclear (Chayakulkeeree et al., 2011).

We now report that Sfh5 is a heme binding protein. The function of a hemoprotein is closely linked to the solvent accessibility of heme. Proteins with deeply buried, solvent-protected hemes, generally tend to be enzymes or heme sequesterers. A higher solvent accessibility correlates with transient-heme binding and release. The unique microenvironment within which a heme is situated, impacts its catalytic and molecule-binding abilities. A hallmark feature of Sec14-like proteins is a hydrophobic chamber at the core of the protein that constitutes its lipid binding domain. We solved a crystal structure of Sfh5 and show that the heme docks within the lipid binding chamber of protein and is highly solvent-protected. We analyzed the spectroscopic properties of the protein and present a comprehensive analysis of the electronic properties of the iron center of the protein.

To our knowledge this is the first instance of a PITP binding heme. As a ubiquitous domain, PITPs can be standalone proteins or multi-modular, as observed throughout the metazoan kingdom. The nature of their physiological ligands is an active area of discovery. A heme-bound

PITP is likely to provoke a re-look at the ligand binding abilities of these proteins and expand their functionality from being mere binders of lipid to being capable of enzymatic action.

Results

Sfh5 is an iron binding protein

Sfh5 was cloned from *S. cerevisiae* and placed in a pET28b(+)vector with N-terminal octahistidine tag. *E. coli* BL21 (DE3) cells transformed with this construct were grown in lysogeny broth (LB) media and protein expression was induced with isopropyl β -D-1-thiogalactopyranoside. Within a few hours, the cells acquired a reddish-brown color that was not seen when plasmids harboring Sec14 were expressed in a similar manner (Figure 4-1A). Upon lysis and purification, recombinant Sfh5 protein was found to have a distinct brown color that was not lost upon dialysis or gel filtration treatments (Figure 4-1B).

This property was not tag-dependent either as expression of a tagless version of Sfh5 in *E. coli* elicited identical phenotype. To confirm the identity of the bound cofactor, we digested the recombinant protein with 5% HNO₃ and performed inductively coupled plasma mass spectrometry with the clarified supernatant. The protein was found to be associated with iron. For 133 μ M protein, the iron concentration was found to be 93 μ M and protein i.e. an iron to protein stoichiometry of 0.7 to 1 was observed.

Sfh5 binds heme

To determine if Sfh5 proteins from other fungal species showed similar characteristics, we purified Sfh5 from *Candida albicans* (Sfh5_{CA}) and noticed a similar brown color. Colored proteins are generally associated with divalent metal cofactors, capable of *d*-orbital transitions and co-ordinate

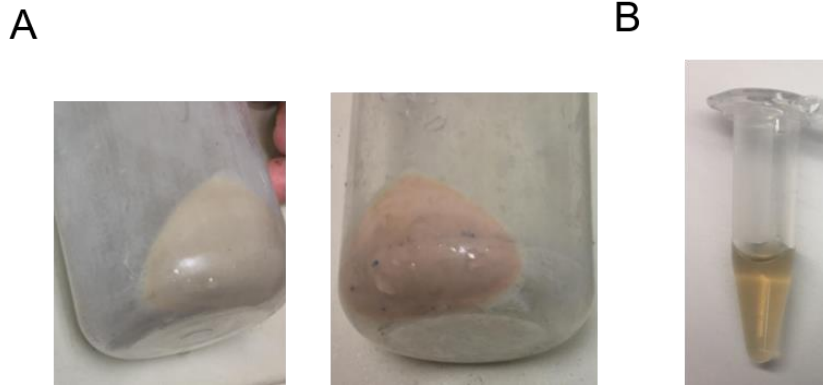


Figure 4-1. Visual properties of *E. coli* cells when expressing Sfh5 and picture of the purified protein

(A) On left, image of an *E. coli* cell pellet prepared from a bacterial culture expressing recombinant Sec14 from *S. cerevisiae*. The pellet of *E. coli* expressing Sfh5 is provided on the right side for contrast.

(B) Recombinant purified Sfh5p at a concentration of 5 mg/ml (~150 μ M).

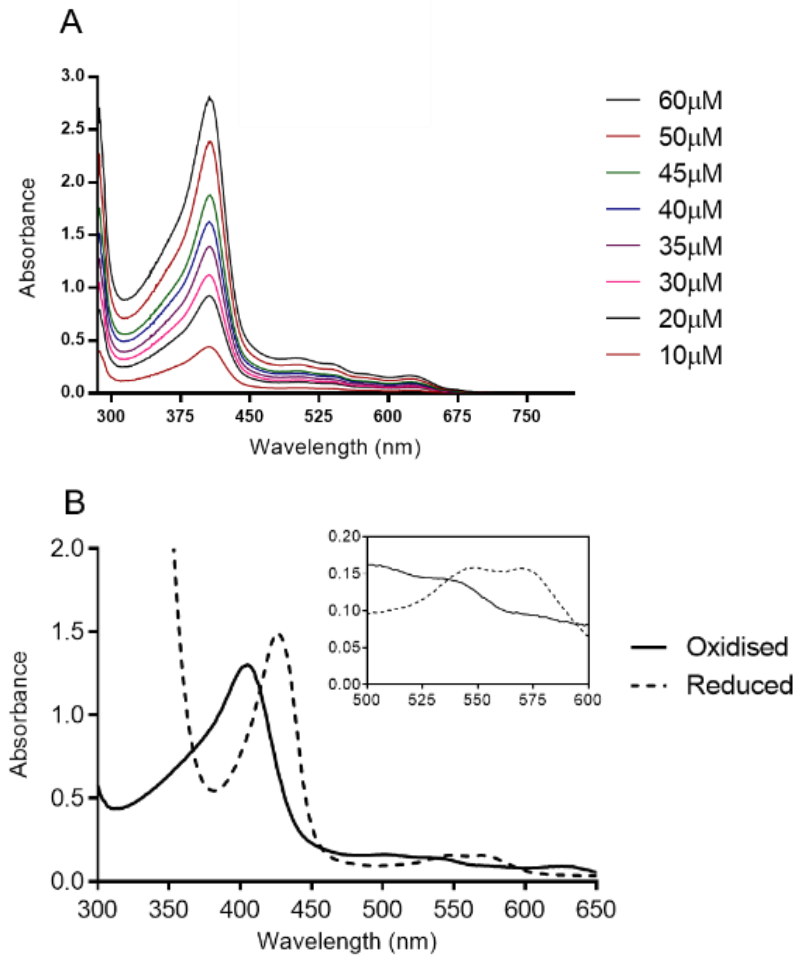


Figure 4-2. Recombinant Sfh5 protein binds heme

A) UV-vis spectra of Sfh5 protein at multiple concentrations was measured in a Cary 50 spectrophotometer.

B) Spectra of a 35 μ M solution of Sfh5 was taken before and after reduction with a strong reducing agent, sodium dithionite. The inset focuses on the spectra between wavelengths 500-600nm.

bond formation. Absence of cysteine in the Sfh5_{CA} amino acid sequence allowed us to rule out the involvement of a sulfur-mediated chromophore such as a [Fe-S] cluster. We used ultraviolet spectroscopy to gain further insights into the spectroscopic features of Sfh5. A distinctive spectrum emerged with an absorption maximum of 404nm that was identified as the classical (Soret) γ peak associated with heme proteins. The intensity of the peak increased in a manner dependent upon the protein concentration (Figure 4-2A). Upon reduction with excess sodium dithionite, the Soret peak shifted to 426 nm. Additional spectral features emerged in the reduced sample at 550 nm and 568 nm wavelengths, that were associated with the characteristic α and β bands of protoporphyrin groups (Figure 4-2B). Taken together these data indicate that Sfh5 is *bona fide* heme binding protein.

Structural features of Sfh5

To understand the structural basis of heme binding in Sfh5, we determined its crystal structure. Among yeast PITPs, Sfh5 and Sec14 share the lowest homology with 17.4% identity and 33% similarity. Sfh5 formed brown rod-shaped crystals (Figure 4-3A). Attempts to phase the diffraction dataset by using previously solved structures of PITPs as search models, failed (Sha et al., 1998; Schaaf et al., 2008; Ren et al., 2014). So we exploited our knowledge of presence of iron in Sfh5 and used the iron anomalous signal at Cu K α edge to obtain phase information. Upon refinement, a 2.7Å structure was obtained (Table 4-1).

The solvent content of the final structure was ~64% which was likely due to the geometry of Sfh5 crystals in the unit cell (Figure 4-3B). In an asymmetric unit, Sfh5 crystallized as a homotrimer with each of the three monomeric units, binding a molecule of heme (Figure 4-3C). Adopting a Sec14-like fold, with 8 α helices, 5 β strands, 5 short 3_{10} helices and a β -hairpin turn, Sfh5 retains the major structural elements associated with Sec14 (Sha et al., 1998; Schaaf et al.,

2008; Ren et al., 2014). A tripod motif formed by helices A1, A3 and A4 characterizes the N-terminal, but unlike Sec14, the loop connecting A1/A3 (A2/A3 in Sec14) is expanded to host another helix, A2. The central hydrophobic chamber is defined by a 5 β sheet floor with two α helices A5-A6 on one side. Helix A7 and an extension loop gated the chamber. Compared to the isostructural A10/T4 helix of Sec14, the Sfh5 helical gate is shifted by 15.8 Å towards the pocket thereby describing a “closed” conformation of the protein. Phe228 at the C-terminus of the conserved gating motif KKFL (KPFL in Sec14 and Sfh1) interacts with Lys192 of adjacent helix A6 to stabilize the closed conformation. Hydrophobic interactions between Val229 on the loop extending from helix A7, and Ile195 of helix A6 also contribute to gate closure (Figure 4-3D).

In all Sec14-fold proteins, the conformational dynamics of helical gate are governed by a gating module composed of a network of hydrogen-bonded substructures. The string motif is one such element that assumes a strict 3_{10} -helix pose in Sec14 but loosens up in Sfh5 to form what we term a pseudo-string motif. Residues extending from this motif do not fold into 3_{10} -helices or β sheet structures as seen in Sec14. Instead, they loop around the hydrophobic chamber before forming an α helix, away from the pocket surface.

Heme binding motif

The most remarkable feature of the structure was the presence of electron density consistent with a heme *b* molecule within the hydrophobic chamber (Figure 4-4A, B). The porphyrin ring plane runs parallel to β sheets B3-B5 and helix A6, making 25 van der Waal contacts with pocket residues. The heme molecule was sequestered just beneath the protein surface, but buried. A calculation of solvent exposed surface area (SASA) for bound heme was found to be a 8 Å² as compared to 835 Å² for free heme, that is, a less than 1% value, reflecting the buried nature of heme (Figure 4-4C). Opening of the gating helix of the cavity was predicted to enhance solvent

Table 4-1. Crystal structure model refinement parameters for Sfh5

| | |
|---|----------------------------------|
| <u>Data collection</u> | |
| Wavelength (Å) | 1.5498 |
| Space group | P4 ₃ 2 ₁ 2 |
| a, b, c (Å) | 205.13, 205.13, 68.27 |
| α, β, γ (°) | 90,90,90 |
| Resolution (Å) | 41 - 2.7 (2.8 - 2.7)* |
| <i>R</i> _{merge} | 0.291 (1.736) |
| <i>R</i> _{pim} | 0.049 (0.545) |
| <i>I</i> /σ <i>I</i> | 13.5 (0.8) |
| Completeness (%) | 98.5 % (85.3) |
| Redundancy | 32.2 (9.1) |
| CC _{1/2} % | 0.996 (0.303) |
| <u>Refinement</u> | |
| Resolution (Å) | 41 - 2.7 |
| <u>No. of reflections</u> | |
| Total | 1302155 (34845) |
| Unique | 40447 (3831) |
| <i>R</i> _{work} | 0.236 |
| <i>R</i> _{free} | 0.269 |
| No. of atoms | 7257 |
| Protein | 7123 |
| Ligand | 129 |
| Water | 5 |
| <u>B-factors (Å)²</u> | |
| Protein | 117.1 |
| Ligand | 79.4 |
| Water | 71.8 |
| <u>R.M.S. deviations</u> | |
| Bond angles, rmsd (°) | 0.006 |
| Bond angles, rmsd (°) | 2.37 |
| <u>Ramachandran plot</u> | |
| Ramachandran favoured (%) | 95.32 |
| Ramachandran allowed (%) | 4.68 |
| Ramachandran outliers (%) | 0 |

*Values in parenthesis are for the highest resolution shell

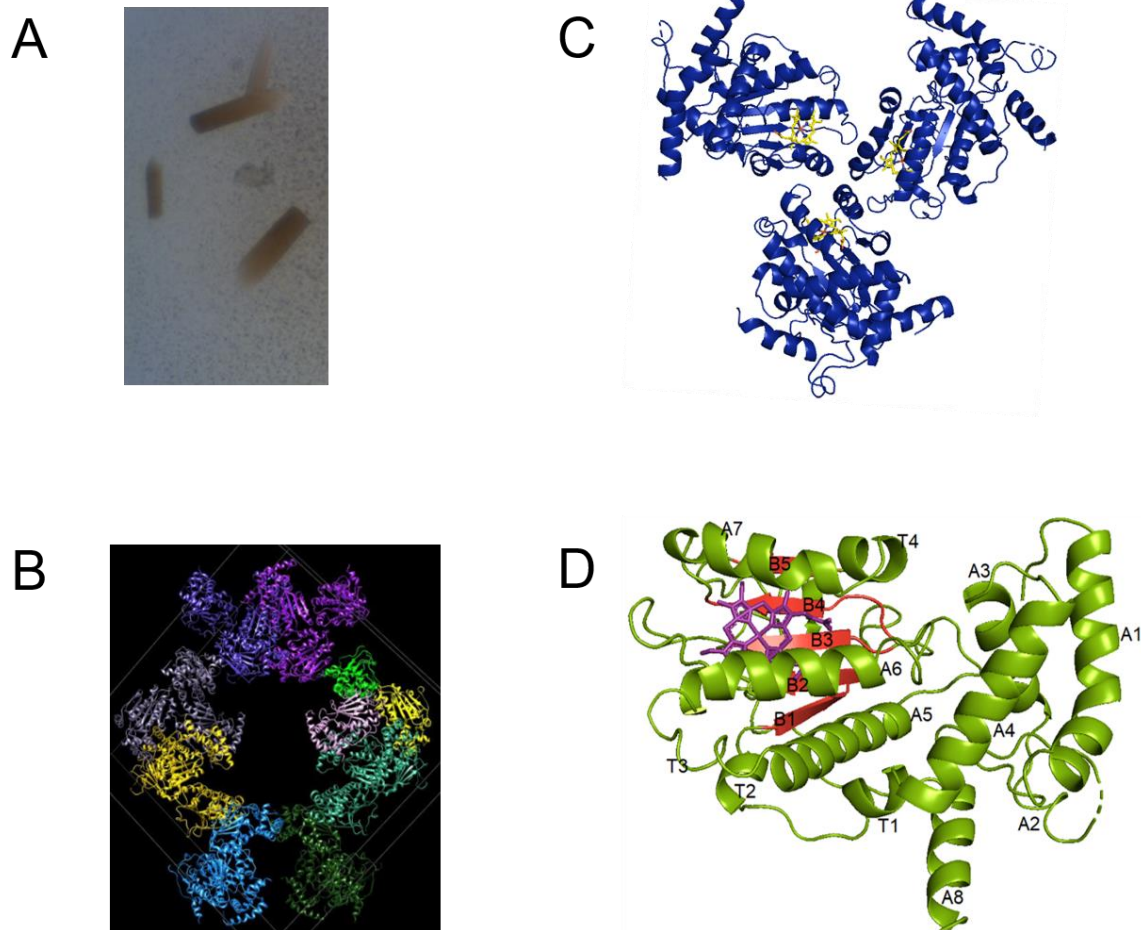


Figure 4-3. Structural features of Sfh5 protein

(A) Reddish brown crystals of Sfh5

(B) The unit cell in which Sfh5 crystallizes.

(C) The asymmetric unit showing a trimeric Sfh5, is rendered in navy blue, the heme center of each monomer is depicted in yellow.

(D) Secondary structure elements of Sfh5.

accessibility of heme. So we simulated an “open” conformation of the protein by repositioning its gating helix with rest of the structural features kept intact (Figure 4-4B). As expected, the SASA value for heme now increased to 55 Å² or 6.5% of free heme. When compared to other heme bound proteins, these values are on the lower end of the spectrum for known SASA values, indicating that the heme is bound tightly to the protein and is likely not exchangeable (Schneider et al., 2007).

A central feature of heme binding in Sfh5 is the coordination of its iron center by Tyr175, part of a loop protruding from β3 sheet in the hydrophobic floor. At 2.4 Å distance, the metal coordination between iron and -OH of the tyrosine is clearly observed in the 2Fo-Fc electron density map (Figure 4-5A). Coordinating with four more nitrogen atoms from the pyrrole subunits of the porphyrin ring, the iron was determined to be in a pentacoordinate state as no distal ligand was detected. His173 is positioned orthogonally with respect to the heme plane, making two distinct interactions with it. The imidazole side chain interacts with the tyrosinyl-OH through hydrogen bonding while concurrently interacting with one of the heme propionates through its imidazole imine. Tyr175 and His173 taken together, form part of a ‘molecular wire’ that connects the iron center of heme with one of its two propionate moieties (Figure 4-5B). An aspartate residue present between Tyr175 and His173 was found to have its sidechain oriented away from the iron center, ruling out any possibility of interaction with the heme iron center. An alignment of fungal Sfh5 homologs indicates that residues His173, Asp174 and Tyr175 form a highly conserved motif.

The second heme propionate is positioned to make electrostatic interactions with Lys209 and Arg148. Other contacts of the heme molecule with the protein included hydrophobic interactions between the heme vinyl/methyl moieties and isoleucine, leucine and valine residues (Ile187, Val194, Ile195, Val214, Val221, Val229, Leu206) present in the lipid binding pocket of Sfh5.

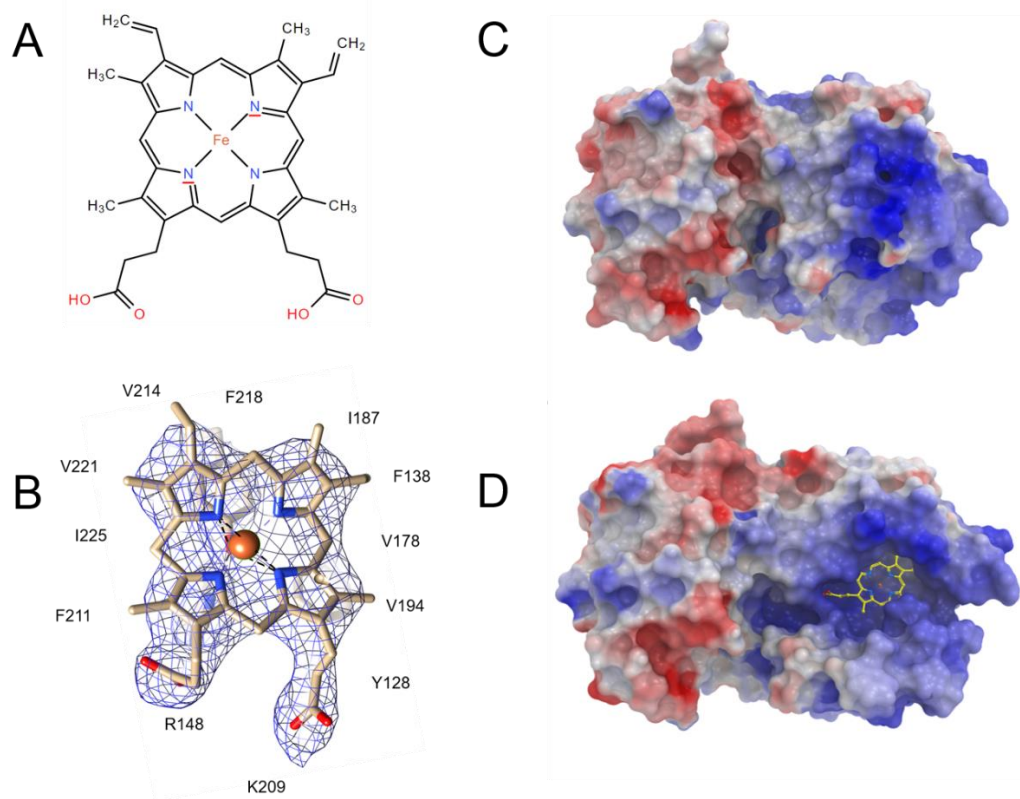


Figure 4-4. Surface electrostatic potentials of “closed” and “open” forms of Sfh5

(A) Structure of a heme *b* molecule

(B) Representative electron density of heme *b* as observed in Sfh5 crystal structure. The $(2F_o - F_c)$ map was calculated with experimentally observed structure factor amplitude F_o and the actual calculated structure factor amplitude F_c ; the map was contoured at 1.2σ .

(C) Electrostatic rendering of the “closed” form of heme bound Sfh5. Electropositive regions are colored in blue while electronegative regions are colored red. Grey regions represent neutral electrostatics.

(D) Electrostatic rendering of the “open” form of heme bound Sfh5. Coloring scheme is same as above.

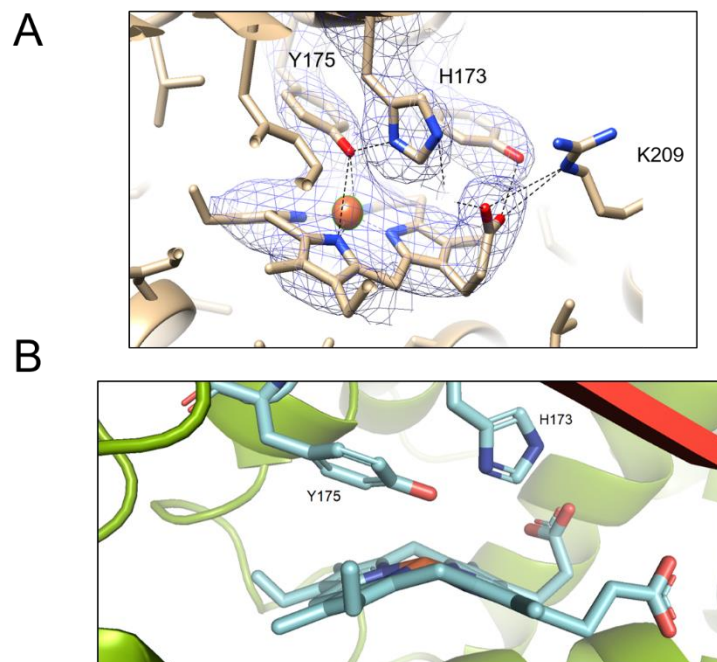


Figure 4-5. The iron co-ordination architecture of Sfh5 protein.

(A) 2Fo-Fc map showing the electron density associated with heme and its coordinating residues (rendered at 1.2σ).

(B) The iron atom is directly coordinated by Y175. A histidine side chain, H173, straddles the heme plane orthogonally, interacting with tyrosinoyl -OH and the -COOH group of one of the propionates.

When the Sfh5 and Sfh1 PL-binding pockets were superimposed with their ligands, the heme appears to be straddling between the distal acyl chains of PL-bound Sfh1. Although we did not detect a bound phospholipid in the hydrophobic pocket, the secondary structure elements associated with PtdIns binding residues are well conserved in Sfh5. As with all non-classical SFH proteins, no residues corresponding to the binding elements for PtdCho are found in Sfh5.

Reduction Potential of Sfh5p

The redox potential of a hemoprotein is closely related to its function. When the axial ligand of heme consists of strong electron donors, the redox potential values are generally negative. We determined the Fe^{III}/Fe^{II} reduction potential of heme bound Sfh5, by measuring the distribution of electrons between the protein and a dye with known redox potential using sodium dithionite as a reductant. The reaction was monitored through a UV-vis spectra and based on the Nernst plot, the redox potential of Sfh5 protein was estimated to be -246 mV (vs. NHE) which was in the expected range (Kaluka et al., 2015) (Figure 4-6A,B).

Mutational analysis of heme-binding ligands of Sfh5

To probe the role of axial ligand in determining the electronic configuration of heme, we made mutant versions of the protein. A Tyr175Ala mutation totally abrogated any heme binding, as did the more conservative Tyr175Phe mutation. The His173Ala mutation, retained heme binding properties, albeit diminished, as judged from the pictures of the WT and mutant proteins at the same concentration (Figure 4-7A). The metal content of the protein as determined by ICP-MS also indicated that mutant versions no longer bind iron. In WT Sfh5, the iron and protein concentrations were 93 μ M and 133 μ M, respectively, or 0.70 Fe/protein molecule. The amount of heme-loading in H173A mutant molecules was only 21% with 29 μ M Fe and 136 μ M protein. Y175F and Y175A

versions of Sfh5 were effectively unable to bind any iron. Loss of Soret band signals in the mutant proteins confirmed that the proteins did not bind heme as tightly as the WT protein (Figure 4-7B).

Heme containing proteins have been reported to display pseudo-peroxidase activity due to the ability of heme center to engage in one- or two-electron chemistry with peroxides. (Hamza, et. al., 2014). We tested if Sfh5 behaved similarly and if that could be used to distinguish heme-binding proteins from their apo forms. Protein fractions were run through a non-reducing SDS-PAGE and transferred to nitrocellulose membranes before being probed with a luminol/enhancer and peroxidase-based reagent for chemiluminescent staining of heme. Peroxidase-responsive staining was observed in Sfh5 containing fractions but not with Y175F version of the protein (Figure 4-7C). Taken together, these data indicate that mutations in proximal residues renders Sfh5 defective to heme binding.

Electron Paramagnetic Resonance and Mössbauer spectroscopy study of Sfh5

To understand the impact of H173A and Y175A mutations on the magnetic and electronic properties of the iron center we used electron paramagnetic resonance (EPR). In the 10 K X-band EPR spectrum, WT Sfh5 exhibited an axial signal with $g_{\perp} = 5.85$ and $g_{\parallel} = 2.0$, as is typical of High-Spin Fe^{III} heme centers with the rhombicity parameter $E/D \approx 0$. (Figure 4-7). The EPR signal exhibited by the His173Ala mutant had the same features as WT heme, suggesting that Sfh5 heme is populated by high spin Fe^{III} heme with $E/D \approx 0.02$. Tyr175Ala mutant showed no signals for heme. We also made two mutants that are predicted to selectively abolish PtdIns binding in Sfh5 – Tyr68Ala and Thr233Ala. Both these mutants bound heme robustly and displayed typical spectra indicating that abolishing PtdIns binding has no effect on heme binding. (Figure 4-8).

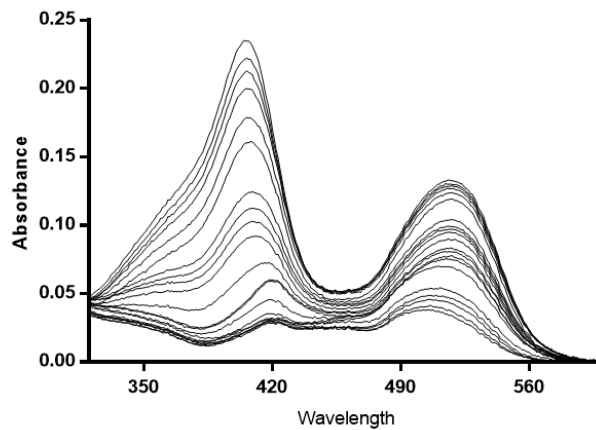
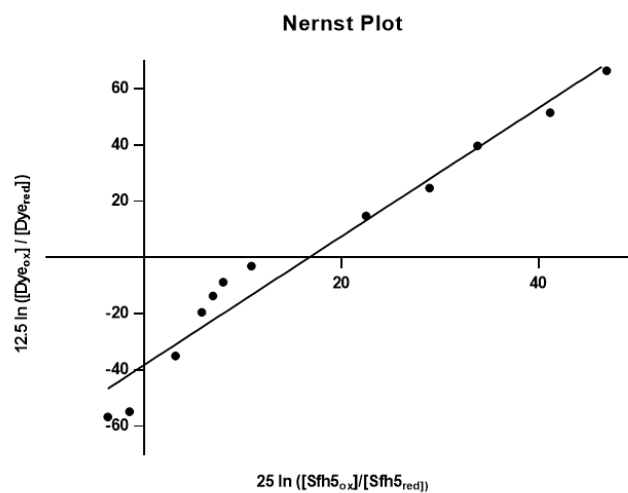
A**B**

Figure 4-6. Determination of Reduction Potential of Sfh5 protein

(A) UV-vis spectra of one electron reduction of Sfh5 and two electron reduction of Safranin T dye by titration with sodium dithionite.

(B) Linear Nernst Plot of the titrations. Dye_{ox}/Dye_{red} stand for ratio of oxidized vs. reduced Safranin T dye, and $Sfh5_{ox}/Sfh5_{red}$ refer to oxidized vs. reduced protein.

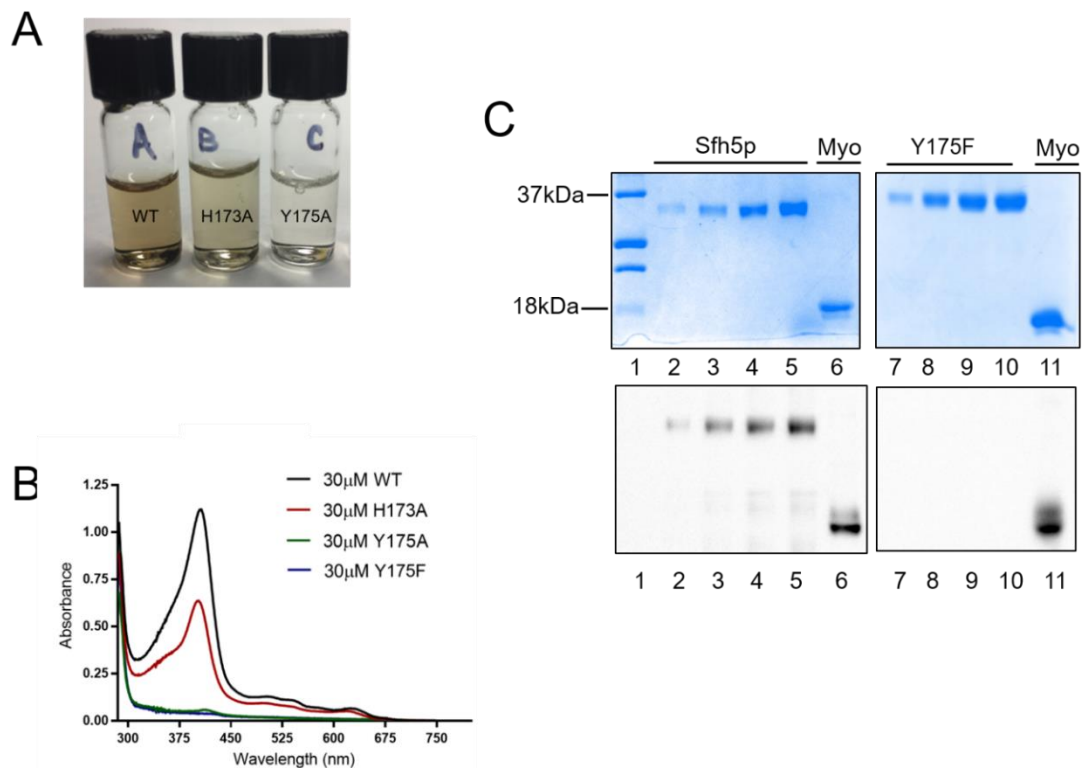


Figure 4-7. Mutations in proximal residues renders Sfh5 defective to heme binding

(A) The purified proteins: WT Sfh5 and mutants H173A and Y175A. The concentration of all proteins was fixed at 5 mg/ml (~250 μM).

(B) UV-vis spectra of Sfh5, H173A, Y175A and Y175F proteins. The concentration of all proteins was fixed at 1 mg/ml (~30 μM).

(C) Top: non-reducing SDS-PAGE with proteins as indicated. Lane 1, molecule weight ladder; lane 2, 0.5 μg WT; lane 3, 1 μg WT; lane 4, 2 μg WT; lane 5, 4 μg WT; lane 6, 2 μg myoglobin; lane 7, 0.5 μg Y175F; lane 8, 1 μg Y175F; lane 9, 2 μg Y175F; lane 10, 4 μg Y175F and lane 11, 2 μg myoglobin. Below: SDS-PAGE gels performed in duplicate were transferred to a PVDF membrane and a chemiluminescent blot performed as described.

A low-temperature, low-field Mössbauer spectrum of WT Sfh5 labeled with Fe⁵⁷ was also obtained (Figure 4-9). The solid red line is a simulation assuming two $S = 5/2$ Fe^{III} heme sites that we call L and S. According to our simulations, the L site has larger average hyperfine couplings and the S site has smaller average hyperfine couplings. Fitting spectra of different preparations of protein required somewhat different relative intensity ratios for the two sites. In contrast, the Mössbauer spectrum of His173Ala mutant suggested that its heme center can be simulated by assuming only the L site (Figure 4-9). The magnetic hyperfine interactions associated with the L site partially collapsed by around 150 K (data not shown) whereas those for S site did not.

The collapsed L site could be fitted to a quadrupole doublet with the same parameters as was used to simulate the mutant Mössbauer spectrum. We hypothesized that the two sites reflect a difference in protonation of the heme center. Since the H173A mutant exhibited the L site exclusively, we further hypothesize that the protonation state involves the proximal histidine residue and that the L site reflects the unprotonated state. We will refer to this as the LS two-site model in the discussion.

Heme-free Sfh5 protein has improved PtdIns-transfer ability in vitro

The mutant versions of Sfh5 protein were tested for their [³H PtdIns] transfer abilities between membranes *in vitro*. Sec14 was used as a control throughout the experiment. A gradient of protein amounts was tested in the assay. Sfh5^{H173A} mutant displayed enhanced PtdIns transfer abilities when compared to wild type Sfh5p. This effect was even more pronounced when Sfh5^{Y175A} was assayed for activity. Compared to 6.3% transfer when 25µg WT protein was assayed for activity, the Sfh5^{Y175A} mutant showed three-fold higher transfer. These results indicate that removal or loss of heme has no effect on protein folding, instead, it leads to an enhancement in the PtdIns binding abilities of Sfh5 (Figure 4-10).

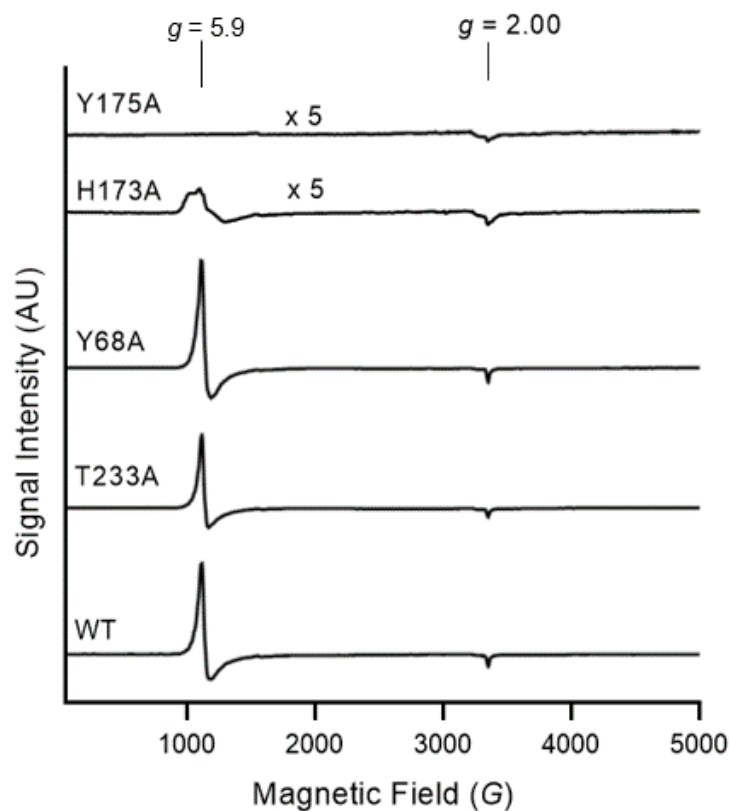


Figure 4-8. Electron Paramagnetic Resonance spectra for Sfh5 protein and mutants.

250 μ M recombinant proteins in their native buffers were taken in Wilmad Suprasil tubes and frozen under liquid nitrogen. All spectra were collected at a temperature of 4K with a 5000G magnetic sweep. A 1mM Cu-EDTA solution was used as a reference to calibrate the readings.

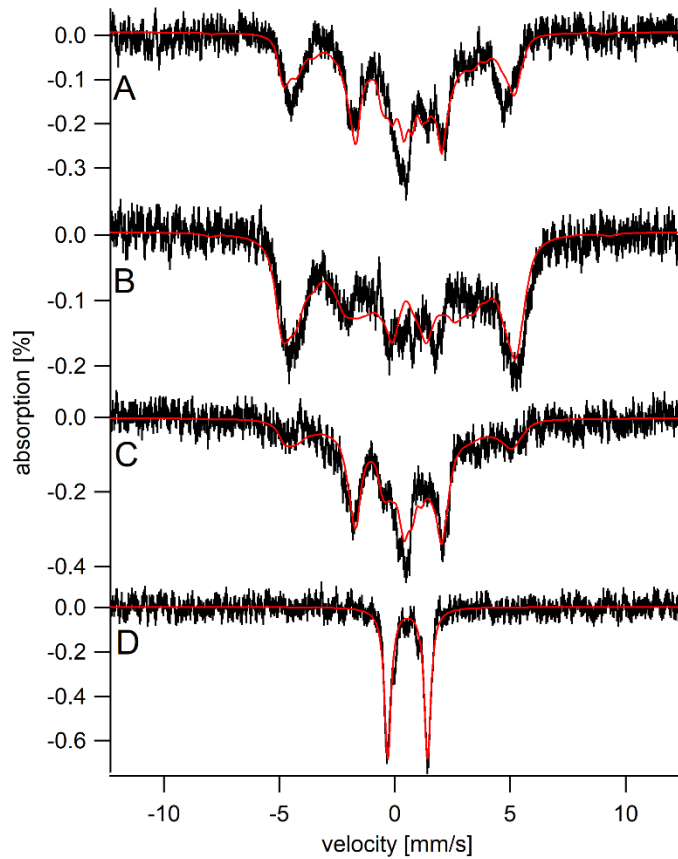


Figure 4-9. Mössbauer spectra of Sfh5p and mutants

The letters A-D in the figure indicate the following: A, WT Sfh5p; B, High temperature (150K) spectra of WT protein; C, H173A Sfh5p ; D, WT Sfh5p spectra post reduction with 20mM Sodium Dithionite.

A field of 0.05 T was applied parallel to the gamma radiation. Overall simulations are indicated by red lines. In the Mössbauer fitting of the reduced sample (D), the spectra from (A) was deducted from the original sample, leaving behind a doublet that represented reduced heme.

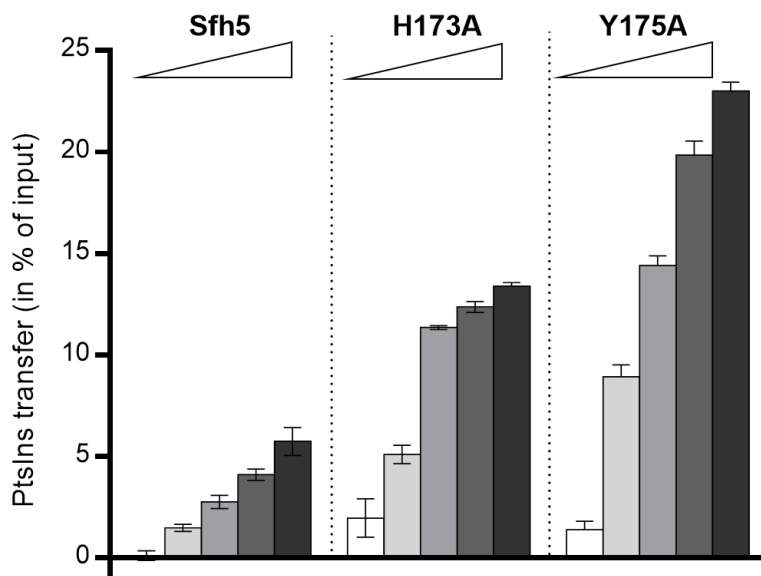


Figure 4-10. PtdIns transfer assay with purified, recombinant Sfh5 protein

The total input of [³H] PtdIns per reaction varied between 9234-2390 cpm. The background was scored between 677-973 cpm. The amount of each protein used in the assay varied from 5μg to 25μg in steps of 5 μg. The percentage transfer values for Sfh5 showed a protein amount dependent increase, as did all the other mutants. The maximum transfer percentage for Sfh5 was 6.3% when 25μg protein was used in the assay. This number increased to 14% for His173Ala and 23% for Tyr175Ala.

Mutant Sfh5 variants complement *sec14-1^{ts}* at restrictive temperatures

To probe the role of mutant Sfh5 in complementing *sec14-1^{ts}*, we used a temperature sensitive strain of Sec14 that is conditionally lethal at 37°C. Rescue of growth at restrictive temperature by the mutants being tested would indicate an ability to mimic Sec14-like functions *in vivo*. Our *in vitro* data suggested that heme-free versions of Sfh5 would be superior than WT protein in complementing *sec14-1^{ts}*. To test that we expressed Sfh5 and its mutant variants from a high expression plasmid. Sfh5 has been previously shown to have poor *sec14-1^{ts}* complementation abilities and our results report the same. In contrast, we observed that Sfh5^{Y175F} mutant rescued the *sec14-1^{ts}* associated growth defects in a very robust manner whereas the Sfh5^{H173A} variant failed. These results essentially phenocopy the results obtained through *in vitro* assays. Moreover, they provide indirect evidence of Sfh5 binding heme *in vivo* (Figure 4-11).

Discussion

The data reported here demonstrate that Sec14-homolog, Sfh5, is a heme binding protein. This is the first time that a phosphatidylinositol transfer protein has been shown to associate with heme. The iron center of Sfh5-heme stays predominantly in the Fe^{III} state and is coordinated axially by a tyrosine residue. Histidine is a coaxial ligand of Sfh5 which does not make direct contact with the iron center, but nevertheless has a significant effect on iron binding. This dual axial tyrosine/histidine motif for iron coordination has been seen in other proteins but they are always supplemented by amino acids as distal ligands. Sfh5 has no distal amino acid ligands that coordinate with heme.

The retention of chemiluminescent activity by the protein despite treatment with SDS indicates that the heme associates strongly with the protein. Our attempts to extract the heme using

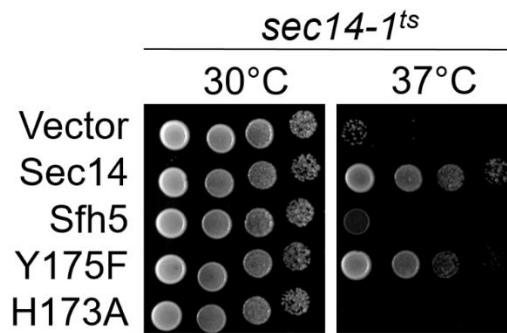


Figure 4-11. *In vivo* complementation assay with Sfh5 mutants.

Sfh5 was expressed under the strong *PMA1* promoter and expressed from a 2 μ plasmid. The WT and mutant variants of Sfh5 were transformed in *sec14-1^{ts}* strains and the *URA*⁺ colonies were selected. Serial dilution of transformants were made on a YPD plates. The plates were incubated at the indicated temperatures for 48 hrs. before imaging.

an organic solvent such as methyl-ethyl kethone always led to the degradation of protein. It is possible that the heme is protected within the lipid binding pocket of the protein and inaccessible to organic solvents. It was remarkable that removal of heme by generation of specific mutants resuscitated PtdIns transfer activity in the protein. This indicates that presence of heme acts to physically prevent any loading of PtdIns molecule in the protein cavity.

It could be possible that Sfh5 binds freshly produced heme from the mitochondria and coordinates that with specific signaling events at membranes elsewhere. Given how easily heme intercalates within membranes, it is possible that Sfh5 exchanges its bound heme at membranes to potentiate PIP signaling. The purpose and downstream consequences of that signaling, however, are not clear.

Sfh5 could also be a heme sequestering protein. Overexpression of Sfh5 in *E. coli* leads to a strong concomitant production of heme as well, with Sfh5 essentially functioning as a ‘heme sink’. However, Sfh5 has never been implicated in any role whatsoever related to heme production or degradation in yeast. This hypothesis also begs the question that if Sfh5 is a heme sink, does it ever act as a ‘heme source’? That is, whether the heme ligand is exchangeable like its other ligand, PtdIns. Our data indicates once the heme is tightly bound and cannot be exchanged. It is feasible that movement of the helical gate guarding the lipid binding chamber may afford the bound heme some mobility, but that remains to be formally demonstrated.

Sec14-like proteins are regarded as nanoreactors that coordinate metabolic signals to boost PIP signaling events. These metabolic signals are generally lipids, that are considered as secondary ligands of PITPs. In this regard, heme seems to behave in an opposite manner – its binding suppresses PIP signaling by the protein. Given that heme is not a “second ligand” of Sfh5 in a

conventional sense, it is possible that there are additional lipid-like ligands of Sfh5 that remain unrecognized.

With respect to the Mössbauer spectrum, we do not know the chemical differences responsible for the L vs. S sites of the protein but propose that they reflect differences in the hydrogen-bonding. We propose that the Tyr175 ligand is hydrogen-bonded to one of the His173 nitrogens in the S site but not in the L site. The absence of this hydrogen-bond in the L site should render the tyrosinate oxygen a harder base, and this should diminish the electron delocalization around the Fe^{III} ion which should, in turn, increase the hyperfine coupling as observed for the L site. According to the LS two-site model, the H173A mutant exhibits the L spectroscopic site because its proximal histidine ligand and the associated hydrogen-bonding is absent. The situation is undoubtedly more complicated than this, because the other imidazole nitrogen of H173 in WT protein is hydrogen-bonded to one of the propionate carboxylate side-chains of the porphyrin ring. Thus, there is a hydrogen-bonding network that electronically connects the porphyrin ring, the propionate side-chain, the proximal histidine, the tyrosinate oxygen, and the heme Fe^{III}. In the His173Ala mutant, this entire network, including both hydrogen-bonding interactions, is absent. Thus, the L state of the mutant may not be exactly the same as the L state of the WT protein; the latter may lack only one hydrogen-bonding interaction.

The heme site of Sfh5 is reminiscent of the active site of catalases and also the heme binding site of certain carrier proteins. Catalases catalyze the dismutation of hydrogen peroxide into water and molecular oxygen, $2\text{H}_2\text{O}_2 \rightleftharpoons 2\text{H}_2\text{O} + \text{O}_2$. They contain heme *b* centers in which the iron is coordinated on the proximal side of the ring by a tyrosinate oxygen (Diaz et al., 2012, Glorieux et al., 2017). However, catalases contain two distal side residues that play important

roles in catalysis, including a histidine and an asparagine (Borges et al. 2014). Our concern in assigning Sfh5 as a catalase is the absence of the residues on the distal side of the heme.

An alternative possibility is the Progesterone Receptor Membrane Component 1 (PGRMC1; Dap1 in yeast). It is a heme binding protein that uses a tyrosinate axial ligand on the proximal side (Cahill et al., 2017). The heme iron in PGRMC1 is 5-coordinate high spin, with the Fe^{III} state dominating. Like Sfh5, there are no distal histidine or asparagine residues. Although its exact function is not known, PGRMC1 is involved with heme-binding, cytochrome P450 interactions, and membrane trafficking (Hughes et al., 2007; Cahill et al., 2017). PGRMC1 locates to the mitochondrial outer membrane where it regulates (inhibits) ferrochelatase activity (Piel et al., 2016). More investigation is needed for Sfh5 to determine if it has PGRMC1 like activities or not. This work lays down a solid foundation for a more detailed and exhaustive study of the relationship between heme and phosphoinositide signaling.

Materials and Methods

Protein expression and purification.

Sec14p was purified as described previously (Khan et. al., 2016). For Sfh5p, a pET28b(+) vector harboring His₈-Sfh5 was transformed into *E. coli* BL21(DE3) cells and grown in lysogeny broth (LB) medium at 37°C. Upon reaching OD₆₀₀=0.5, protein expression was induced with 100μM isopropyl β-D-1-thiogalactopyranoside and the culture grown overnight at 16°C. Cells were harvested by centrifugation at 4°C and the temperature maintained for all subsequent steps. For lysis, cell pellets were resuspended in buffer A (300 mM NaCl and 25 mM Na₂HPO₄ at pH 7.0) with 1mM PMSF and passed through French Press twice at 10,000 psi for protein extraction. The lysate was clarified by centrifugation at 2800g and then at 27,000g. The resulting soluble fraction

was incubated with Co^{2+} resin (TALON, Clontech) in the presence of 10mM imidazole for 5 hours, followed by a thorough wash with buffer A plus 20mM imidazole. Reddish brown fractions of protein were purified using a four-step gradient of buffer A, supplemented with 50mM, 100mM, 200 mM and 350 mM imidazole. The protein purity was judged by SDS-PAGE. Homogenous fractions were pooled and subjected to two rounds of dialysis against buffer A, followed by size-exclusion chromatography on Sephadex 200 column (GE Healthcare). Aliquots of protein were stored at -80°C and used within a month.

For producing Sfh5 with ^{57}Fe -labeled heme, *E. coli* BL21(DE3) cells were transformed with the His₈-Sfh5-pET28b(+) plasmid and a pre-inoculum was grown overnight in LB medium at 37°C . Subsequently, the cells were washed twice in a modified M9 minimal medium (42 mM Na_2HPO_4 , 22 mM KH_2PO_4 , 8.5 mM NaCl, 18.5 mM NH_4Cl , 2 mM MgSO_4 , 0.1 mM CaCl_2 with 20mM glucose) and grown in the same media plus $40\mu\text{M}$ $^{57}\text{FeCl}_3$ at 37°C till $\text{OD}_{600}=0.5$ was reached. In this case, protein expression was induced with 100mM IPTG for 36 hours at 16°C . The cells were then harvested and protein purification done as initially described.

Metal analysis of protein

The metal content of WT and mutant proteins were determined by ICP-MS. Proteins of known concentrations were digested overnight at 80°C in the presence of trace-metal grade nitric acid. Precipitated material was removed by centrifugation and the supernatant collected for analysis. Perkin Elmer Elan DRC II ICP-MS machine was used in collision cell mode (He, 4.5 mL/min) and with a skimmer to minimize polyatomic interferences. A standard Micromist nebulizer (Glass Expansion, Australia) was used to introduce the sample. The dwell time for ^{56}Fe analysis was 100ms.

Crystallization and optimization of crystals.

A search for crystallization conditions was performed at the Hauptman–Woodward Medical Research Institute with >1500 cocktails (Luft et al. 2003). One condition produced brown, rod-shaped crystals within a day of incubation at 16°C. This hit was reproduced and refined in-house using sitting-drop vapor diffusion technique. Diffraction quality crystals were obtained when 300 nL of 10mg/ml protein was mixed with an equal volume of a cocktail containing 0.1 M potassium thiocyanate, 0.1 M sodium citrate (pH 4.2) and 15.5%-26% PEG 4000. Prior to X-Ray analysis, the crystals were soaked in 20% ethylene glycol for cryoprotection and quickly frozen under liquid nitrogen.

Structure determination and model refinement

Data collection was done on 23-ID beamline of Advance Photo Source (APS) at Argonne National Laboratory, Chicago, IL, USA, with three different crystals at 8 keV (1.5498Å) and the space group was determined to be $P4_32_12$. Using *HKL2000* the data was indexed, integrated, merged and scaled with anomalous flags on [Otwinowski and Minor, et al., 1997]. *Xtriage* predicted the anomalous signal for iron from the merged dataset to extend to 3.6Å. For initial phasing, the resolution was set at 3.2Å and for subsequent model building and refinement, the resolution was extended to 2.7Å. Structure was solved using Phenix Autosol Wizard by single wavelength anomalous diffraction method using iron anomalous signal from three heavy atom positions in the asymmetric unit (Adams et al., 2010). The solution was then submitted to Autobuild and a partially built model was obtained. Upon inspection of the same, a well-defined electron density consistent with heme *b* was found which correlated with the found heavy atom positions. The coordinates and geometry definition files for the heme ligand were generated with Phenix Elbow (Moriarty et al., 2009) The initial model was improved by manual rebuilding in COOT (Emsley and Cowtan et

al., 2004). The final structure was deposited in the RCSB protein database and validated. All protein structure figures were generated with Schrodinger.

UV-visible Absorbance Spectroscopy

All absorbance measurements were carried out using Cary Varian Bio 100 UV-vis spectrophotometer (Varian) at room temperature. The slit width for all measurements was 1 nm and spectra was collected at a rate of 500 nm per minute. Quartz cuvettes were used for all measurements.

Reduction Potential Measurements

The reduction potential of Sfh5 was measured following established protocols (Kaluka et al., 2015). 10 μ M Sfh5 protein was taken as purified (i.e. oxidized) in buffer A (300 mM NaCl and 25 mM Na₂HPO₄ at pH 7.0) and mixed with 10 μ M of Safranin T dye for which redox potential is already known (-289 mV vs. NHE). The solution also had 50 mM glucose oxidase, 10 μ M glucose and 10 mM catalase to generate a micro-anaerobic environment. The mixture was titrated with a solution of 100mM sodium dithionite. UV-vis spectra was recorded after 5 minutes of every addition to allow the system to stabilize. Ratio of oxidized to reduced Sfh5p was determined at 404nm, while Safranin T was monitored at 530nm. Linear Nernst plots were tabulated with the values, considering two-electron reduction for the dye and one-electron reduction for the protein.

EPR Spectroscopy

Purified proteins were taken in a Wilmad Suprasil tube and gently frozen under liquid nitrogen and stored in it until measurements were made. EPR spectra was collected on an X-band EMX spectrometer (Bruker Biospin Corp) with a bimodal resonator and cryostat for maintaining a low temperature of 4K. A 1 mM solution of CuSO₄-EDTA was used as a standard. All spectrum involved a 5000G sweep with an average amplitude of 30Db.

Mössbauer Spectroscopy

Low-field (0.5 T), low-temperature (5K) Mössbauer spectra were collected using a model MS4 WRC spectrometer (See Co. Edina, MN). Variable field (0-6 T), 4.2 K spectra were collected using a model LHe6T spectrometer. Both instruments were calibrated using an α -Fe foil at room temperature. Approximately 800 μ l of recombinant proteins of concentration 1.5mM were taken in a Mössbauer cup, frozen over liquid nitrogen and stored at -80°C until use.

Yeast Media and Methods

The yeast strain used in this study was CTY1-1A (*MATa ura3-52 lys2-801 his3 Δ -200 sec14-1^{ts}*) (Cleves et. al., 1991). Genetic methods and media conditions are same as previously described (Kearns et. al., 1998, Khan et. al. 2016).

PtdIns Transfer Assays

The assays were performed by methods previously established (Schaaf et al., 2008). Recombinant Sfh5 proteins were pre-incubated with acceptor liposomal membranes in 300 mM NaCl, 25 mM Na₂HPO₄, pH 7.0 for 30 minutes at 37°C. Donor membranes were rat liver microsomes, labeled with [³H]PtdIns. They were added to initiate the assay, and reactions were incubated for an additional 30 minutes at 37°C. [³H]PtdIns transfer activities are represented as a percentage of radiolabel transferred during the course of the reaction.

References

A.L. Hughes, D.W. Powell, M. Bard, J. Eckstein, R. Barbuch, A.J. Link, P.J. Espenshade, Dap1/PGRMC1 binds and regulates cytochrome P450 enzymes, *Cell Metab.* 5 (2007) 143–149.

Adachi, S.; Nagano, S.; Watanabe, Y.; Ishimori, K.; Morishima, I. *Biochem. Biophys. Res. Commun.* 1991, 180, 138–144.

Adams, P.D., Afonine, P.V., Bunkóczi, G., Chen, V.B., Davis, I.W., Echols, N., Headd, J.J., Hung, L.W., Kapral, G.J., Grosse-Kunstleve, R.W., et al. (2010). PHENIX: a comprehensive Python-based system for macromolecular structure solution. *Acta Crystallogr. D Biol. Crystallogr.* 66, 213–221

Alfonso-Prieto, M.; Borovik, A.; Carpena, X.; Murshudov, G.; Melik-Adamyan, W.; Fita, I.; Rovira, C.; Loewen, P. C. “The Structures and Electronic Configuration of Compound I Intermediates of *Helicobacter pylori* and *Penicillium vitale* Catalases Determined by X-ray Crystallography and QM/MM Density Functional Theory Calculations” *J. Am. Chem. Soc.* 2007, 129, 4193.

Alfonso-Prieto, M.; Oberhofer, H.; Klein, M. L.; Rovira, C.; Blumberger, J. Proton Transfer Drives Protein Radical Formation in *Helicobacter pylori* Catalase but Not in *Penicillium vitale* Catalase *J. Am. Chem. Soc.* 2011, 133, 4285-4298.

Bominaar, E.L., Ding X.Q., Gismelseed, A., Bill, E., Winkler, H., Trautwein, A.X., Nasri, H., Fisher J., and Weiss R. (1992) “Structural, Mossbauer, and EPR investigations on two oxidation states of a five-coordinate high spin synthetic heme. Quantitative interpretation of zero-field parameters and large quadrupole splitting” *Inorg. Chem.* 31, 1845-1854

Borges P.T., Carlos Frazao, Cecilia S. Miranda, Maria A. Carrondo and Celia V. Romao (2014) “Structure of the monofunctional heme catalase DR1998 from *Deinococcus radiodurans*” *FEBS Journal* 281 (2014) 4138–4150

Cahill, M.A., Medlock, A.E. (2017) “Thoughts on interactions between PGRMC1 and diverse attested and potential hydrophobic ligands” *J. of Steroid Biochemistry and Molecular Biology* 171, 11-33.

Cleves AE, McGee TP, Whitters EA, Champion KM, Aitken JR, Dowhan W, et al. Mutations in the CDP-choline pathway for phospholipid biosynthesis bypass the requirement for an essential phospholipid transfer protein. *Cell.* 1991;64(4):789-800.

Diaz A, Loewen PC, Fita I & Carpena X (2012) Thirty years of heme catalases structural biology. *Arch Biochem Biophys* 525, 102–110.

Emsley, P., and Cowtan, K. (2004). Coot: model-building tools for molecular graphics. *Acta Crystallogr. D Biol. Crystallogr.* 60, 2126–2132.

Fita I; Rossmann, MG (1985) “The Active Center of Catalase” *J. Mol. Biol.* 185, 21-37.

Ghosh, K., Thompson, A. M., Goldbeck, R. A., Shi, X., Whitman, S., Oh, E., Zhiwu, Z., Vulpe, C., and Holman, T. R. (2005) Spectroscopic and biochemical characterization of heme binding to yeast Dap1p and mouse PGRMC1p. *Biochemistry* 44, 16729–16736.

Glorieuxa, C., and Calderon, P.B. “Catalase, a remarkable enzyme: targeting the oldest antioxidant enzyme to find a new cancer treatment approach” *Biol. Chem.* 2017; 398(10): 1095–1108

Holic R, Simova Z, Ashlin T, Pevala V, Poloncova K, Tahotna D, et al. Phosphatidylinositol binding of *Saccharomyces cerevisiae* Pdr16p represents an essential feature of this lipid transfer protein to provide protection against azole antifungals. *Biochimica et biophysica acta.* 2014;1842(10):1483-90.

Jeoung, H.-H., Pippig, D.A., Martins B.M., Wagener N., Dobbek H. “HTHP: A Novel Class of Hexameric, Tyrosine-coordinated Heme Proteins” *J. Mol. Biol.* (2007) 368, 1122–1131

Kaluka D., Batabyal D. Chiang BY, Poulos T.L. and Yeh S.-R. (2015) Spectroscopic and Mutagenesis Studies of Human PGRMC1. *Biochemistry* 2015, 54, 1638–1647.

Kearns MA, Monks DE, Fang M, Rivas MP, Courtney PD, Chen J, et al. Novel developmentally regulated phosphoinositide binding proteins from soybean whose expression bypasses the requirement for an essential phosphatidylinositol transfer protein in yeast. *The EMBO journal.* 1998;17(14):4004-17.

Korolnek T, Hamza I. Like iron in the blood of the people: the requirement for heme trafficking in iron metabolism. *Front Pharmacol.* 2014;5:126.

Krishnamurthy P, Xie T, Schuetz JD. The role of transporters in cellular heme and porphyrin homeostasis. *Pharmacol Ther.* 2007;114(3):345-58.

Kielb P., Utesch, P.T., Kozuch, J., Jeoung J.-H., Dobbek, H., Mroginski, M.A., Hildebrandt, P., and Weidinger I. (2017) Switchable Redox Chemistry of the Hexameric Tyrosine-Coordinated Heme Protein. *J. Phys. Chem. B*, 2017, 121, 3955–3964.

Li X, Xie Z, Bankaitis VA. Phosphatidylinositol/phosphatidylcholine transfer proteins in yeast. *Biochimica et biophysica acta.* 2000;1486(1):55-71.

Loewen, P. C.; Carpena, X.; Rovira, C.; Ivancich, A.; Perez-Luque, R.; Haas, R.; Odenbreit, S.; Nicholls, P.; Fita, I. (2004) “Structure of *Helicobacter pylori* Catalase, with and without Formic Acid Bound, at 1.6 Å Resolution” *Biochemistry*, 43, 3089-3103.

Moriarty, N.W., Grosse-Kunstleve, R.W., and Adams, P.D. (2009). Electronic Ligand Builder and Optimization Workbench (eLBOW): a tool for ligand coordinate and restraint generation. *Acta Crystallogr. D Biol. Crystallogr.* 65, 1074–1080.

Oliveira JH, Goncalves RL, Lara FA, Dias FA, Gandara AC, Menna-Barreto RF, et al. Blood meal-derived heme decreases ROS levels in the midgut of *Aedes aegypti* and allows proliferation of intestinal microbiota. *PLoS Pathog.* 2011;7(3):e1001320.

Otwinowski, Z., and Minor, W. (1997). Processing of X-ray diffraction data collected in oscillation mode. *Methods Enzymol.* 276, 307–326.

Piel, R.B., Shiferaw, M.T., Vashisht, A.A., Marcero J.R., Praissman, J.L., Phillips, J.D. Wohlschlegel, J.A, and Medlock, A.E. (2016) A Novel Role for Progesterone Receptor Membrane Component 1 (PGRMC1): A Partner and Regulator of Ferrochelatase. *Biochemistry*, 2016, 55, 5204–5217.

Reid, D.J., Murthy, M.R., Sicignano, A., Tanaka, N., Musik, W.D. & Rossmann, M.G. (1981) “Structure and heme environment of beef liver catalase at 2.5 Å resolution” *Proc. Natl. Acad. Sci. USA* 78, 4767–4771 (1981).

Ren J, Pei-Chen Lin C, Pathak MC, Temple BR, Nile AH, Mousley CJ, et al. A phosphatidylinositol transfer protein integrates phosphoinositide signaling with lipid droplet metabolism to regulate a developmental program of nutrient stress-induced membrane biogenesis. *Molecular biology of the cell.* 2014;25(5):712-27.

Ryan, M.M., Temple, B.R.S., Phillips, S.E., and Bankaitis, V.A. (2007). Conformational dynamics of the major yeast phosphatidylinositol transfer protein Sec14p: Insight into the mechanisms of phospholipid exchange and diseases of Sec14p-like protein deficiencies. *Molecular biology of the cell* 18, 1928-1942.

Ryu CS; Klein K., and Zanger UM (2017) “Membrane Associated Progesterone Receptors: Promiscuous Proteins with Pleiotropic Functions – Focus on Interactions with Cytochromes P450” *Frontiers in Pharmacology* 8, article 159. 1-8.

Sha B, Phillips SE, Bankaitis VA, Luo M. Crystal structure of the *Saccharomyces cerevisiae* phosphatidylinositol-transfer protein. *Nature.* 1998;391(6666):506-10.

Schaaf, G., Ortlund, E.A., Tyeryar, K.R., Mousley, C.J., Ile, K.E., Garrett, T.A., Ren, J., Woolls, M.J., Raetz, C.R.H., Redinbo, M.R., et al. (2008). Functional Anatomy of Phospholipid Binding and Regulation of Phosphoinositide Homeostasis by Proteins of the Sec14 Superfamily. *Molecular Cell* 29, 191-206.

Yosca T.H., Langston M.C., Krest C.M., Onderko E.L., Grove T.L., Livada J, and Green M.T. (2016) “Spectroscopic Investigations of Catalase Compound II: Characterization of an Iron(IV) Hydroxide Intermediate in a Nonthiolate-Ligated Heme Enzyme” *J. Am. Chem. Soc.* 2016, 138, 16016-16023.

CHAPTER V

CONCLUSIONS AND FUTURE DIRECTIONS

In my studies at the Bankaitis Lab, I have been involved in multiple projects aimed at understanding the chemical biology and bioinorganic chemistry of phosphatidylinositol transfer proteins (PITPs). Using long-established techniques of genetic manipulation in *S. cerevisiae*, I discovered a structural feature of Sec14 proteins, that determines their sensitivity to the NPPM class of drugs. This feature, termed the VV motif, enables estimation of NPPM sensitivity/resistance in fungal Sec14-like proteins by mere primary sequence consideration. These discoveries are described in detail in Chapter 2.

The predictive power of this motif was tested in another study where we validated two new chemotypes with anti-Sec14 activity. We elucidated their structure-activity relationships providing a proof-of-principle for fungal Sec14 being an attractive drug target. Chapter 3 summarizes this work.

In chapter 3, I reported the discovery of a novel Sec14-like protein in fungal eukaryotes that bind heme. Establishing Sfh5 as a bona fide hemoprotein, we determined its x-ray crystal structure at 2.7Å resolution. We mapped the unusual electronic properties of the iron center in heme using multiple biophysical approaches. Heme binding could be abrogated, or even enhanced, by making specific mutants in the protein. We also discovered linkages between heme and PtdIns binding that outline their allosteric relationship. Taken together, these findings expand our knowledge of PITPs and the diverse roles they play in cells.

I will now summarize the major conclusions of my work and propose follow up experiments.

Conclusions

Understanding the mechanism of Sec14 inhibitors

As discussed in chapter 2 and 3, we have shown that Sec14 residues V154 and V155 constitute a motif, termed as the VV signature. Presence of this motif, in part or in full, rendered Sec14 homologs susceptible to varying degrees of inhibition by NPPM-like molecules (Khan et al., 2016). Molecular dynamics simulation experiments with V154F/E/M mutations predicted a localized disruption of the lipid binding pocket that co-ordinates the S173-NPPM interaction. Replacing V155 with a charged residue was predicted to have perturbed the S173 coordination envelope in a similar manner, thus rendering the protein insensitive to drug. The predictive power of this motif to test the susceptibility of fungal Sec14 to inhibition was employed against two new chemical scaffolds, picolinamide and benzamide (Pries et al., 2018). As predicted, Sec14 from *Candida albicans* which has MC in place of VV, was immune from the toxic effects of the compounds. In contrast, Sec14 *C. glabrata* with a cognate VV signature was sensitive.

To eliminate the possibility of cross-species interference by the proposed inhibitors, we tested the picolinamide and benzamide drugs against a rat Sec14-like protein, PITP α . Mammalian PITPs do not share sequence or structural similarity with fungal PITPs, despite showing similar biochemical activities *in vitro*. I discovered that the compounds active against Sec14 were ineffective towards PITP α , thereby supporting the notion that these compounds are non-promiscuous nature and have no off targets.

The repertoire of effective fungicides is shrinking due to emerging fungal resistance. In 2017, the Centre for Drug Control (CDC) labelled *Candida auris*, an emerging pathogen, a ‘serious global health threat’. Some strains of *C. auris* are resistant to all FDA-approved drugs, necessitating the development of new classes of drugs. On other hand, only a small part of fungal

proteome has been pharmacologically exploited. My work expands this space to include Sec14 as an attractive new drug target. The study of inhibition from a molecular point of view will provide valuable guidance for development of new pan-fungal drugs.

These conclusions notwithstanding, certain questions remain. The VV signature isn't the only determinant of drug resistance in Sec14. The amino acid residues lining the lipid-exchange pocket of Sec14 from multiple fungal species show remarkable similarity, but they are not identical. Subtle differences in pocket architecture need to be considered if drugs targeting Sec14 from *C. albicans* or *C. auris*, are to be developed.

We also know little about the trajectory taken by the drug while entering the pocket. A successful inhibitory event would presumably involve multiple steps. Defects in initial association of drug with protein surface, or weak interactions with the gating elements of pocket may exclude the molecule from the pocket. Even if accessible, the pocket may eject the drug molecule to supplant it with its more natural ligands - phosphatidylinositol or phosphatidylcholine. While crystallographic structures of proteins complexed with drugs are useful, they generally offer a snapshot of the final binding mode, not the events preceding it. Previous studies have shown that the headgroups of both phospholipid ligands bind Sec14 at distinct sites within the lipid binding pocket. Their acyl chains though, converge at the same space. With these challenges in mind, I propose the following experiments.

Future Directions

Development of small molecule inhibitors against Sec14 from C. albicans and C. auris.

Attempts to crystallize recombinant Sec14 from *Candida* species should be made. To that effect, I had the Sec14 ORF from *Candida auris* (Sec14_{AU}) synthesized commercially and then cloned

into a protein expression vector. The protein expressed stably and with high yields. Recombinant Sec14_{AU} should be purified and attempts made to determine its crystal structure in collaboration with Prof. James Sacchettini's group at Texas A&M.

We also recently screened ~1500 crystallization conditions for Sec14_{CA} at the Hauptman-Woodward Medical Research Institute, Buffalo. One condition produced morphologically well-defined crystals that could serve as leads for further development. The cocktail, termed CAC1, consists of 0.5 M ammonium sulfate, 0.1 M sodium citrate tribasic dihydrate and 1M lithium sulfate monohydrate (Figure 5-1A). The proteinaceous nature of the crystals was confirmed by checking them for tryptophan fluorescence so as to screen out the possibility of any salts crystals. Alternatively, three-dimension computational structure-based approaches could be taken to produce homology models for fungal Sec14s. High resolution structures of *S. cerevisiae* Sec14 and its homologs would serve as templates for such modeling. Sec14 shares 67% identity and 81% similarity with Sec14_{CA} at primary sequence level. For Sec14 from *C. auris*, 69% residues are identical and 79% similar. The low *e*- values for sequence comparison computed through BLAST searches indicate that reliable homology models could be generated. This will allow in-silico approaches to develop new inhibitors for fungal Sec14s.

The current library of Sec14 inhibitors encompass around ~34 compounds built around the NPPM and picolinamide scaffolds. By using computational docking protocols, a diversified library of compounds can be tested to predict Sec14_{CA} or Sec14_{AU} specific binding modes. Many of the candidate compounds are already available commercially. Our preliminary studies have indicated three new scaffolds as promising candidates for anti-Sec14_{CA} activity (Figure 5-1C). These

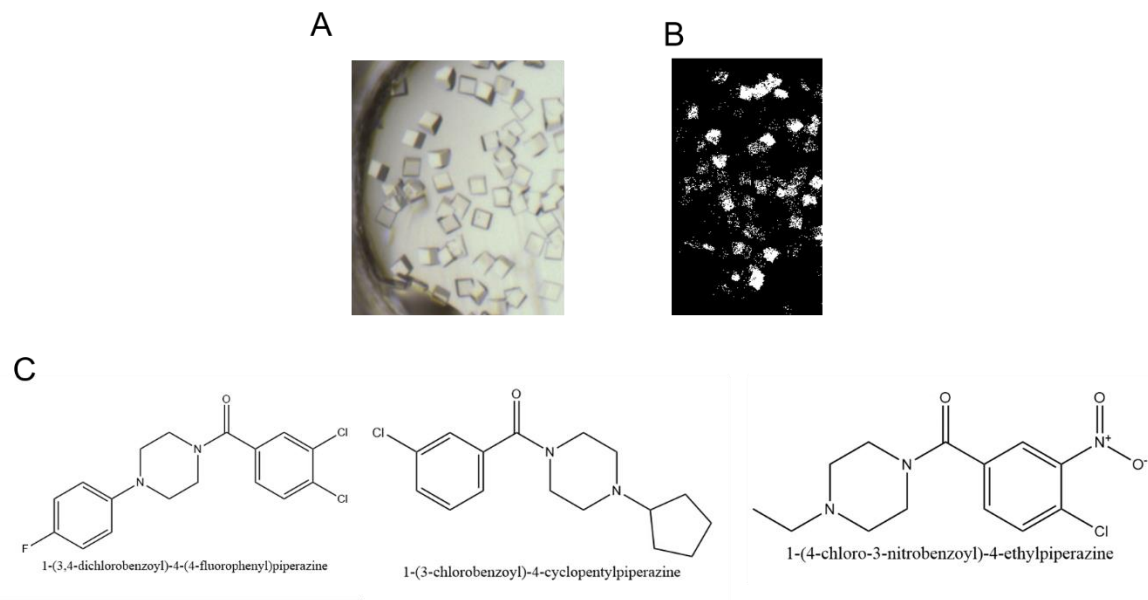


Figure 5-1. Crystallization efforts directed towards Sec14 from *C. albicans* and promising new chemical scaffolds.

(A) Images of putative Sec14_{CA} crystals that were formed in condition CAC1 after 4 days of incubation at 16°C.

(B) The Two-photon excited Ultraviolet Fluorescence images of the same crystals. Presence of tryptophan is indicated by fluorescence in the protein crystals.

molecules are: 1) 1-(3,4-dichlorobenzoyl)-4-(4-fluorophenyl)piperazine, 2) 1-(3-chlorobenzoyl)-4-cyclopentylpiperazine and, 3) 1-(4-chloro-3-nitrobenzoyl)-4-ethylpiperazine. These compounds have a cLogP value below 3.6 which is an indicator of their soluble nature. They should be tested for anti-Sec14_{CA} activity using platforms established in Chapters 2&3.

The ILSB at Texas A&M has an expansive library of chemical scaffolds that could also be used in these tests. Positive hits *in silico* could be cherry-picked from the library and validated in *in vitro* lipid transfer assays. Drugs that “fit” into the lipid binding pockets of Sec14s from *C. albicans* and *C. auris* will need to be redesigned to for optimal results. These approaches are likely to be very helpful in developing new chemotypes that target fungal Sec14s.

Trajectory mapping of phospholipid and drug ligands of Sec14.

The lipid binding pocket of Sec14 can accommodate only one molecule of PtdIns, PtdCho or NPPM at a time. PtdIns headgroup is nestled just under the protein surface while PtdCho and NPPMs dock deep within the pocket. Although high resolution structure of the protein:ligand complexes are useful, they are uninformative as to the trajectories taken by them. A better understanding of the drug pathway may allow design of molecules that associate with the protein in a more favorable manner. To answer these questions, I propose that we exploit new yeast-specific CRISPR-cas9 based technologies that have been recently developed.

Traditional genetic techniques are limited when it comes analyzing mutant profiles of proteins on a large scale. Generating hundreds of mutations concurrently and in a controlled manner is time taking and expensive. Recently, a group led by Dr. Lars Steinmetz (Stanford), with contributions from our lab, has developed a method to introduce thousands of mutations in proteins in very short period of time (Roy et al., 2018). This technique is termed ‘MAGESTIC’, short for “Multiplexed Accurate Genome Editing With Short, Trackable, Integrated Cellular Barcodes”. It

uses the CRISPR-cas9 technology to introduce saturation mutagenesis of a given gene. In principle, using MAGESTIC, every amino acid in the protein can be changed to 19 other natural amino acids, each of which can be tracked and accounted for in a pool of barcoded strains. Thus, for a protein such as Sec14 that has 304 amino acids, a total of 19 times 304, i.e. 5776 distinct strains can be generated.

To test their technique, the authors selected a 35 amino acid stretch in Sec14, from residues 102 to 137 and subjected it to saturation mutagenesis using MAGESTIC. They then challenged this mutant library with NPPM drugs to determine drug resistance or sensitivity. The strains were subjected to drug treatment for multiple generations, thereby allowing identification of a range of mutation with variable phenotypes.

A remarkable feature of this technique is that it allows identification of even those mutational changes that instead of conferring resistance to the protein, end up making them more sensitive to the drug. The authors identified many such mutations that are nowhere near the lipid binding domain, the supposed resting place of NPPMs (Figure 5-2A and Figure 5-2B).

The residues A21 and L22 reside at the loop connecting elements of the tripod motif. The residues P108 and G127 belong to the “gating module” of the protein that controls the helix gating the lipid binding domain. D117 and P120 lie at the loops connecting the β sheets of the lipid binding pocket. None of these residues have been ever identified as significant with respect to NPPM inhibition of Sec14. The fact that they are not in the pocket poses tantalizing questions as to their role in NPPM-protein interactions.

These mutants need to be rigorously characterized as they are likely be involved in interaction of the drug with Sec14 at some point in their trajectories. These would involve testing the mutants to see if they have any subtle defects associated with PtdIns/PtdCho binding and

transfer. Prevailing evidence indicate that PtdIns and PtdCho have distinct binding modes and periods of occupancy within the Sec14 pocket. It can be reasonably presumed that NPPMs follow the trajectories of any of these two lipids, or that it could charter its own independent pathway of binding with Sec14. Analysis of these mutants should be very informative.

As a preliminary experiment, I have been able to show that the reported mutations do indeed confer NPPM resistance to Sec14 but at varied potency. The Pro108, Ala21, Leu22 and Asp117 were indeed able to abrogate inhibition by NPPM to a great degree but, Pro120 and Gly127D did not. These are promising leads that need to be pursued. By expanding this saturation mutagenesis technique to the entire protein, a high definition picture of Sec14-protein interaction can be generated which will allow us to understand the precise molecular mechanism by which NPPMs intoxicate Sec14. This will greatly aid development of rational drugs against Sec14 from fungal pathogens that are so urgently needed.

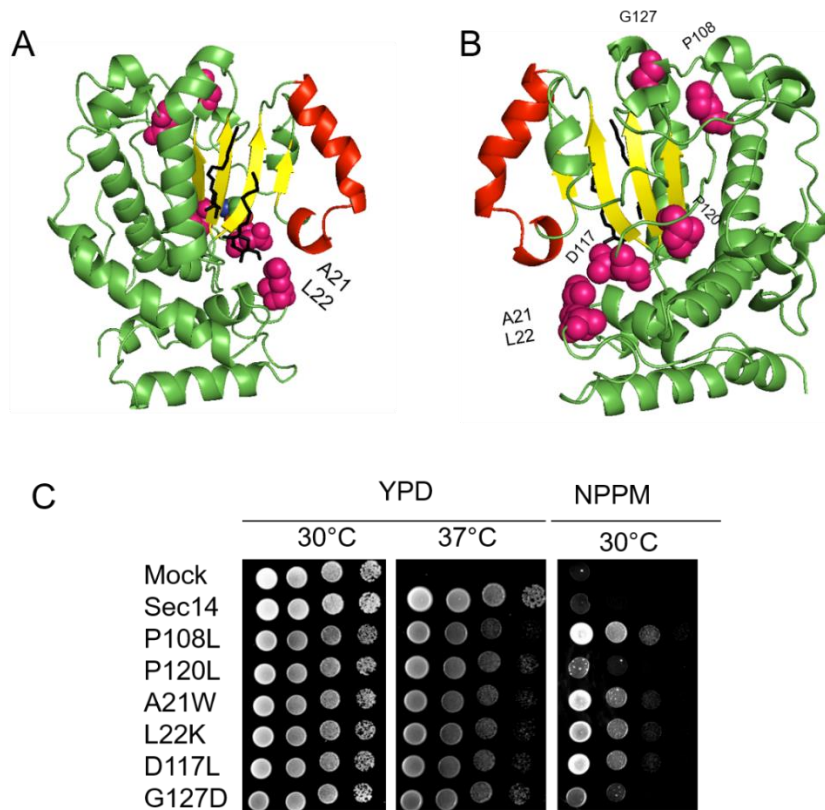


Figure 5-2. Analysis of new Sec14 mutants that do not reside in the binding pocket

(A) Overview of Sec14 crystal structure (PDB ID 1AUA) with select residues that were identified as NPPM sensitive in the MAGESTIC screen by Roy et. al., 2018. The floor of the lipid binding pocket is shown in yellow. An α helix guarding entry to the lipid binding pocket is shown in red. Rest of the secondary structural elements are in green. A ligand docked within the pocket, mimicking PL, is in black. All amino acid residues are shown as pink spheres and labeled. Residues A21 and L22 are located outside the pocket.

(B) A 180° degree flip of the structure shown in (A). The residues D117 and P120 are situated behind the β pleated sheets. Residues G127 and P108 belong to the gating module of the protein

(C) The indicated SEC14 genes were integrated into the *LEU2* locus of a *sec14-1^{ts} spo14 Δ* strain and grown at the indicated temperatures. Expression of each Sec14 protein was sufficient to rescue *sec14-1^{ts}* growth defects at the restrictive temperature of 37°C was demonstrated by comparison of the growth profiles in the left (30°C) and center (37°C) panels of the integrants relative to mock controls. The NPPM^R phenotypes are displayed in the right panel. The plates were incubated for 48 h at the indicated temperatures before imaging.

References

Khan D, McGrath KR, Dorosheva O, Bankaitis VA, Tripathi A. Structural elements that govern Sec14-like PITP sensitivities to potent small molecule inhibitors. *J Lipid Res.* 2016;57(4):650-62.

Pries V, Nocker C, Khan D, Johnen P, Hong Z, Tripathi A, et al. Target Identification and Mechanism of Action of Picolinamide and Benzamide Chemotypes with Antifungal Properties. *Cell Chem Biol.* 2017.

Roy KR, Smith JD, Vonesch SC, Lin G, Tu CS, Lederer AR, et al. Multiplexed precision genome editing with trackable genomic barcodes in yeast. *Nat Biotechnol.* 2018.

Nile AH, Tripathi A, Yuan P, Mousley CJ, Suresh S, Wallace IM, et al. PITPs as targets forselectively interfering with phosphoinositide signaling in cells. *Nature chemical biology.* 2014;10(1):76-84.

APPENDIX A

PLASMID INVENTORY

| Plasmid Name | Description |
|--------------|---------------------------------------|
| pDK285 | Sfh5-6His pET28b (tag at C' terminus) |
| pDK289 | Tagless Sfh5 pET28b |
| pDK293 | 8His-Sfh5 pET28b |
| pDK306 | Sfh5 pDR195 |
| pDK307 | Sfh5 H173A pET28b |
| pDK335 | Sfh5 H173A pDR195 |
| pDK336 | Sfh5 pET28b K14K |
| pDK357 | Sfh5 H173A, Y175A pET28b+ |
| pDK358 | Sfh5 Y175A pDR195 |
| pDK363 | Sfh5 Y175A pET28b+ |
| pDK364 | Sfh5 HYAA pDR 195 |
| pDK365 | Sfh5 W181A pET28b+ |
| pDK366 | Sfh5 T233A pET28b+ |
| pDK367 | Sfh5 Y68A pET28b+ |
| pDK368 | Sfh5 Y68A, T233A pET28b+ |
| pDK370 | Sfh5 Y175F pET28b+ |
| pDK371 | Sfh5 Y175H pET28b+ |
| pDK373 | Sfh5 Y175A Y68A pET28b+ |
| pDK374 | Sfh5 Y175A T233A pET28b+ |
| pDK375 | Sfh5 Y68A pDR195 |

PLASMID INVENTORY

| Plasmid Name | Description |
|---------------------|--------------------------|
| pDK376 | Sfh5 T233A pDR 195 |
| pDK377 | Sfh5 Y175A Y68A pDR195 |
| pDK378 | Sfh5 Y175A T233A pDR 195 |
| pDK379 | Sfh5 Y175F pDR 195 |
| pDK380 | Sfh5 Y175H pDR 195 |
| pDK381 | Sfh5 W181A pDR195 |
| pDK390 | Sfh5 Y175F Y68A pDR 195 |
| pDK391 | Sfh5 Y175F T233A pDR 195 |
| pDK426 | Sfh5 Y175F E204V pDR 195 |
| pDK427 | Sfh5 Y175F K236I pDR 195 |
| pDK428 | Sfh5 Y175F E204V pET28b |
| pDK429 | Sfh5 Y175F K236I pET28b |
| pDK430 | Sfh5 Y175F Y68A pET28b |
| pDK431 | Sfh5 Y175F T233A pET28b |

APPENDIX B

PROTOCOLS OF NOVEL TECHNIQUES

Electron Paramagnetic Resonance Spectroscopy Analysis of Heme-bound Protein

1. Before beginning an experiment, it should be ensured that the Helium tank is at least 30% full. Turn on the compressor, heat exchanger, console and the magnet power supply.
2. Set the desired temperature – usually 10K.
3. Set up a ‘new experiment’. Fix diode current at 200 μ A, sweep time at 300s, attenuation at 40dB, sweep width at 5000, amplitude at 10G and tune the microwave to get stable diode current reading.
4. To collect spectra, switch into the “tune mode”. Then move the tube containing CuEDTA standard into the resonator and pushing it gently until there is resistance.
5. Adjust the frequency slider and the iris to get a symmetric dip reading. The lock offset should be adjusted to get a value close to 0. The diode current should be around 200 μ A
6. Collect EPR spectra without any sample in the machine to establish a baseline reading and rule out any contamination in the resonator.
7. Preparation of CuEDTA standard: Around 200 μ l of 1mM CuEDTA solution was taken in a 250mm Wilmad Suprasil glass tube and gently frozen over liquid nitrogen. This sample serves as a known standard and spectra collected for it.
8. Preparation of protein samples for analysis by EPR: Around 200 μ l of 250 μ M protein in a buffer (250mM NaCl and 25mM Na₂HPO₄) was taken in the glass tube frozen as described above.
9. Between changing samples in or out of the resonator, make sure that the ‘tune mode’ is on and attenuation is set at 40dB.

10. After collection of EPR spectra for each sample, turn off the instrument by executing steps in the reverse order to turning it on.
11. Set the machine to “standby” mode and “disconnect from spectrometer”.
12. Do not save any changes you made to the program. Switch off the magnet power supply, console, heat exchanger and the compressor.

Heme protein Chemiluminescent Assay

1. Heme-bound proteins show a pseudo-peroxidase activity that can be visualized through a chemiluminescent blot.
2. Set up a SDS-PAGE gel with 10% separation and 4% stacking gels according to standard protocol.
3. Mix the protein volumes with a dithiothreitol-free 6X SDS loading buffer. Do not heat the samples.
4. Load the samples on the gel along with a molecular weight marker and run it at 150V till the dye front runs off the gel.
5. Perform electrophoretic transfer of proteins from SDS-PAGE gels to sheets of nitrocellulose membrane according to standard protocol.
6. Ensure that the electroblotting apparatus does not heat up during the transfer.
7. Wash the electroblotted membrane in PBS solution to remove transfer buffer and remove excess liquid with help of an adsorbent paper towel.
8. Prepare a visualisation solution by mixing 1ml of peroxide solution with 1 ml of luminol/enhancer solution as provided in the Pierce SuperSignal West Femto Maximum kit.

9. Place the blots on a plastic wrap and cover it with the visualization solution prepared above.
Incubate it for 5 minutes.

10. Develop the blots through the Biorad Chemidoc imager system.

Determination of the Reduction Potential of a redox active protein

$$E_P = E_{mP} + \frac{RT}{nF} \ln \left(\frac{[P_{ox}]}{[P_{red}]} \right) \quad (1)$$

In the Nernst Equation (1) E_P is the measured potential of a redox protein, E_{mP} is the reduction potential being determined and the contribution of oxidized vs. reduced form of protein is quantified in $\frac{RT}{nF} \ln \left(\frac{[P_{ox}]}{[P_{red}]} \right)$. R and F denote the Gas and Faraday constants respectively, while T denotes the absolute temperature. Number of electrons being lost or gained are denoted by n .

The Soret band (around 404nm) for a heme protein can be taken to approximate the concentration of heme-protein. For a redox active dye, the absorption band (around 500-650nm) can be used to approximate the dye concentration. We assume that protein and dye are in their 'oxidised' forms in the beginning of the assay and as the reaction proceeds, they get 'reduced'. The ratio of oxidized vs. reduced forms can thus be approximated by taking ratio of absorption change for protein or dye. $\frac{[P_{ox}]}{[P_{red}]} = \frac{[A - A_{min}]}{[A_{max} - A]}$ where A_{min} is the residual absorbance at the end of reaction, A is the measured absorbance, A_{max} is the maximum absorbance measured (before adding enzyme). The reduction potential of the protein and dye can be thus represented as (2) and (3) respectively.

$$E_P = E_{mP} + \frac{RT}{nF} \ln \left(\frac{[P_{ox}]}{[P_{red}]} \right) \quad (2)$$

$$E_{Dye} = E_{mDye} + \frac{RT}{nF} \ln \left(\frac{[Dye_{ox}]}{[Dye_{red}]} \right) \quad (3)$$

Considering the electrochemical potential in solution to be equal at equilibrium, i.e.

$$(E_{\text{Dye}} = E_{\text{P}}) \quad (4)$$

we get,

$$E_{m\text{Dye}} + \frac{RT}{nF} \ln \left(\frac{[\text{Dye}_{\text{ox}}]}{[\text{Dye}_{\text{red}}]} \right) = E_{m\text{P}} + \frac{RT}{nF} \ln \left(\frac{[\text{P}_{\text{ox}}]}{[\text{P}_{\text{red}}]} \right) \quad (5)$$

We know that the Fe^{III} to Fe^{II} reduction is a one-electron process, while the reduction of Safranin T dye is a two-electron process. So, equation (5) can be expressed as:

$y = (E_{m\text{P}} - E_{m\text{D}}) + x$ (6). Where $x = 25 \ln \left(\frac{[\text{P}_{\text{ox}}]}{[\text{P}_{\text{red}}]} \right)$ and $y = \frac{25}{2} \ln \left(\frac{[\text{Dye}_{\text{ox}}]}{[\text{Dye}_{\text{red}}]} \right)$. This assumes the form of a linear equation of the form $y = mx + C$ where C is the y-axis intercept of the graph. From the known reduction potential value for Safranin T dye, the reduction potential of the protein can be calculated.